CHARACTERIZATION AND DETERMINATION OF EROSION DAMAGE RESULTING FROM LIQUID JET IMPACT

A Thesis Submitted

to the

Victoria University of Manchester

By

GEOFFREY WELLS VICKERS

M.Sc., C.Eng., M.I.Prod.E.

as part of

the requirements for the degree of

Doctor of Philosophy

University of Manchester

Institute of Science and Technology

August 1972

ProQuest LLC.
789 East Eisenhower Parkway
P.O. Box 1346
Ann Arbor, MI 48106 – 1346

To Mother and Father

CONTENTS

		Page
Acknowledgments		
The Author		
Synopsis		
CHAPTER 1	INTRODUCTION	1
1.1	Occurrence of erosion	1
1.2	Simulation techniques	3
	.1 Wheel and jet	3
	.2 Liquid jet	4
	.3 Projectile apparatus	4
	.4 Magnetostriction oscillators	4
1.3	Factors influencing erosion	5
1.4	Present investigations	7
CHAPTER 2	LIQUID JET AND ANCILLARY APPARATUS	8
2.1	Repetitive water jet equipment	8
2.2	High speed jet gun	9
	.1 Description of gun	9
	.2 Calibration	10
2.3	Jumbo jet apparatus	11
	.1 Description of equipment	11
	.2 Calibration	12
2.4	Split-platen pressure cell	12
	.1 Design of pressure cell	13
	.2 Calibration and analysis of response	13
2.5	Measurement of jet velocity using photocells	16

CHAPTER 3	FORMATION OF EROSION CRATERS	18
3.1	Introduction	18
3.2	Development of impact craters	19
	.1 Fully annealed ∝-brass	19
	.2 Perspex	23
3.3	Threshold velocity	24
3.4	Effect of jet velocity on erosion	26
3.5	Conclusions	28
CHAPTER 4	SURFACE CONDITION	30
4.1	Introduction	30
4.2	Surface finish	31
	.1 Experimental procedure	31
	.2 Results and discussions	32
	.3 Conclusions	33
4.3	Chromium plated mild steel	34
4.4	Anodised aluminium	35
4.5	Shot peening	35
CHAPTER 5	PRE-STRESS AND PRE-STRAIN	37
5.1	Equipment	37
	.1 Uniaxial loading fixture	37
	.2 Biaxial loading	38
5.2	Experimental procedure	39
5.3	Experimental results and discussion	40
	.1 Erosion of ∝-brass specimens	40
	.2 Erosion of Perspex specimens	43
5.4	Conclusions	44
5.5	Pre-strain	45

CHAPTER 6	JET IMPACT ON CONVEX, CONCAVE AND FLAT INCLINED SURFACES	46
6.1	Introduction	46
6.2	Theoretical jet impact	48
	.1 Jet impact on convex surfaces	48
	.2 Jet impact on concave surfaces	48
	.3 Jet impact on flat inclined surfaces	51
6.3	Experimental results and discussion	52
	.1 Convex and concave surfaces	52
	.2 Flat inclined surfaces	54
6.4	Conclusions	55
CHAPTER 7	PENETRATION AND PERFORATION	56
7.1	Introduction	56
7.2	Experiments and discussion	57
	.1 Penetration of plasticine	57
	.2 Perforation of lead and aluminium plates	60
7.3	Conclusions	61
CHAPTER 8	IMPACT STRESSES	63
8.1	Introduction	63
8.2	Experimental procedure	66
8.3	Experimental results and discussion	67
	.1 Direct impact stress	67
	.2 Surface shear impact stress	69
	.3 Direct impact stress on inclined surfaces	71
	.4 Surface films	72
	.5 Fluid flow on impact	73
8.4	Conclusions	74

REFERENCES 75

APPENDIX I 84

TABLE I 86

TABLE II 87

ACKNOWLEDGMENTS

The author wishes to express his gratitude to Professor W. Johnson for encouragement and guidance throughout the course of these investigations.

The technical assistance of many members of the department is gratefully acknowledged - in particular Mr. A. D. Kidd for his valuable assistance with work in the latter chapters, Mr. G. Robinson for help with equipment design, Mr. H. Vernon who made the high velocity gun, Mr. T. Lees for work on the pressure cell, Mr. J. Howe for all photographic work and Mr. R. Blower for assistance with electronic problems. Appreciation is also extended to Mr. D. Ryder and his colleagues of the Metallurgy Department, Dr. H. Kenyon and Dr. J. B. Hawkyard for numerous discussions.

Finally the author wishes to thank the Science Research Council for its support of this work.

THE AUTHOR

The author was born in Leicester in 1943. He was employed by the British United Shoe Machinery Co. Ltd. as an Apprentice in 1959 and took O.N. Cert and H.N. Dip. at Leicester Polytechnic and Dip. Eng. Prod. at Birmingham University. Subsequently he spent four years as Production Controller of the Knife and Die Factory of B.U.S.M. Co. Ltd.

In 1969 he joined the Mechanical Engineering Department of Manchester University Institute of Science and Technology and was awarded the degree of M.Sc. for research on dynamic loading of structures in 1970.

SYNOPSIS

To investigate erosion phenomena, two different equipments have been developed. Equipment (i) projects high speed small diameter liquid jets at 450 to 800 m/sec and equipment (ii) projects 50 mm diameter low velocity jets at a speed of up to 46 m/sec.

The formation and development of erosion craters are examined, criteria are obtained for threshold velocities for single and multiple impacts and the relationships of jet velocity to the induction period and rate of mass loss are derived. The effects of impact against surfaces of varying roughness and also chromium plated, anodised and shot peened surfaces are studied and the influence on erosion characteristics are considered.

Experiments on targets subjected to uniaxial and biaxial tensile and compressive stresses are described and some analysis is given.

Damage resulting from jet impact on convex, concave and flat inclined surfaces is reported on and the essential features are analysed in terms of stress wave phenomena. Penetration of large blocks of material and the perforation of thin plates by water jets have been investigated.

The large diameter jet was used in conjunction with a pressure cell to determine the stresses engendered during impact on perpendicular and inclined surfaces and novel and unexpected results are found and are reported.

CHAPTER ONE

CHAPTER ONE

INTRODUCTION

On impact with a solid surface a liquid drop produces a very high compressive stress in the vicinity of the area of contact, lasting for a few microseconds, which is followed by rapid outward radial flow causing erosive shearing of the surface. An insight into the intricacy and complexity of water drop impact, with water, is given admirably by Worthington.[136]

1.1 OCCURRENCE OF EROSION

Erosion manifests itself in three spheres of technology which are of importance at the present time. One is the erosion of aircraft, helicopter and missile surfaces when flying through rain.[52,44,119] Damage may result on the forward facing surfaces such as wing edges or radomes at speeds of a few hundred miles per hour and at Mach 1 to 2 a single impact causes serious deformation. The limiting altitude for rain as usually accepted, is 10,000 metres although discrete cells of Cumulo Nimbus clouds can occur as high as 17,000 metres particularly in the tropics. Thus many aircraft fly relatively slowly up through the rain and achieve their highest speeds above the rain level. However, with all-weather operational requirements of, for example, fighter aircraft at low altitudes, erosion is a very real problem.

The broad requirement stated by Fyall[51] is that erosion must not hazard the vehicle during a single encounter and that as a long-term aim erosion should not make structural replacement necessary before the end of the service life of the component. Air-worthiness requirements for supersonic aircraft are also given by Edwards[33].

The size of rain drops encountered by aircraft is given by Blanchard [10,86], from wind tunnel experiments, as 10 mm diameter maximum with the most likely size ranging from a few millimetres down to the small sizes formed when drops disintegrate [81]. Frequency of impact is assessed [24,95] as one

every two seconds with 1 inch per hour rainfall and an aircraft speed of 500 mph.

The second sphere of importance is the damage of turbine blades rotating in wet steam. In large modern turbines the blade tips may reach 600 m/sec and at the low-pressure end the wetness of the steam may be about ten per cent. Recent studies [20,23,57] have shown that most of the water is present in very fine droplets which move with the steam over the surface of the blades causing no damage. Some large drops of up to 1.4 mm diameter condense on the stationary blades and are pulled into the path of the moving blades by the action of the steam. The resulting erosion occurs just behind the leading edges of the moving blades.

To alleviate the damage protective shields [4,5,43,98,116] of cobalt-chromium alloy or high speed tool steel are placed on the last few rows of running blades. Also, increased separation between fixed and moving blades is partially successful as is a reduction of the water content of the steam or insertion of drainage slots in the trailing edges of the blades [116].

The third feature is the damage resulting from cavitation, on many mechanisms functioning in a liquid environment - for example ships propellors, valves, pumps etc.. The process is one of bubble formation and collapse in a liquid as a result of the surrounding pressure changes. It has been shown [7,64,90] that a high speed liquid jet forms by involution of the far side of the cavity - the jet passes through the bubble and strikes the solid surface. In this respect cavitation, a more widely researched topic, has similarity with water drop erosion. An extensive survey of cavitation is given by Knapp et al [92] and also in references 9, 74, 75, 76, 123, 124, 126, and 135. A favourable comparison between water drop erosion and cavitation has been made by a number of people including Canavelis [21] and Hammitt et al [65].

The high stresses generated in liquid impact is used to advantage in cutting rock and coal. This is achieved by a water cannon which fires several jets per second with typical velocities of 1,200 m/sec and stagnation pressures [28]

of 50,000 to 5 million lbf./in^2. The jets thus produced rapidly crush and erode even granite rock and may be used for ocean floor excavation. Data on cutting granite by pulsed water jets in air and underwater is included in a review by Ostrovskii[103].

1.2 SIMULATION TECHNIQUES

Laboratory testing of materials for resistance to liquid drop impact has produced numerous differing approaches. Essentially the multiplicity of these is due to attempts to avoid the break-up of the small single water droplets into a fine mist when accelerated to 17 m/sec in air;[93] overcoming the problem of securing the appropriate relative speed has had to be attempted by other means. Some typical approaches are given below.

1.2.1 Wheel and jet

This is an early method developed by Honegger [79] and later modified by Gardner [56] and de Haller [31] which is still in current use. It consists of a disc or arm which is rotated at high speed with a specimen mounted at the periphery. A jet of liquid ejected parallel to the axis of the wheel impinges on the specimen once per revolution. The speed of impact may reach 700 m/sec and with a number of jets placed equally around the circumference or a number of targets inserted round the disc, many thousands of impacts are made per minute. Impingement speed and the rate of impact is limited by the time of recovery of the liquid jet between impacts.

A rectangular contact area is generated by the impact of the flat target on the cylindrical jet. However, the method has been extended by directing the liquid jet through a nozzle block [36] to produce many small droplets. The damage produced, more closely resembles the random nature of rain-drop erosion. Alternatively, Lapp et al [94] and Fyall et al [49] allow a fine water spray to fall on to specimens mounted on arms with their axis of rotation vertical.

1.2.2 Liquid jets

Bowden and Brunton [11] first used liquid jets to examine erosion. The method consists of ejecting liquid from a steel die by means of a projectile acting as a fast-moving piston. The liquid is initially held in position by a disc which spreads during extrusion to prevent leakage. Turbulent break-up of the jet is minimised by a die entrance angle of 120^{o} and other critical orifice geometry.

A mushroomed-shaped jet is produced at velocities of up to 1,200 m/sec which is suitable for examining erosion. The upper limit of jet velocity is determined by the bursting strength of the die. The jet profile is completely altered if a concave menicus is used; micro-jets form in advance of the main jet as shown in references 13 and 87.

This type of gun and also a modified repetitive lower velocity gun are used in the work and are described in Chapter 2.

1.2.3 Projectile apparatus

A method developed by Jenkins [80] uses a projectile carrying a specimen which is fired at a stationary drop suspended on a thin web fabricated from filaments of polymethylmethacrylate. The size of drop may be up to 2 mm and impact speeds of 1000 m/sec are attainable.

It is not a repetitive method and therefore restricts the number and precise positioning of impacts. Also recovery of the projectile after impact without causing further damage to the specimen is difficult. However, as impact is against a spherical drop at high speeds, it is a useful technique.

1.2.4 Magnetostriction oscillators

Gaines [54] and later Kerr [88] and Rheingans [107] were among the first to use magnetostriction oscillators. It consists of a vibrating nickel rod to which a specimen is attached and immersed in liquid. Cavities form on the rarefraction side of the rod and collapse in compression as the rod returns. Specifications were set in 1956 by a sub-committee of ASME which included a resonant frequency of 6,500 c/sec and an amplitude of vibration of 0.003,42 inches. These

oscillators had the disadvantage of working on audible frequencies and severely limiting the tube life. Improved water cooled equipment is now in use [35,75] with a resonant frequency of 20,000 c/sec.

With similarity between cavitation and erosion this type of equipment is used to advantage to rapidly rate the erosion resistance of materials.

1.3 FACTOR INFLUENCING EROSION

The important parameters of erosion have been considered by many investigators. As the types of damage are markedly dissimilar materials are classified into four groups [77]; glasses, plastics, ceramics and metals; any comparisons are normally confined within these groupings. A nomogram is given by Thirvnengadam [122] which outlines the erosion resistance of a wide range of materials.

Impact velocity is of prime importance [45,48,77,89] as metal damage increases as the second, third or even higher power of velocity, while in ceramics and glasses the dependence may be as large as six to ten [113,133]. Prediction of rain erosion destruction might be expected to vary linearly with velocity and hence impact pressure, or even with velocity squared from energy considerations, but it is apparent, particularly with glasses and ceramics, that above certain critical velocities failure occurs suddenly and any increase in these velocities gives corresponding catastrophic failure.

Considerable work has been undertaken to relate material properties to erosion [6,19,30,66,79,105] and indicates that hardness, notch impact strength and elastic moduli have a definite influence although exceptions do exist. Hobbs[73,76] deduced erosion indices from studies of the induction period and erosion rate for many ferrous and non-ferrous metals and found hardness to be the main factor. He was also able to correlate damage volume with strain energy at the ultimate strength in simple tension.

Although the approach of relating erosion to quasi-static material properties indicates general tendencies its inherent limitation is the applicability of such

properties to the dynamic liquid impact situation. The average material strength properties are circumscribed by the strength of the most vulnerable points of the impact surface, - the present tendency is to move towards specialised erosion tests similar to a fatigue approach.

Impact pressure is reduced according to the cosine of the angle of impact [50] and Hoff et al [77] has shown that only the normal component of the velocity of impacting rain drops is responsible for erosion. The size of rain drops determines the area of damage and thus directly affects mass loss. Elliott et al [36] found that larger droplet size prolongs the induction period but with longer impact duration the growth rate of cracks is increased and thus mass loss is intensified.

Temperature of water, at least for cavitation experiments with copper, [76] show a maximum erosion rate at 50°C. Experiments with wheel and jet apparatus in a reduced pressure environment indicate that air pressure has little effect although with small water droplets the induction period is most greatly reduced at a pressure of 300 mm of mercury because deceleration of liquid droplets in front of the moving specimen does not occur [78].

Impurities in rain drops do not significantly influence erosion - even an aqueous salt solution has no mechanical effect. Carbon tetrachloride gives rise to the same form of damage as water but inflicts twice the rate of mass loss [66] whilst mercury intensifies the rate of erosion by three to twenty times [55] depending on target material.

One of the recent major objectives has been to establish a mathematical model with fluid and material parameters as input data. Heymann [69,70,72] presents an approach for predicting material loss based on empirical data and dimensionless values such as 'normalised erosion resistance' (Ne) and 'rationalised erosion rate' (Re). He relates these quantities by

$$Ne \cdot Re = \left[\frac{Vo}{K}\right]^{\alpha}$$

here the constants K and α are given for droplet and jet impact. Thiruvengadam [123, 125] bases his model on probability of fatigue failure of particles after a given time while Hof [78] relates the rate of erosion (mean depth of penetration) to the kinetic energy impinging on the target, a material parameter and the efficiency of energy transfer. Hammitt [62] working within this framework relates impingement and cavitation data. These models have only had a limited success and it seems to be agreed that there is much further to go [34, 41, 106].

1.4 PRESENT INVESTIGATIONS

In this work a number of facets of erosion investigation have been covered including how and why materials, surface condition, or external stresses influence erosion and also examining stress wave and flow characteristics of the jet to find answers. The topics where deemed necessary are dealt with in separate chapters together with details of relevant literature.

The equipment used included a repetitive low velocity water jet gun, a single shot high velocity liquid gun and a large diameter low velocity single jet gun termed a 'jumbo jet gun' and dealt with in Chapter 2. As a general introduction Chapter 3 covers typical erosion craters in ductile and brittle materials, criteria for the onset of erosion or threshold level, and the correlation of erosion with impact velocity. Surface condition and protective films, prestressing of targets, and the impact on inclined and curved surfaces are discussed respectively in Chapters 4, 5, and 6. Chapter 7 deals with the penetration of thin plates and a semi-infinite medium while impact pressures and their variation with time is treated in Chapter 8.

CHAPTER TWO

CHAPTER TWO

LIQUID JET AND ANCILLARY APPARATUS

2.1 REPETITIVE WATER-JET EQUIPMENT

This equipment was developed by Dr. H. F. Kenyon of A.E.I., Trafford Park and is described in detail in A.E.I. research reports, see ref. 87. A similar apparatus based on this design has been built and described by Hammitt [63, 129].

Essentially it consists of a spring loaded mass, 9, which impinges every two seconds on a diaphram, 4, housed under a conical die, 3, as shown in Fig. 2.1. The die chamber is filled automatically with water through a needle valve, 7, and excess water is sucked off from the die face, 1. With the die nozzle completely filled with water an approximately flat topped mushroom shaped jet is formed at speeds of up to 220 m/sec, as given in Fig. 2.2. The jet speed may be reduced by adjusting the driving spring, 10, compression on the impacting mass. Calibration of water jet velocity with driving spring deflection is given in Fig. 2.3.

Integral with the apparatus is a spark photography unit which enables jet profiles and velocities to be obtained at intervals down to 1μsec.

Specimens are mounted in a holder 16 mm above the die orifice so that they can be re-located in the same position after removal for examination. Between jets a short blast of compressed nitrogen is played on the target to remove any trapped water.

The consistency of jet speed at 16 mm stand-off distance was taken by measuring the speeds of a sample of 100 consecutive jets using the two photocell method described later. The jet of 60 m/sec has a standard deviation of $1\frac{1}{2}$ m/sec whilst the fastest jet of 220 m/sec has a standard deviation of $4\frac{1}{2}$ m/sec.

2.2 HIGH SPEED JET GUN

To increase the scope of investigations beyond those obtainable with the repetitive jet gun, a single shot high velocity gun was constructed. It was designed to fire a smooth topped jet of water with a velocity greater than supersonic aircraft speeds (1,400 mph).

In principle the gun is similar to one described by Bowden and Brunton [11] where a projectile is fired at a die filled with fluid thus extruding a jet from the small orifice at one end of the chamber.

2.2.1 Description of gun

A photograph of the apparatus is given in Fig. 2.4 with the die section shown schematically. It consists essentially of a stainless steel gun barrel, $9\frac{1}{2}$ mm I/Dx 25 mm O/Dx 1 m long, held rigidly to a base plate by two quick release clamps. A silencer located at one end of the barrel butts up to a steel block which is fastened to the base plate and houses the die centrally with the gun barrel axis - a location screw enables die and barrel to be aligned.

The die is formed from a rectangular piece of stainless steel measuring 70 x 40 x 20 mm with a handle attached to facilitate removal after firing. A small chamber of 12 mm diameter in the die block has a 120^{O} conical end and a short nozzle through which the liquid jet is expelled. Surfaces of the die are smooth and the profile of the nozzle is blended with that of the cone. Liquid is held in the die chamber by a disc of reinforced rubber gasket material. Two dies were made with 1.64 and 2.0 mm diameter nozzles - the former corresponds to the nozzle diameter used in the repetitive water gun.

A $9\frac{1}{2}$ mm diameter x 12 mm long lead projectile is fired at the die chamber using an industrial Rapid Hammer Major 0.38 in calibre stud gun which fits on to the gun barrel with a screwed adaptor collar. To prevent accidental firing of the gun it is necessary to apply an axial thrust of 20 lb to the handle. A number 'two' yellow cartridge was normally used and it was found that to obtain consistent firing conditions the lead projectile had to be a

close push fit in the barrel. The velocity of the projectile and thus the velocity of the liquid jet was reduced by positioning the projectile further down the barrel - hence a range of impingement velocities were obtainable.

To determine the jet shape and motion the spark photography unit, developed by Kenyon 87, was adapted to fit this apparatus. It consists of a light source and photocell situated diametrically across the die nozzle. As the jet interrupts the light beam a spark between tungsten electrodes is triggered off giving an 'instantaneous' exposure of the jet profile on a photographic plate. At a convenient and variable time interval a further exposure of the jet profile is taken which enables a distance versus time plot to be made of the water jet.

A more rapid and convenient method was also developed to measure jet velocity utilising two photocells a known distance apart. This is described later but the light sources are shown in position in Fig. 2.4.

2.2.2 Calibration

A shadowgraph of the resulting liquid jet is given in Fig. 2.5 which shows the jet to be smooth topped without microjets or break-up over some distance of travel and thus suitable for erosion experiments. An interesting feature is the shock wave travelling in advance of the water jet. From Fig. 2.7 which shows the distance travelled by the jet versus time, the jet velocity at a distance of 16 mm from the die face was found to be 780 m/sec. This may be reduced to 450 m/sec by altering the gap between the projectile and the cartridge although below this speed the necessary air gap produces unreliable firings.

Some preliminary tests on Perspex were made. At stand-off distances of up to 20 mm targets showed typical damage with a central undamaged area and an annulus of ring cracks. With larger stand-off distances the damage became random and more extensive as the jet started to break up prior to impact.

A micrograph of a section of 6 mm thick Perspex plate which has been impacted by a water jet travelling at 780 m/sec is shown in Fig. 2.6. Three distinct sections are apparent which include surface damage from direct impact, spallation as the incident compression wave is reflected from the rear surface in tension and crazing under the surface caused by shear stress fracture.

A number of fluids were used in the die including, tap water, distilled water, deaerated water, hot water, oil and mercury. They made little difference to the resulting damage on Perspex with the exception of mercury which had much deeper shear damage.

2.3 JUMBO JET APPARATUS

In an attempt to quantify the stresses engendered during liquid impact, it was decided to project a large diameter liquid jet on to a calibrated pressure cell. The scale effect was not considered important as surface tension is very small in comparison to likely impact stresses. The following equipment was developed to give a smooth topped liquid jet of high enough velocity, and a pressure cell of sufficient sensitivity to produce full scale oscilloscope deflection (see Chapter 8).

2.3.1 Description of equipment

A detailed drawing and photograph of the apparatus are given in Figs. 2.8 and 2.9. They show a 100 mm diameter piston with an integral push rod sliding in a stainless steel cylinder. The end of the cylinder is restricted to form a 120° tapered, highly polished die with 50 mm diameter nozzle through which liquid may be ejected. A phosphor bronze split bush guides the push-rod and piston, and the complete assembly is secured to a concrete base by a 175 mm diameter by 2/3 m long steel tube.

The piston is activated by the tup of a spring loaded drop hammer - the force being transmitted through an I - section beam pivoted on a 75 mm diameter steel shaft to give a velocity ratio of driven (piston) to driver of 2.

Slides on either end of the beam secure a constant area of contact for even transmission of load. A quick release splash guard is fitted around the pressure cell before each test and the water caught in a tank surrounding the base of the die.

The drop hammer, comprises a tup of 70 lb mass with a terminal velocity of approximately 10.5 m/sec. For ease of experimentation it was modified to automatically rewind after each drop. The modifications shown in Fig. 2.8 comprise a 3 phase, $\frac{1}{4}$ h.p. motor with 60 to 1 worm and wormwheel reduction box, brake and a knock-off switch positioned at the top of the stroke.

2.3.2 Calibration

A number of high speed films were taken of unimpeded water jets as they emerged from the die orifice. The Hycam camera was triggered by the 'event' with a microswitch, actuated by the falling tup, positioned at a height corresponding to the film delay time. Fig. 2.10 shows a typical jet at instances of travel similar in profile to the smaller jets discussed previously.

Distance of jet travel against time, taken from the high speed films, indicate a constant speed water jet - at least over a distance of 2/3 metre. The velocity is taken as 46 m/sec with an estimated error of 1 or 2 m/sec in the five jets analysed. This velocity is in good agreement with the design calculations where kinetic energy of the descending tup was equated to the work done extruding water and also accelerating a large inertia beam with end masses.

2.4 SPLIT-PLATEN PRESSURE CELL

The pressure cell is used in conjunction with the jumbo jet equipment to measure the transient liquid impact stress distribution as shown in Fig. 2.8. It was designed in collaboration with Dr. J. B. Hawkyard and Dr. G. H. Daneshi and is a modified version of the pressure cell described by them in reference 29.

The main differences are that this pressure cell measures shear as well as direct stresses, is six times more sensitive but restricted to a lower working load.

2.4.1 Design of pressure cell

The cell consists of two blocks of aluminium butting squarely on either side of a 3 mm thick aluminium plate, as shown in Fig. 2.11. A series of strain gauge rosettes - comprising three $1\frac{1}{2}$ mm long 350 Ω gauges with an inclination of 45^{o} between gauges - were attached with RTC epoxy resin on both sides of the plate, directly opposite and $1\frac{1}{2}$ mm from the top working surface. The mating platens have small clearance grooves at the top to eliminate interference with the strain gauges and leads. Water is prevented from penetrating into the clearance slot and destroying the strain gauges by the gap being filled with strain gauge cement on assembly.

The blocks are held firmly together by a metal frame and also screwed to a base plate. An extension of the base plate allows the cell to fit into a slideway for precise positioning above the die orifice.

It is worth noting that a pressure cell with strain gauges cast into a block of polymer was contemplated. However, with the uncertainty of dynamic calibration this was not pursued but might be worth while for low strain, static work.

2.4.2 Calibration and analysis of response

Calibration is conducted quasi-statically and as the elastic modulus of aluminium is not influenced by rate of loading the results are relevant to the dynamic case.

An analysis of the pressure cell may be obtained by assuming the central platen, to which the strain gauges are attached, is in a state of plane or biaxial stress; this is justified as the plate is relatively thin and the elastic modulus of araldite is much smaller than that of aluminium. Thus it may be shown that the direct pressure σ_p, on the pressure cell is given by

$$\sigma_p = B.\ Q_2 + C.\ (Q_1 + Q_3) \qquad (2.1)$$

where B and C are pressure cell constants and Q the strain gauge readings. Subscripts refer to strain gauge directions as given in Fig. 2.11. The surface shear stress, τ, is given by

$$\tau = G(Q_1 - Q_3) \qquad (2.2)$$

where G is the modulus of rigidity.

Also the principal stresses, σu, σv, are given by

$$\sigma_{u,\,v,} = A\,(Q_1 + Q_3) \pm \frac{B}{\sqrt{2}}\sqrt{(Q_1 - Q_2)^2 + (Q_2 - Q_3)^2} \qquad (2.3)$$

where $A = C + (B / 2)$

In the absence of Q_1 and Q_3 strain readings the direct pressure, σ_p, may be adquately represented by

$$\sigma_p = D\ Q_2 \qquad (2.4)$$

The first uniform pressure calibration was achieved by applying a load to the platen face via a block of constrained plasticine [29]. The load may be assumed to be evenly distributed, i.e. negligible surface friction, as the shear strength of plasticine is small in relation to calibration pressures. Strain gauge readings were taken at stress increments of 0.2 Tf/in^2 and are shown in Fig. 2.12. The overall variation in slope between vertical gauges was five per cent and for inclined gauges it was three per cent. Values of the constants in equation (2.1), (2.2), (2.3) and (2.4) may be obtained from the calibration curve as

$A = 7 \times 10^6$ lb f/in^2

$B = 17 \times 10^6$ "

$C = -1.5 \times 10^6$ "

$D = 15.3 \times 10^6$ "

Further calibration to include surface shear stresses was provided by compressing $3\frac{1}{2}$ in diameter x 0.3 in high lead billets on the platen and recording the friction hill. The strains resulting from an axial load of 15 ton f. are shown in Fig. 2.13 and both vertical and inclined gauges indicate a constant frictional stress.

From equation (2.1) the pressure gradient may be shown to be 3,780 lbf/in^2 /in. (The comparable figure from equation (2.4) gives zero error when $Q_2 = Q_1 - Q_3$ and 6% error when $Q_2 = 3\ (Q_1 - Q_3)$. Simple analysis of 'friction' hills with constant shear stress, τ, provides the expression

$$\frac{d\sigma}{dr} = - \frac{2\tau}{h} \qquad (2.5)$$

where h is the current height and $d\sigma_r/dr$ is the radial gradient of axial pressure given above. Thus the surface shear stress is τ = 557 lbf/in^2 which upon substitution into equation (2.2) with

$Q_1 - Q_3 = 175 \times 10^{-6}$ from Fig. 2.13 gives

$$G = 3.2 \times 10^6 \text{ lbf/in}^2$$

This is similar to the accepted modulus of rigidity for aluminium.

Equations (2.1), (2.2), (2.3) and (2.4) may therefore be used, with the given constants, to determine direct, surface shear and principal stresses from the strain readings resulting from any applied load.

As adjacent pairs of strain gauges are connected to opposite sides of a Wheatstone bridge it may be shown[32] that change of bridge voltage, E_{bd}, is given by

$$E_{bd} = \frac{1}{2} \cdot F \cdot Iac \cdot Rg \cdot Q \qquad (2.6)$$

where F is gauge factor (1.995 for gauge 2 and 1.925 for gauges 1 and 3)

Iac is bridge current (determined from recommended power dissipation of gauges as 25 m A)

Rg is strain gauge resistance (350 Ω)

Q is strain gauge reading

Thus from equations (2.4) and (2.6) the direct stress, σ_p, may be written as

$$\sigma_p = 1760\ E_{bd2} \quad lbf/in^2 \qquad (2.7)$$

where E_{bd2} is the oscilloscope deflection in milli volts.

Similarly from equations (2.2) and (2.6) the surface shear stress, τ, may be written as

$$\tau = 381\ (E_{bd1} - E_{bd3})\ lbf/in^2 \qquad (2.8)$$

and again E_{bd1} and E_{bd3} are measured in milli volts.

2.5 MEASUREMENT OF JET VELOCITY USING PHOTOCELLS

To measure quickly and conveniently water jet velocity and also check repeatability a method utilising two photocells was used. The photocells were secured on perspex tubes and mounted in an aluminium holder as shown in Fig. 2.14. They are spaced 10 mm apart and 11 mm from the die face so that their intermediate position corresponds to the target impact height.

The light source consisted of a 12 v, 6 watt bulb with a focusing lens positioned to give minimum thickness to a converging beam of light on the axis of the water jet. Alignment of the photocell with the light source was made to minimise the resistance of the illuminated photocell.

The sequence of operation is that the water jet interrupts the first light beam causing a high resistance at the photocell thus changing the output potential of the photocell circuit, shown in Fig. 2.15, from 5 to 6 volts to 10 to 12 volts. This increase in voltage triggers-off the Decimicrosecond Chronometer and as the water jet interrupts the second light beam the output voltage of the duplicate photocell circuit is similarly increased which stops the timer. From the time interval for the jet to travel a known distance

average speed of travel may be calculated.

As the photocells and light beams are only 10 mm apart, precise measurement of this distance needs to be made. To this end a steel ball of 25 mm diameter was dropped down the water jet axis on to a thin lead block on to the die face: interrupting both light beams as it fell. The time interval thus recorded with the ball falling from a known height gives, using equations of motion, an accurate measurement of light beam spacing.

An estimate of the errors incurred in measuring jet velocity by this method is given in Appendix I and for a jet travelling at 220 m/sec the error is $\pm$ 1.2 per cent.

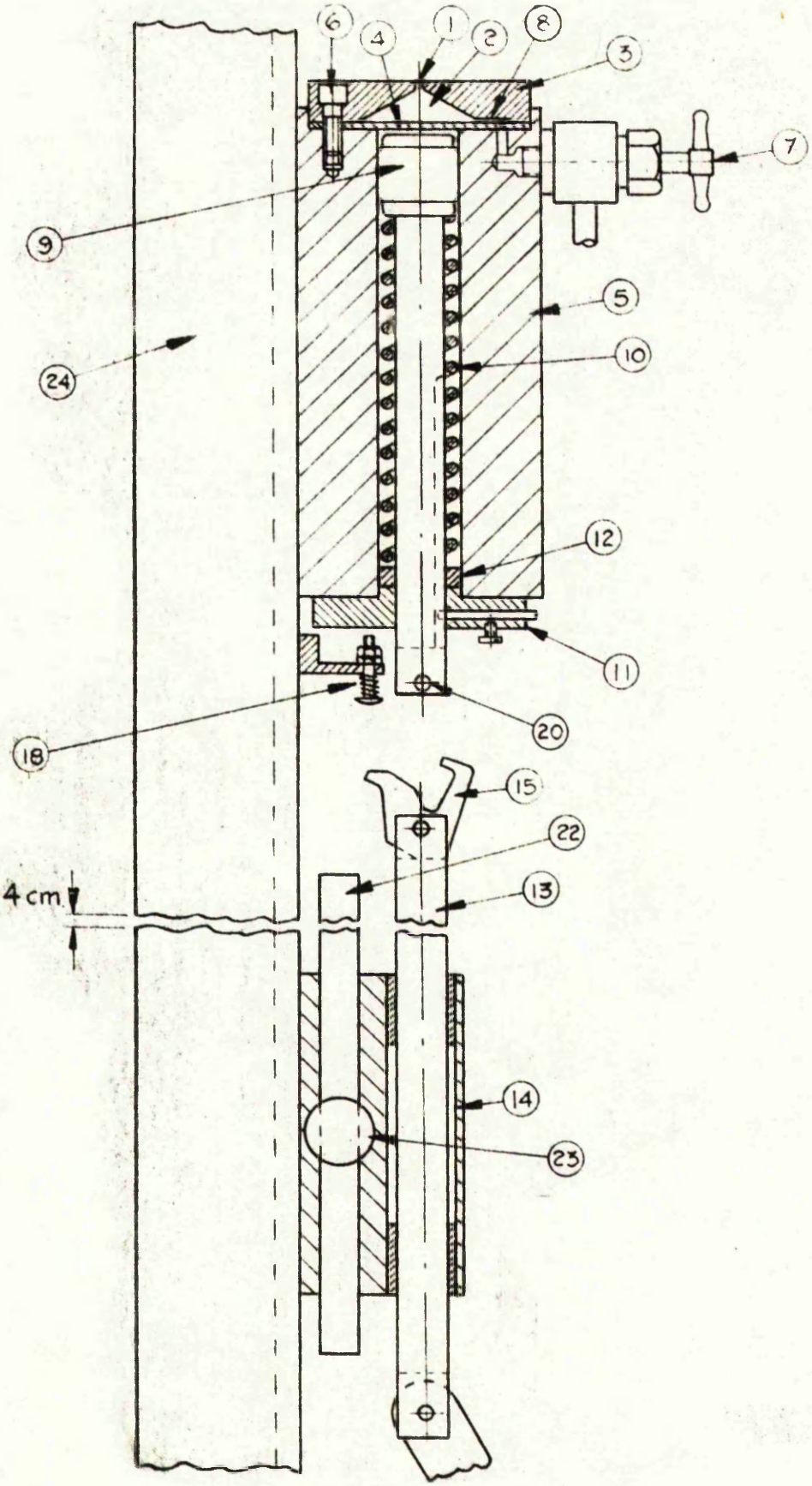

SCALE 1:2

FIG. 2·1 SECTIONAL DIAGRAM OF REPETITIVE JET APPARATUS

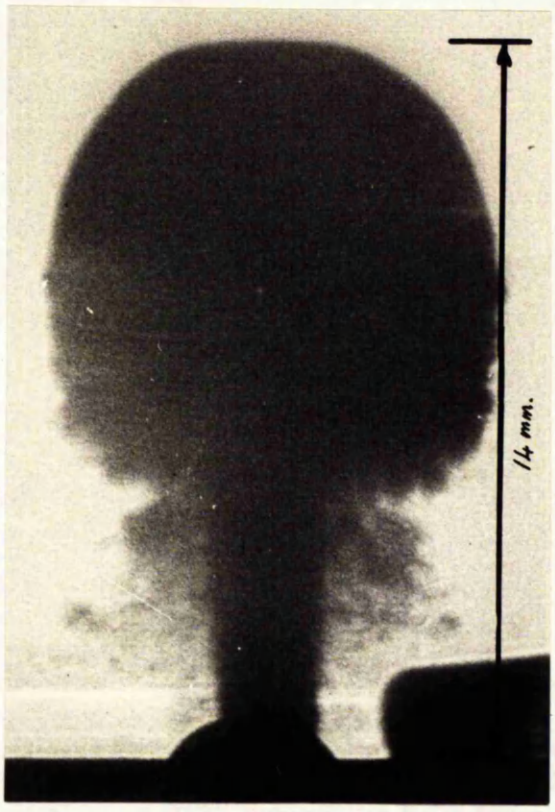

FIG. 2·2 INSTANTANEOUS JET PROFILE

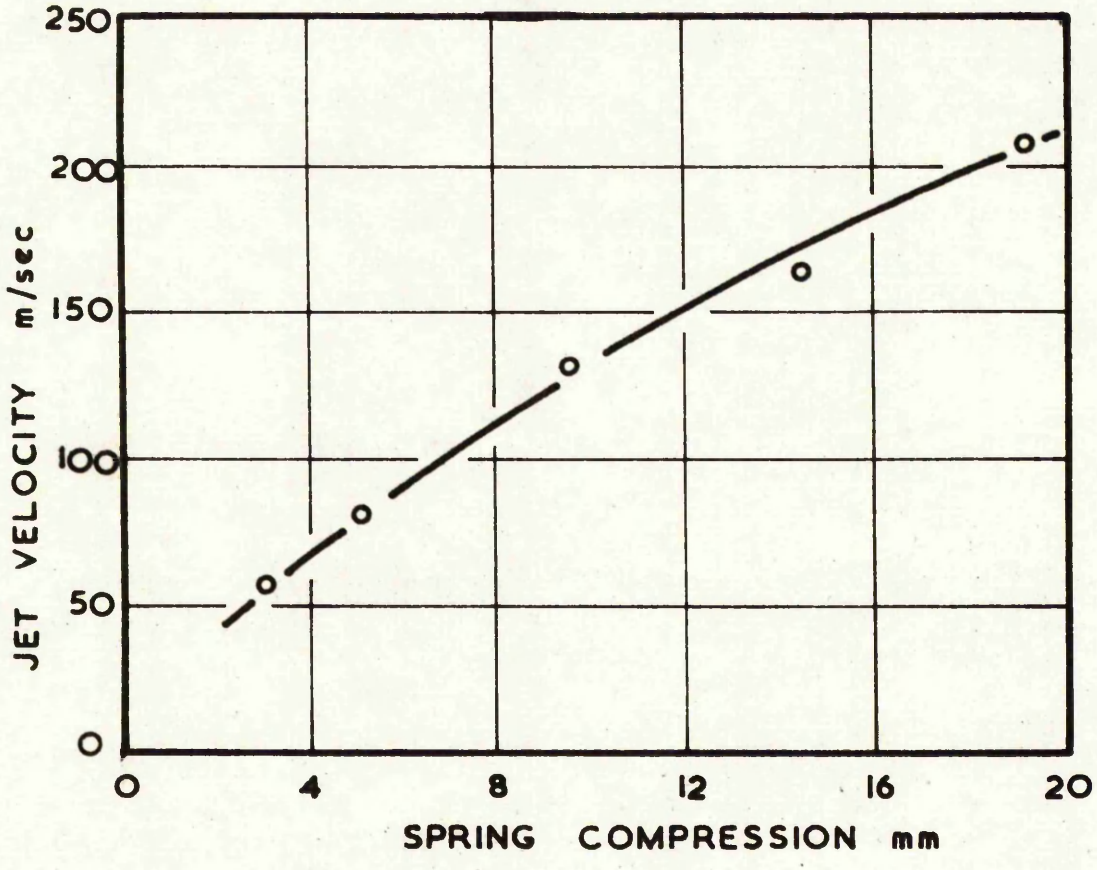

FIG. 2·3 JET VELOCITY VERSUS SPRING COMPRESSION

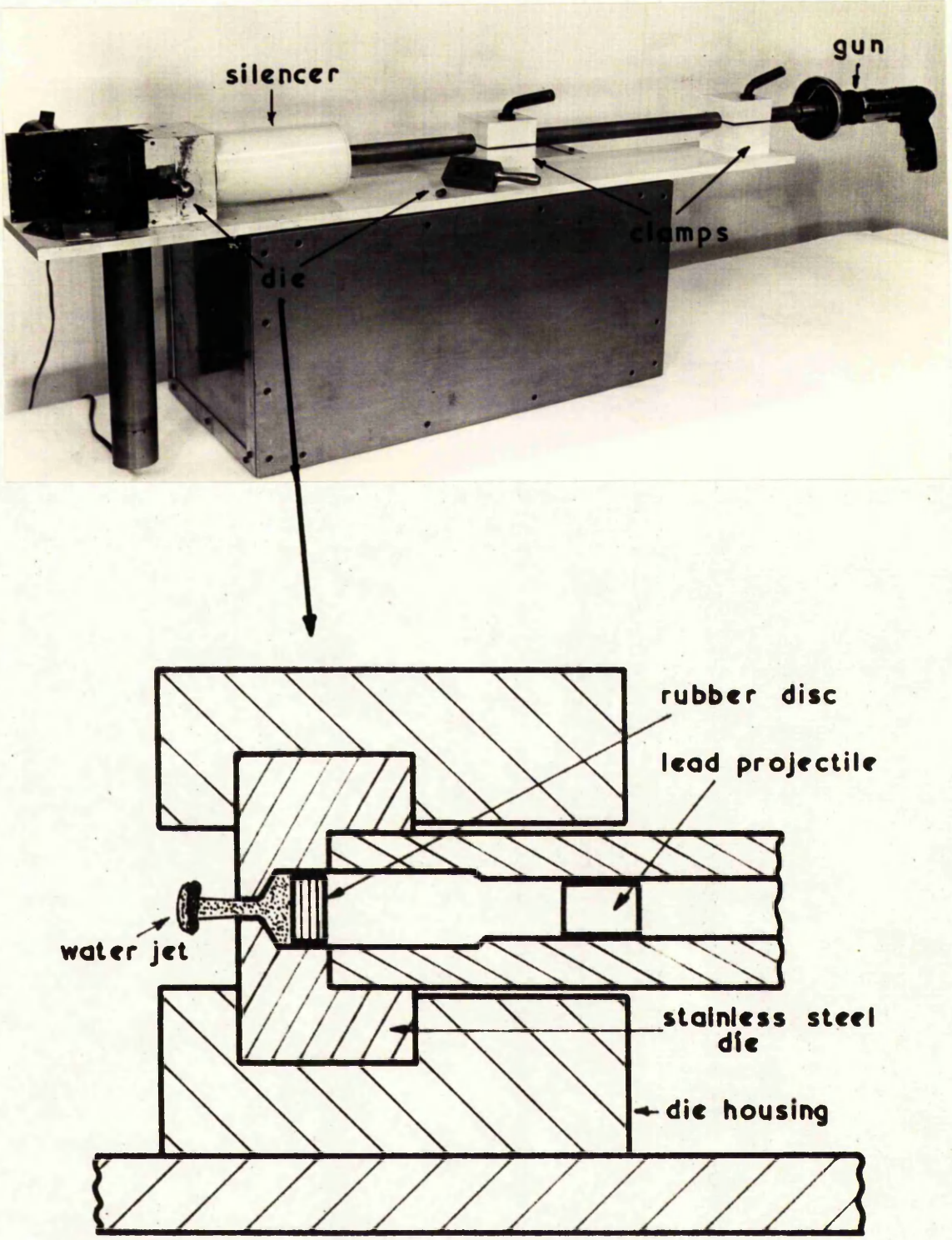

FIG. 2·4 HIGH SPEED WATER JET APPARATUS

FIG. 2.5 SHADOWGRAPH OF 780 m/sec WATER JET

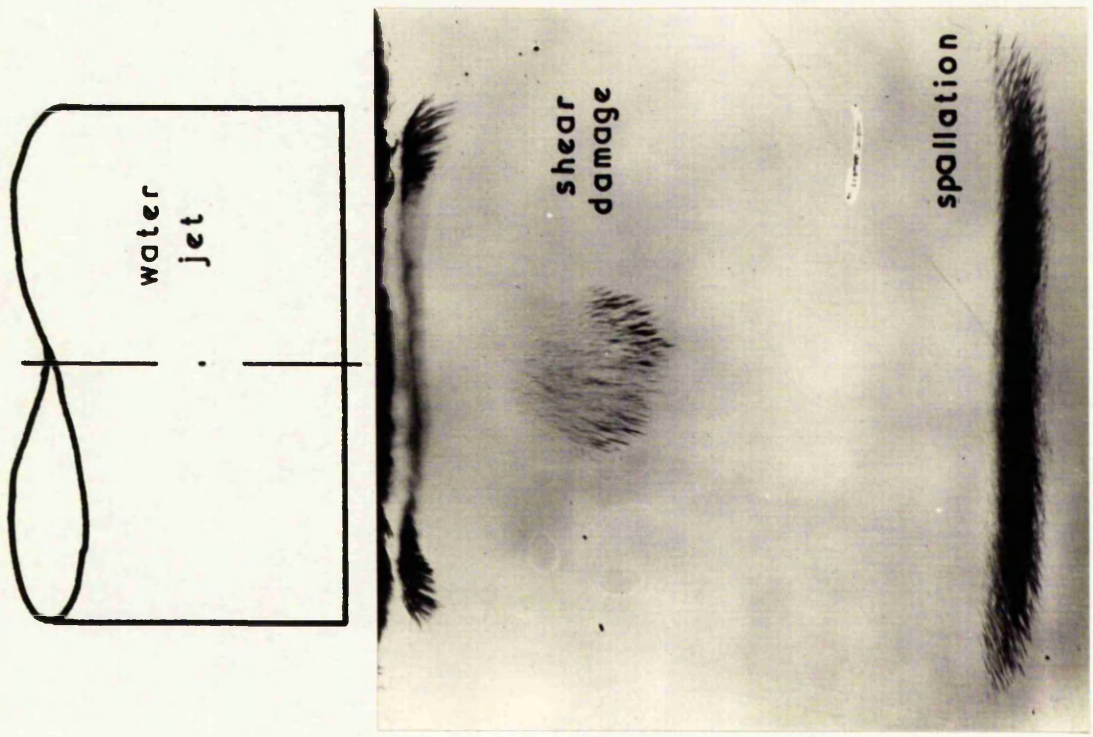

FIG. 2.6 MICROGRAPH OF PERSPEX PLATE

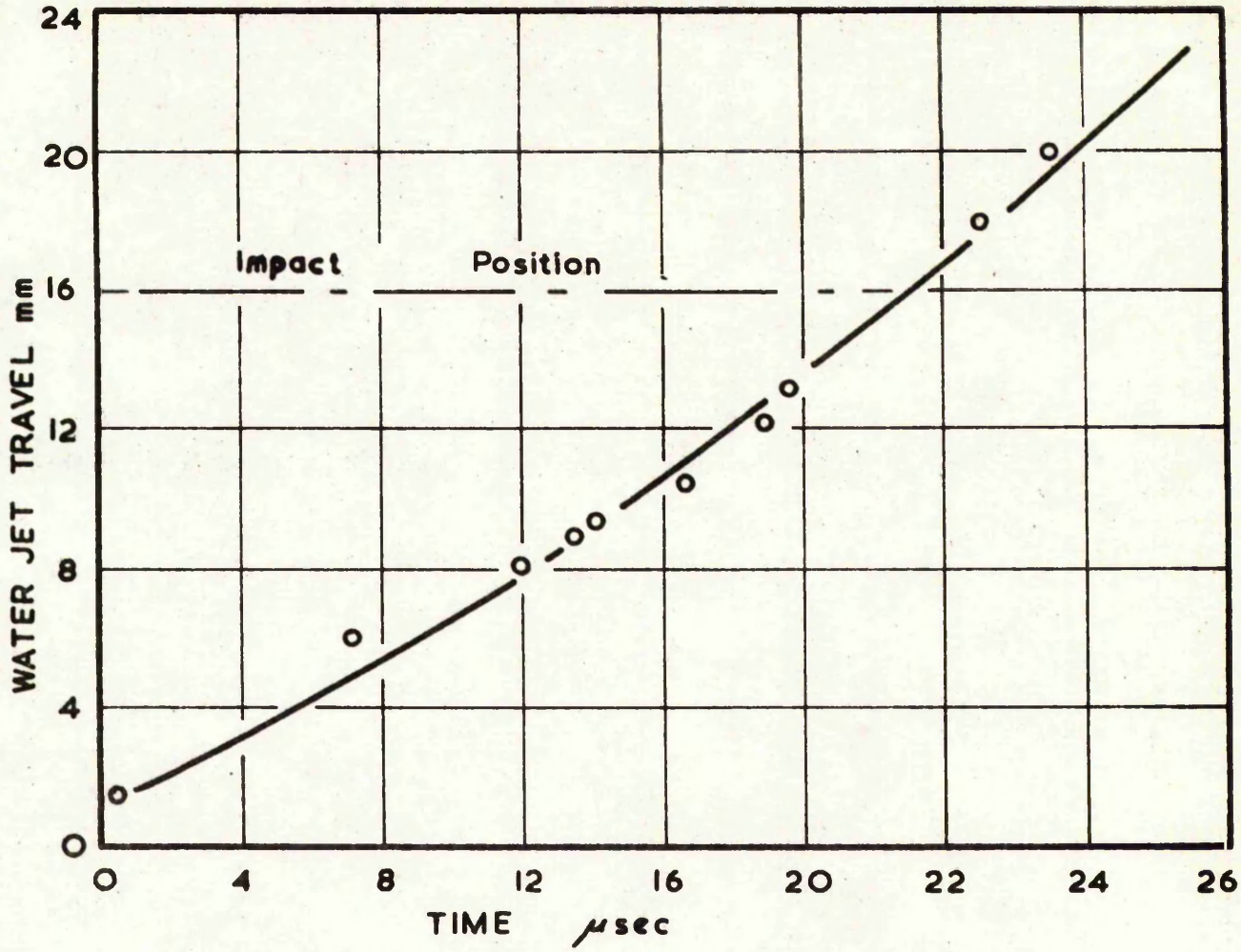

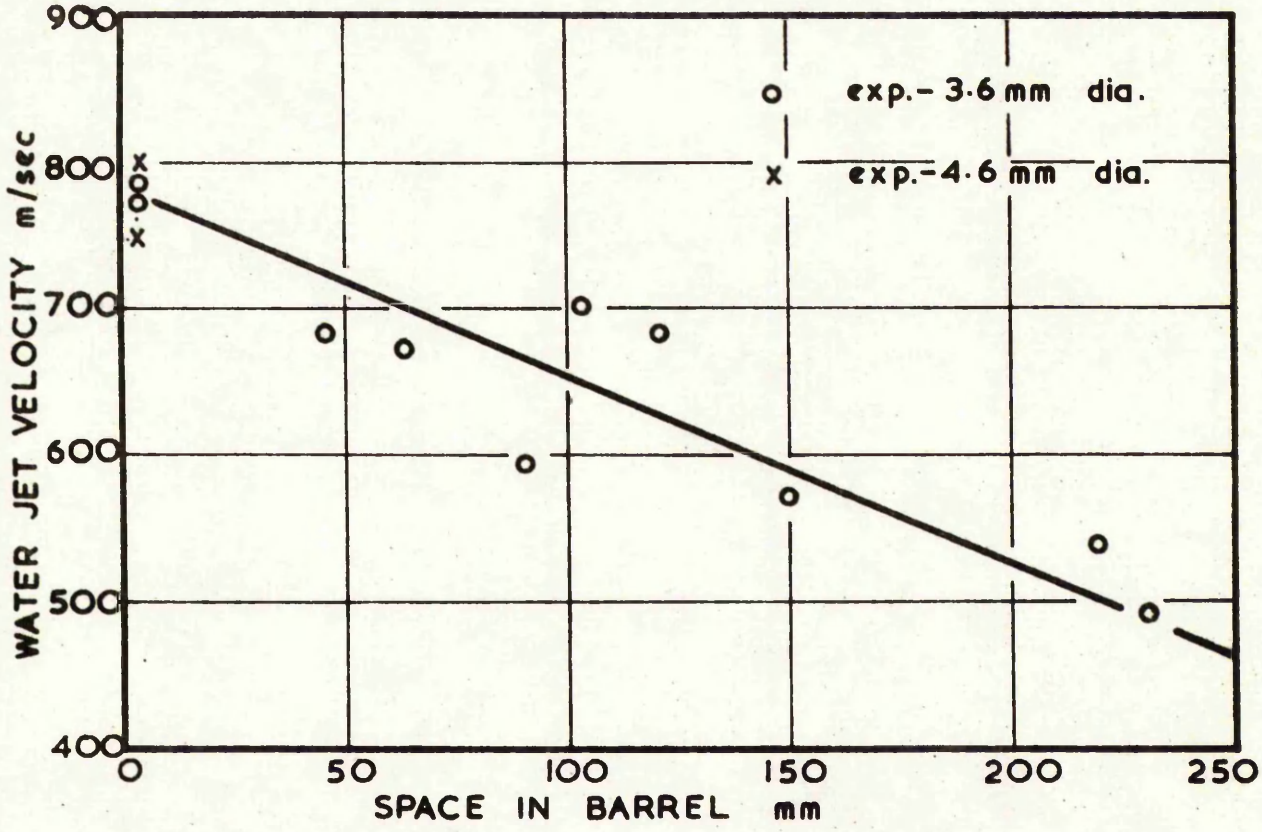

FIG. 2-7 WATER GUN CHARACTERISTICS

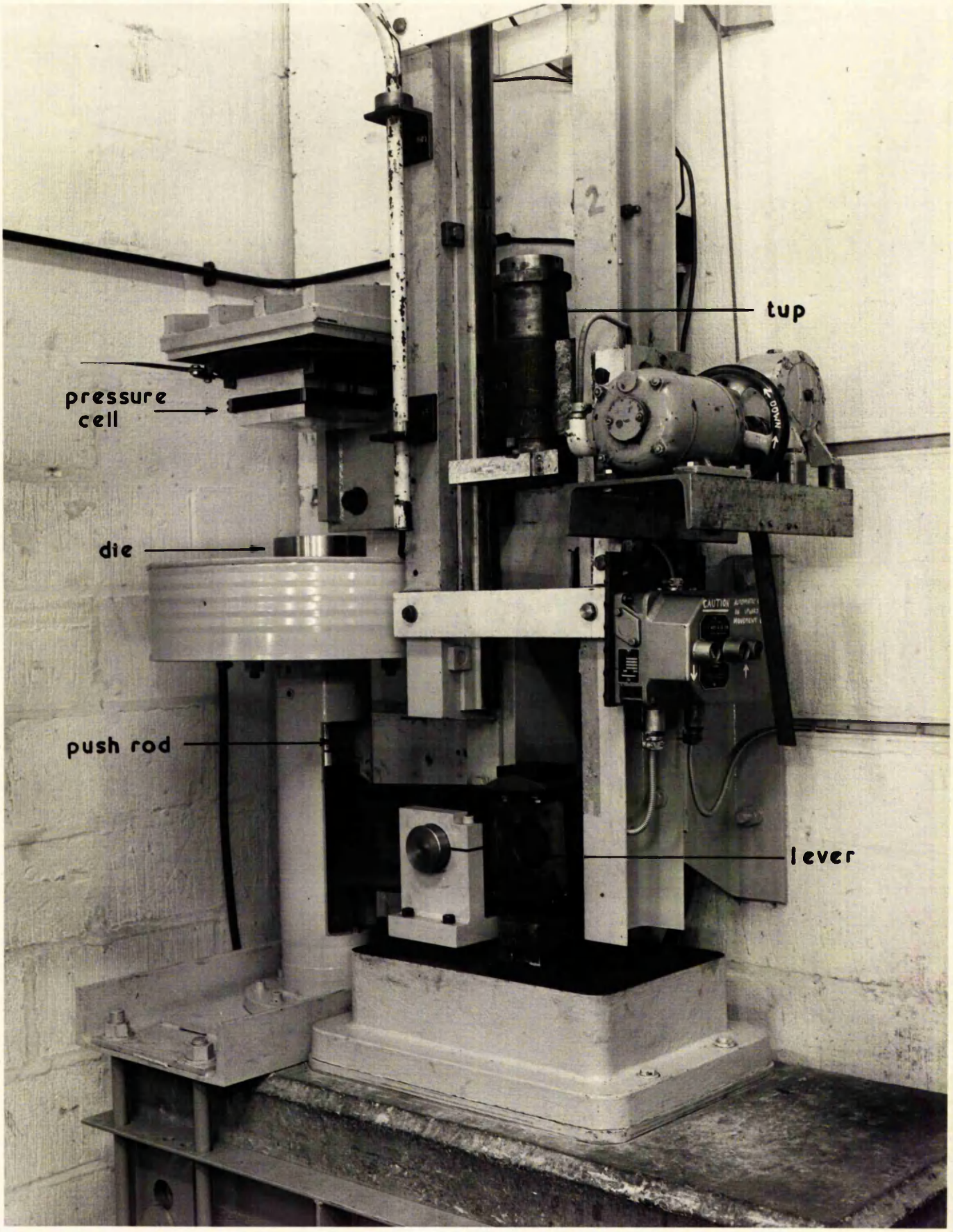

FIG. 2·8 JUMBO JET APPARATUS

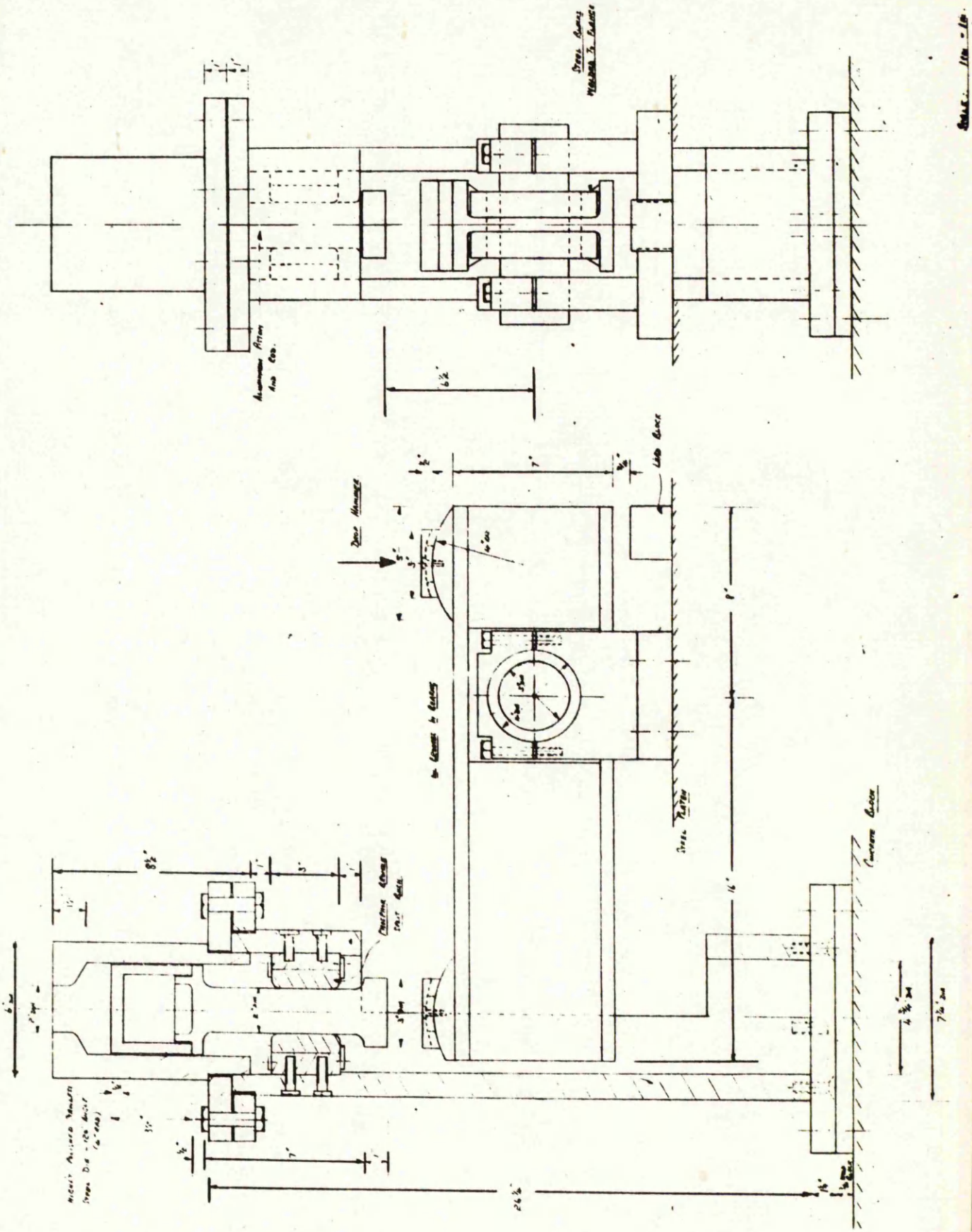

FIG.2·9 SECTIONAL DIAGRAM OF JUMBO JET APPARATUS

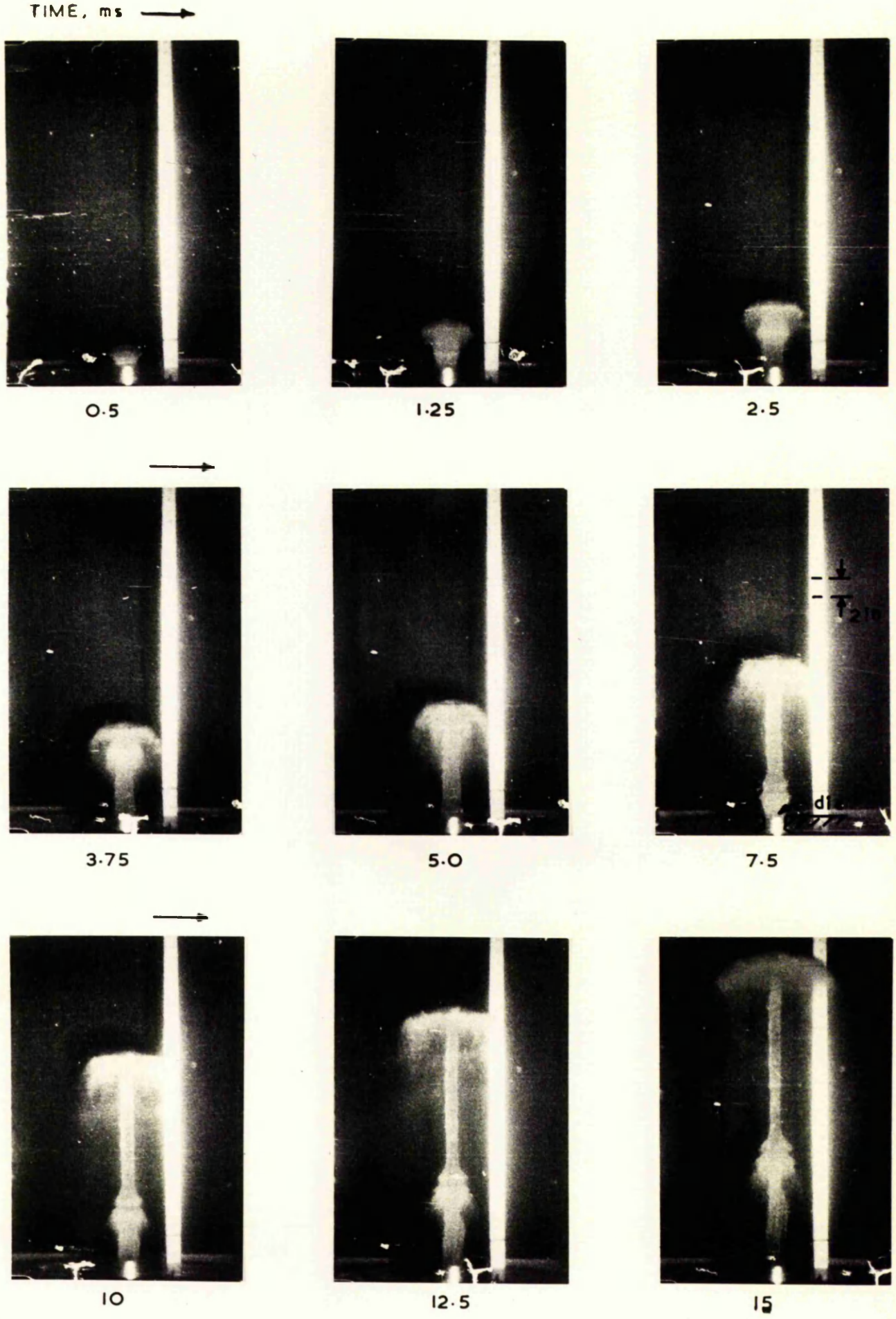

FIG. 2·10 INSTANTANEOUS PROFILE OF UNIMPEDED WATER JET

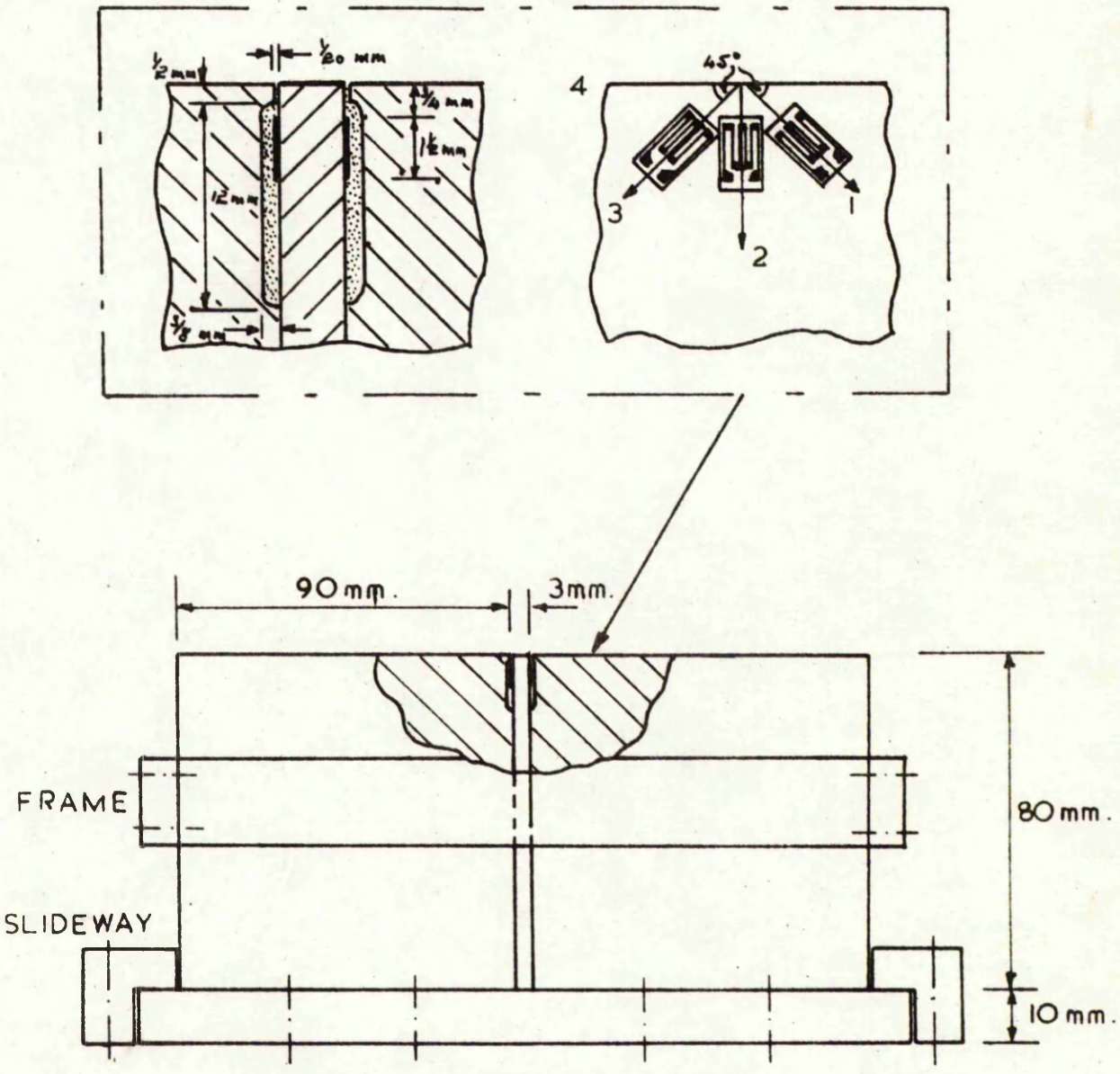

FIG. 2·11 SPLIT – PLATEN PRESSURE CELL

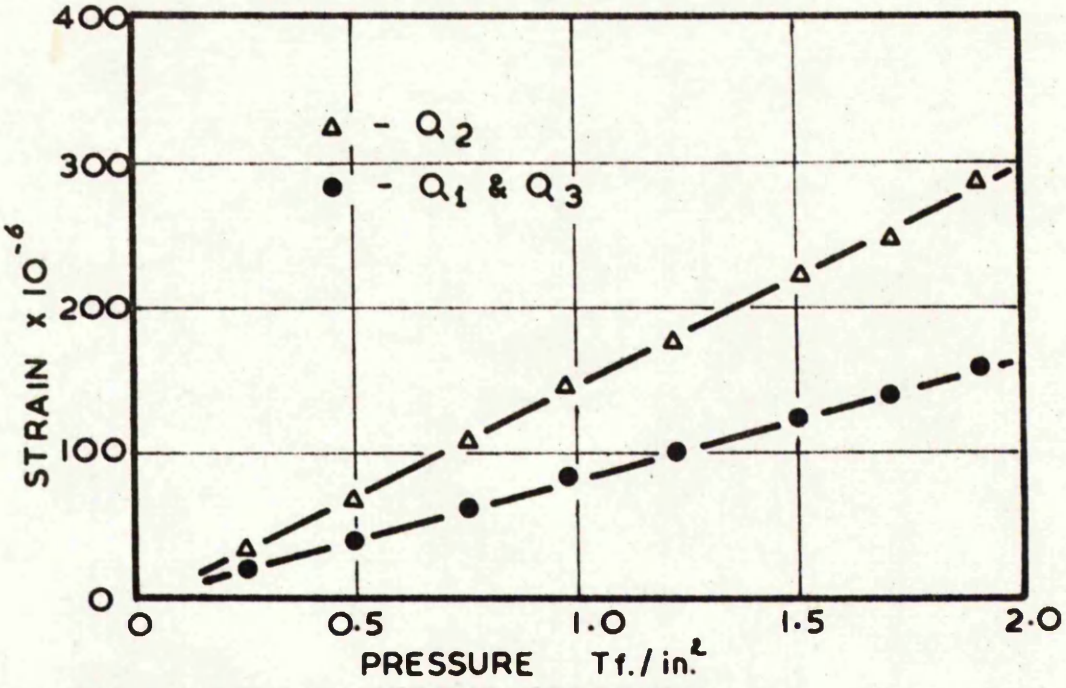

FIG. 2·12 STRAIN VERSUS PRESSURE

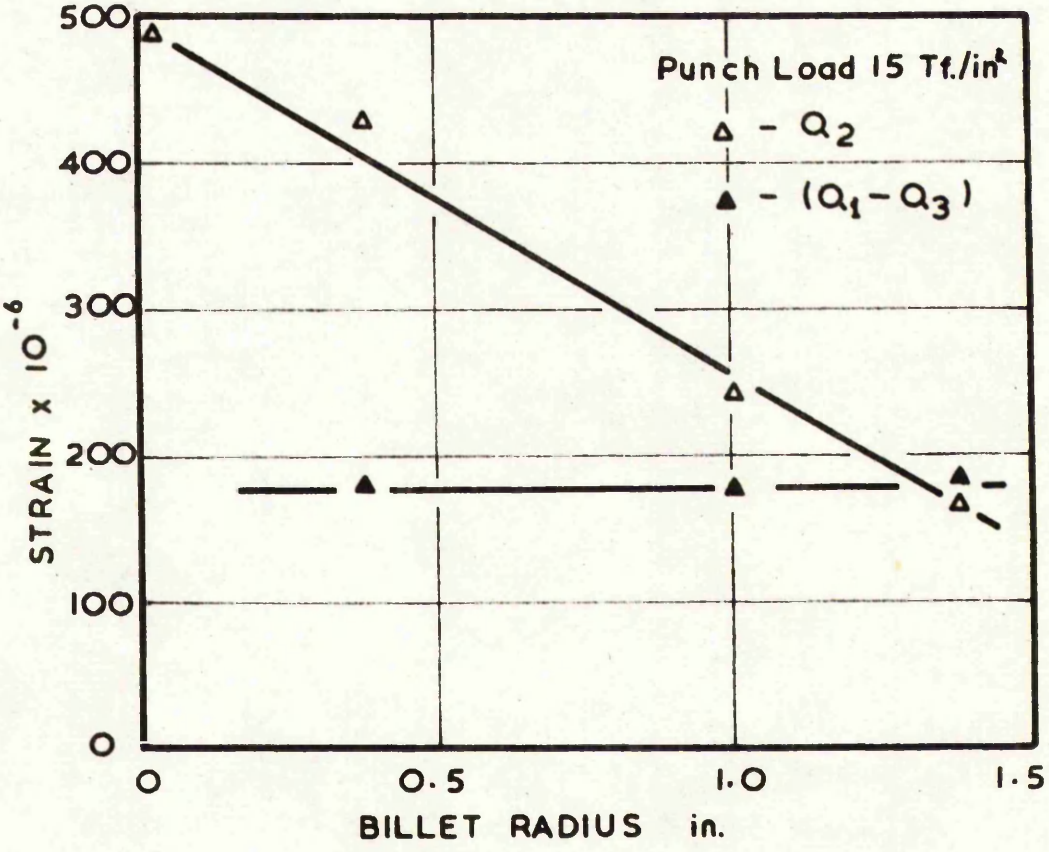

FIG. 2·13 STRAIN VERSUS BILLET RADIUS

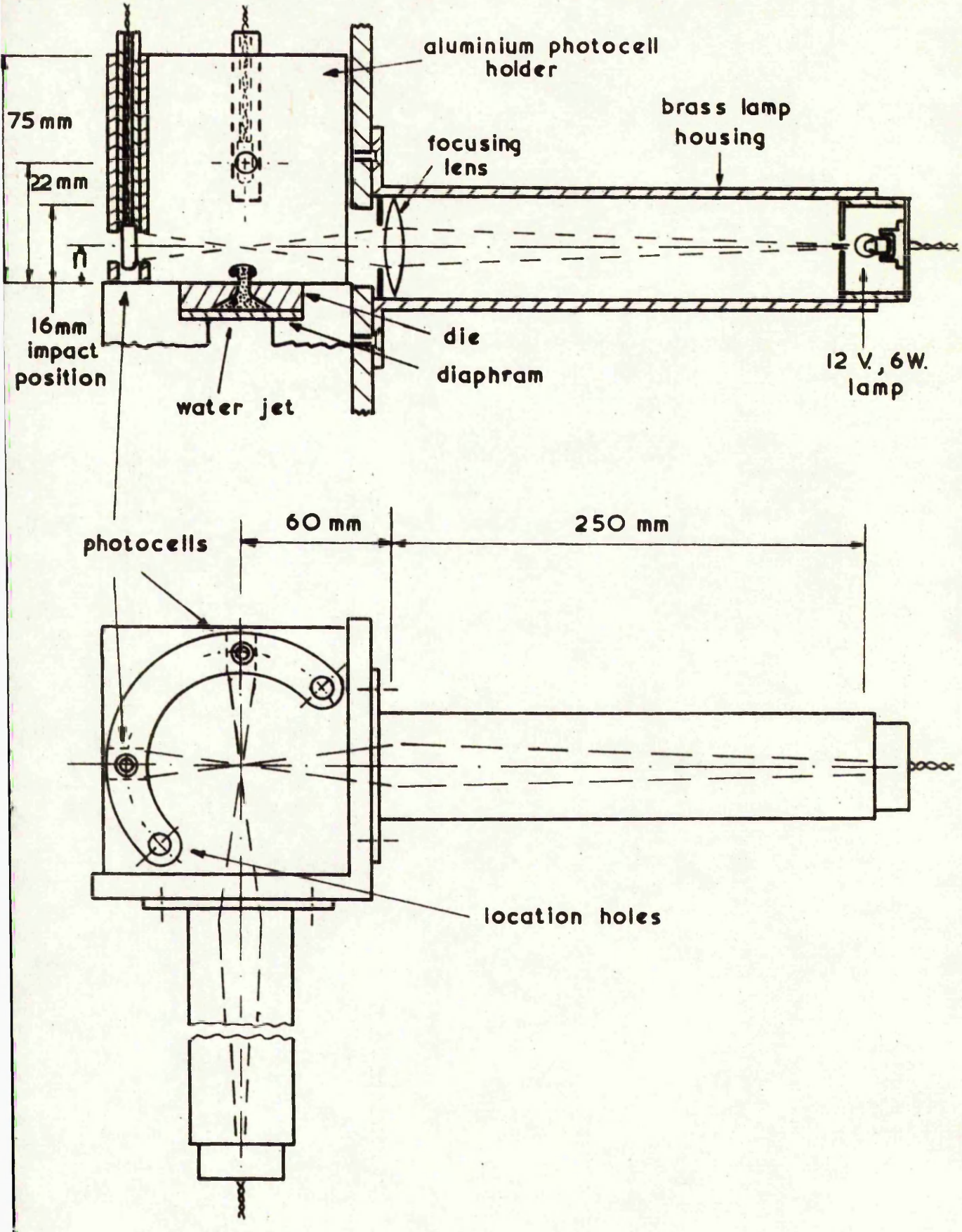

FIG. 2·14 DIAGRAM OF PHOTOCELL VELOCITY MEASURING APPARATUS

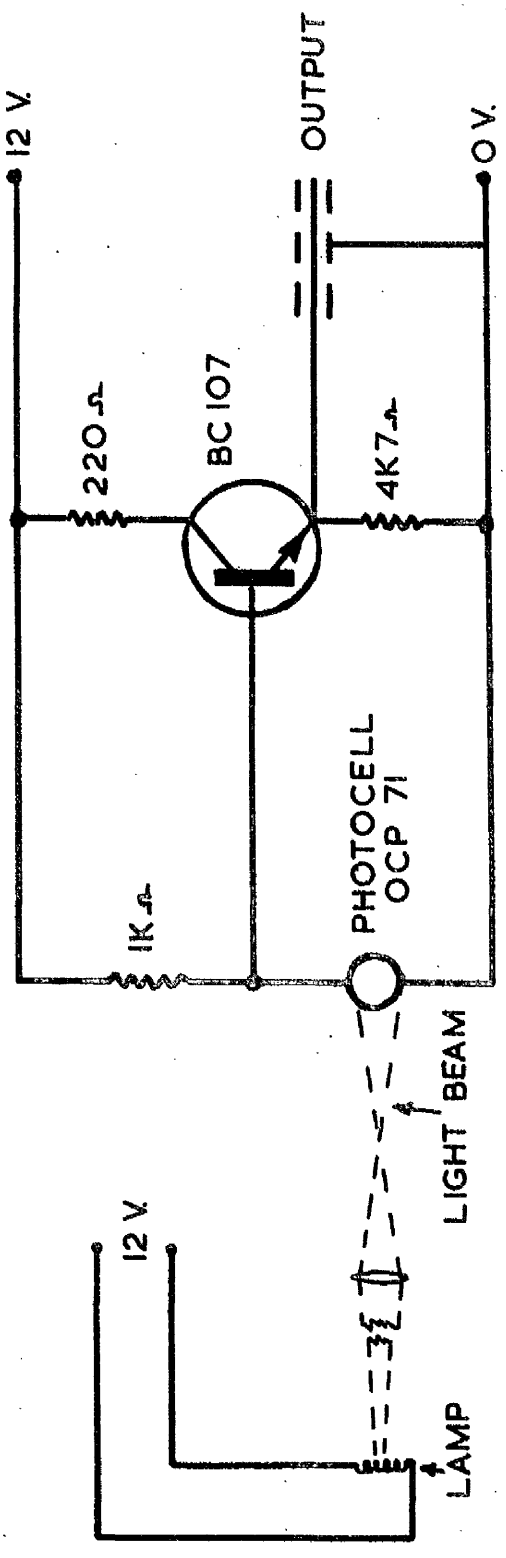

FIG. 2·15 DIAGRAM OF PHOTOCELL CIRCUITRY

CHAPTER THREE

CHAPTER THREE

FORMATION OF EROSION CRATERS

3.1 INTRODUCTION

The formation and development of erosion craters in a ductile and a brittle material resulting from repetitive liquid impact are examined as are the threshold velocities for single and multiple impacts and the relationship of jet velocity to the induction period and the rate of mass loss.

Two target materials, Polymethylmethacrylate or Perspex and α- brass, were selected to give results pertaining to completely different properties.

Perspex erodes readily, is transparent so that propagating cracks can be easily seen, is elastic almost up to the point at which fracture occurs and its uses are fairly wide-ranging.

Fully annealed α-brass, on the other hand, is a very ductile, single phase alloy which is well suited to metallographic examination and is likely to deform plastically under impact pressure. Also, the material is not highly strain rate sensitive at room temperature. From the viewpoint of an experimental material it is extremely useful.

The surface of the specimens were prepared by progressively applying a number of grades of fine emery paper and then polishing on 6 and 1 μm polishing wheels.

Five jet impact speeds were used ranging from 218 m/sec down to 36 m/sec. The water-hammer pressure, estimated using equation (8.3) and using c = 1500 m/sec varied from 308 to 51 M newtons/m^2. These impact stresses are shown in relation to the tensile stress-strain diagram of α-brass and Perspex in Fig. 3.1. The lowest velocity is approximately equivalent to the yield stress of α -brass and the highest impact pressure is greater than its ultimate tensile strength. The two lower impact pressures are below the tensile fracture stress of Perspex, the lowest being approximately half the

fracture stress.

3.2 DEVELOPMENT OF IMPACT CRATERS

Specimens were mounted in a holder 16 mm above the die orifice, so that they could be re-located in the same position after removal for examination. At intervals during the erosion process the specimens were thoroughly cleaned and carefully weighed on a micro-balance. Initially, the depth of the crater was measured from the graph print-out of a Talysurf machine. A number of recordings were taken across the impression and showed good consistency, but after the surface had become roughened and pitted an optical microscope was used.

3.2.1 Fully annealed α-brass

(i) Plastic indentation phase

With the fastest jet at 218 m/sec an impression was made during the first impact. It consisted of a flat circular region, approximately two-thirds the projected diameter of the jet, tapering at the outside up to the original surface of the specimen, as indicated in Fig. 3.2. The depth of this compressed region gradually developed and grew as the number of impacts increased in an almost linear manner up to a maximum of 40 μm at 150 impacts as is evident from Fig. 3.3; thereafter it remained constant throughout the erosion process. The grains in the crater were clearly marked with many slip lines or extrusions, and during its deepening the inner diameter of the depression did not change and the outer diameter altered only marginally. A central conical hole formed which was approximately twice the depth of the depression and this deepened with the number of impacts. However, the conical hole continued after the outer compressed region had reached its maximum depth; in fact, it deepened rapidly to about twenty times the final depth of the compressed region. The central hole developed as the deepest part of the erosion crater as described below.

The proportions of the impression remained remarkably constant

throughout the crater development process; the cycle of events was repeatable. In the later stages of the plastic indentation phase there was a build-up of metal at the rim of the hole to about 20-30 μm in the case of the 218 m/sec jet and 5 μm for the 110 m/sec jet. During this stage there was no measurable material loss but once the compressed region had reached a maximum depth, pits developed and material was lost. The final depth of the compressed area was less than the penetration achieved by pressing a rigid cylindrical indenter of 3 mm diameter into a flat specimen at the equivalent impact stress level. For comparison, a water jet of 218 m/sec produced a central compressed region of 40 μm while the depth of plastic penetration by a rigid indenter at the equivalent static stress was 70 μm and similarly for the 161 m/sec water jet was 6 μm whilst the quasi-static penetration was 22 μm. Part of this disparity may be explained by reference to the low rates of strain in the static test as against the high rate with liquid jet impact.

Jets at the two lower impingement velocities (and to a lesser extent the third) resulted in negligible initial compression and all three generated impact stresses smaller than that required by a rigid indenter in penetrating the flat surface of a semi-infinite medium. (This is given by Tabor [118] as three times the yield stress of the medium).

(ii) Central hole

The establishment of the well defined and repeatable central hole and the reason for its formation is the most perplexing feature of the process. One might be tempted to ascribe this phenomenon to a Munroe microjet travelling in advance of the main jet, as described by Bowden [13]. However, shadowgraphs of the jet profile over the complete length of travel of the jet show quite clearly that it had a smooth, almost flat, top. Electron scanning micrographs, shown in Fig. 3.4, of an impression formed in a lead target after one impact give some insight into the development. Small craters can be seen to exist within

the otherwise smooth dish-like crater which presumably develop to form the conical central hole. The small craters might form through some high pressure pulse within the jet.

(iii) Erosion phase

The second phase of the erosion process in ∝-brass involved the development of surface irregularities, which comprised many slip bands or extrusions, being progressively sheared and torn out of the surface as water from the outer part of the jet flowed radially outwards, see Fig. 3.5. A schematic diagram of the stresses that exist in surface protrusions is given by Engel [38, 39].

It was noticeable that this area of pick-up or shearing occurred only on an annulus corresponding to the tapered outer ring connecting the flat central impression with the original surface. Fig. 3.6 shows a section through the impression after 300 impacts. The central hole and compressed region, although consisting of many slip lines and protuberances, showed no signs of shearing, whereas the outer ring consisted mainly of sheared material.

(iv) Confirmatory tests for 'dead zone'

It appears that the outer ring is the only region where rapid outward movement of the jet occurs. In effect the central impacting liquid of the jet is initially held in position as a 'dead zone' exerting only a compressive stress at impact whilst the outward flow is produced from liquid behind the leading edge of the jet. This hypothesis was substantiated by two simple tests.

In the first, the jet impinged on a lightly silvered surface. Naturally the silvering was not removed by a compressive stress but was readily removed by any shearing action. The results of such a test showed that a central area of silver was untouched and hence subject only to a compressive stress, while an outer ring of silver had been completely removed. With a jet velocity of 218 m/sec the diameter of the circle of untouched silver was 2.05 mm which

corresponded exactly to the inner diameter at this velocity of the ring crack in Perspex and the ring of sheared material in α -brass. The circle diameters for jets at both velocities were approximately two-thirds the estimated jet diameter at impact, although this latter magnitude was not accurately measurable because of the fine mist at the leading edge of the jet.

For the second test a multicoloured low strength projectile was fired at a solid surface, with the aim of freezing the jet action at an intermediate stage. A section through the deformed projectile consisting of concentric coloured rings of plasticine, is given in Fig. 3.7. It also confirms that the central impact area is held in its initial position and the sideways flow of material is supplied from the outer part of the projectile or jet behind the leading edge.

These two tests confirm the hypothesis and may explain why a ring crack forms but does not progressively develop to form a complete circle of concentric ring cracks as would be expected if flow occurred progressively from the outside of the jet as suggested by Bowden and Brunton [11] for jet impact.

A similar phenomenon was reported by Brookes, Tobias and Ali [14] who subjected metal specimens to many impacts between a pair of forging dies and noticed that die wear was confined mainly to an outer annulus where radial material movement took place.

(v) Development of crater

In the development of the erosion crater, the area of sheared surface material increased until a complete ring was visible which appeared as a very bright area under the microscope. Inside this ring a few minute depressions or pits were formed, where the shearing action of the water had removed rather deeper particles of material. Numbers of these pits formed and became elongated radially, gradually joining up to form radial channels. Pitting

marked the onset of measurable mass loss. Gross plastic deformation continued and some of the material was forced outwards and upwards forming a distinct outer lip to the crater. Concerning this stage in our experiments many replicas were taken and examined under an electron microscope, but little meaningful information was gleaned.

The area affected by shearing spread outwards and slightly inwards with number of impacts. Fig. 3.9 shows the variation of outer and inner diameter with number of impacts for all the five jet velocities. It can be seen that the outer diameter of the sheared region remained constant for some time and then increased to a maximum affected area. This increase always coincided with the onset of steady state erosion or mass loss. The maximum area of influence was smaller with slower velocity jets.

The inner diameter of the annulus subjected to shearing decreased slightly with number of impacts and as the central hole widened quite rapidly, the two eventually met and the whole impacted area formed many rugged interconnecting fissures and pits, as shown in Fig. 3.8.

Erosion depth in the central hole and outer ring for the three fastest water jets is plotted in Fig. 3.10. The central hole is deeper than the outer ring but both increased in depth with number of impacts, tending towards a maximum which is a function of velocity. However, the depth of the many pits at the final stages of erosion was variable and could not accurately be determined.

3.2.2 Perspex

With a material which is elastic almost to fracture there was no initial plastic deformation as occurred in α-brass. With the three fastest jets a series of short discrete cracks developed in the surface during the first impact in the form of a ring between 1.8 mm and 3 mm diameter as indicated in Fig. 3.11. Of the other two jets which induce impact stresses below the

fracture stress, no cracks appeared initially but they did develop after 250 and 1,700 impacts respectively. The crack initiation in these two cases, is thought to be due to a fatigue mechanism particularly as the stress level is well below the elastic limit and fracture stress, and as the complete ring was formed at almost the same time. The cracks, once formed, propagated in a brittle manner as the scanning electron micrograph of an opened crack shown in Fig. 3.12.

The ring cracks spread outwards and downwards, undermining the surface. As the water effected its shearing action, a strong influence was exercised on the particles causing cracks to join up with the surface and slivers of material were released. Sometimes these slivers were 2 - 6 mm long. The small inward progression of the ring crack appeared to be associated with a gradual chipping off of the protruding circle of undamaged material.

The progress of the widening of the ring crack with number of impacts is shown in Fig. 3.13. It is interesting to note that, although the development of the outer diameter and its maximum value is affected by the jet velocity the inner diameter, after the first few impacts, is not. This is similar to the behaviour of α-brass.

The depth of impression also increased during the erosion process as demonstrated by Fig. 3.14. The fine penetrating cracks did not lend themselves to precise measurement and as a consequence there was some spread in the results. The depth did tend towards a maximum but there was no sharp cut-off as is observed with some materials.

3.3 THRESHOLD VELOCITY

Recent interest has centred on the existence of an impact velocity, termed the threshold velocity, below which the phenomenon of erosion does not occur. Thiruvengadam [123] gave as the criterion for this the dynamic yield strength for single impacts and the endurance or fatigue strength for multiple impacts.

The present work confirms Thiruvengadam's criterion for brittle materials but not for ductile materials. In Perspex the conditions producing impact stresses in excess of the fracture stress led to a ring crack after the first impact, whilst the two jets developing less than the fracture stress required many impacts to develop what were probably fatigue cracks.

In α-brass, however, the impact stress for four of the five conditions was in excess of the yield strength and one other was just slightly less. The two fastest jets, which generated impact stresses above that required by a rigid indenter to plastically deform the surface, produced compressed regions immediately, whilst the third and fourth did so after approximately 40 and 500 impacts respectively. All these four jets then produced erosion, at a rate depending on velocity. With the fourth jet, after 20,000 impacts, a lightly compressed region of approximately 3μm deep was formed but no measurable mass loss occurred. However, a distinct ring was formed and small pits had started to develop. The slowest jet, which generated an impact stress just below the yield stress, made only a slight impression in the surface after 2,000 impacts but did not develop even after a further 20,000 impacts. Certainly no ring markings and no pits developed so that it may be assumed that the threshold velocity had just been reached. Thus the threshold velocity in α-brass, and possibly other ductile materials, is determined for single impacts by the stress required by a rigid indenter to plastically penetrate the flat surface of a semi-infinite medium (i.e. three times the dynamic yield stress) and for multiple impacts by the dynamic yield stress.

Hancox and Brunton [66] have reported results in which copper is eroded by a jet of speed 24 m/sec, and which causes an impact stress 15% below the average yield strength. Thomas [127] further analysed this problem and shows that it is due to the formation of small depressions at soft spots within the material. He points out that in most methods of loading, the load is taken by the strongest points in the indented area whilst under liquid impact the load is applied over

the whole area and therefore weak points are vulnerable.

Thus it appears that the dynamic yield strength criterion suggested for multiple impacts is circumscribed by the strength of the weakest points of the impact surface, because once a weak spot has caused surface undulation the fierce shearing action across the outer ring of the impact area will soon create pitting. However, using yield strength as a criterion, even with this limitation, would appear to be more appropriate than using the fatigue or endurance limit.

3.4 EFFECT OF JET VELOCITY ON EROSION

If in the erosion process the mass or volume of material lost is recorded against number of impacts (or time if the number of impacts per minute remains constant), then a characteristic curve is obtained shown in Fig. 3.15 for α-brass. Heymann [69] discusses this type of curve in detail. There is an initial period when no mass is lost, during which time plastic deformation takes place (or in the case of Perspex, ring cracks form). As pits start to form in the outer ring some mass is lost and this reaches a steady rate of mass loss as pits develop, elongate and join together. This steady state period may be 'linear', as with α-brass, or may gradually reduce as in the case of Perspex, shown in Fig. 3.16. After heavy surface damage which tends to break up the impinging jet and, according to Plesset and Devine [104] and Hammitt [62] trap a protective layer in the depression, the rate of mass loss tends to level off.

Two important features are

(i) the incubation or induction period; this is given by the intercept on to the abscissa of the steady state portion of the mass loss curve, i.e. AB produced to N_1 in Fig. 3.15; this defines the number of impacts required for erosion to be initiated under a given set of conditions;

(ii) the erosion rate, or the volume loss per impact, is related to the slope of the steady state portion on the graph of Fig. 3.15

and gives a measure of rate of volume loss once erosion has started.

Erosion is usually subsumed under one indefinite index when dealing with velocity. For instance, Hoff [77] et al, when subjecting metals and polymers to impact by jets at velocities from 150 to 380 m/sec, specified an 'overall increase in destruction' proceeding according to the 5th to 7th power of velocity. Hancox and Brunton [66] show that surface damage, expressed as a reflectivity index, was proportional to the 2.7th power of velocity in Perspex.

The magnitude of the induction period, N_1, and the erosion rate, have been taken from Figs. 3.15 and 3.16 for α-brass and Perspex respectively and plotted against velocity, but in spite of the few results available particularly for α-brass, they do disclose, to some degree, a quantifiable relationship. Fig. 3.17 shows jet velocity plotted against the induction number of impacts N_1 for Perspex and α-brass. Both curves suggest a hyperbolic relationship and when plotted in logarithmic co-ordinates, it is found that

(i) for Perspex, $N_1 = \frac{k}{V^{5.7}}$ and

(ii) for α-brass, $N_1 = \frac{k'}{V^{3.2}}$

k and k' are undetermined constants.

Evidently onset of erosion in Perspex is more sensitive to impact velocity than α-brass by two to three orders of magnitude.

Relating erosion rate and velocity as above it was found that

(i) for Perspex, the erosion rate, $\frac{dM}{dN} = h . V^{4.5}$

and

(ii) for α-brass, " " " $\frac{dM}{dN} = h' . V^{3.5}$

h and h' are undetermined constants, M denotes volume and N number of impacts.

It appears that once erosion has started the rate of mass loss is influenced by impact velocity more in Perspex than in α-brass, but not to as great a degree as is the induction period.

3.5 CONCLUSIONS

Craters formed in a ductile and a brittle material due to water jet impact have been shown to have different modes of development, as described.

Considering the ductile material, the craters in α-brass initially consist of flat circular depressions whose diameter is two-thirds of the impinging jet. There is no measurable mass loss as the impression deepens to a maximum with number of impacts. This maximum value is about the same as that penetration achieved by the specimen by a rigid indenter quasi-statically loaded to the equivalent impact stress. A central conical hole forms in the crater to a depth approximately twice that of the surrounding compressed region and as the number of impacts increases, this depth ratio is maintained. Plastic compression eventually ceases, whereupon an annulus forms which is subject to shearing as water flows rapidly across the surface. A series of pits form which deepen and extend radially to cause gross plastic deformation.

The behaviour of the brittle material is quite different; no initial indentation is evident in the Perspex and a band of short discrete cracks form, affecting an area similar to that subjected to shearing in α-brass.

Some characteristics of the water jet have been discussed in relation to the crater development, and in particular it is proposed that the central region of the impacting liquid is initially held relatively stationary exerting mainly compressive stress on the surface, while outward flow occurs from the region behind the leading edge. Some corroborative evidence has been given to substantiate this view.

The existence of a threshold velocity, below which the phenomenon of erosion does not occur, has been confirmed for these two materials. Criteria for predicting such values are,

(i) for Perspex

(a) for single impacts, the dynamic yield strength,

(b) for multiple impacts, the fatigue or endurance strength,

(ii) for α-brass

(a) for single impacts, three times the dynamic yield strength (or the stress required by rigid indenter to plastically penetrate a flat surface),

(b) for multiple impacts, the dynamic yield strength.

The impinging jet velocity has been shown to affect the induction period, or the number of impacts to initiate erosion; it varies with the reciprocal of jet velocity raised to the 5.7th power for Perspex and to the 3.2th power for α-brass. Once erosion has commenced, the rate of mass loss is also affected by jet velocity. For Perspex, mass loss varies with jet velocity raised to the 4.5th power, while for α-brass it varies with jet velocity raised to the 3.5th power.

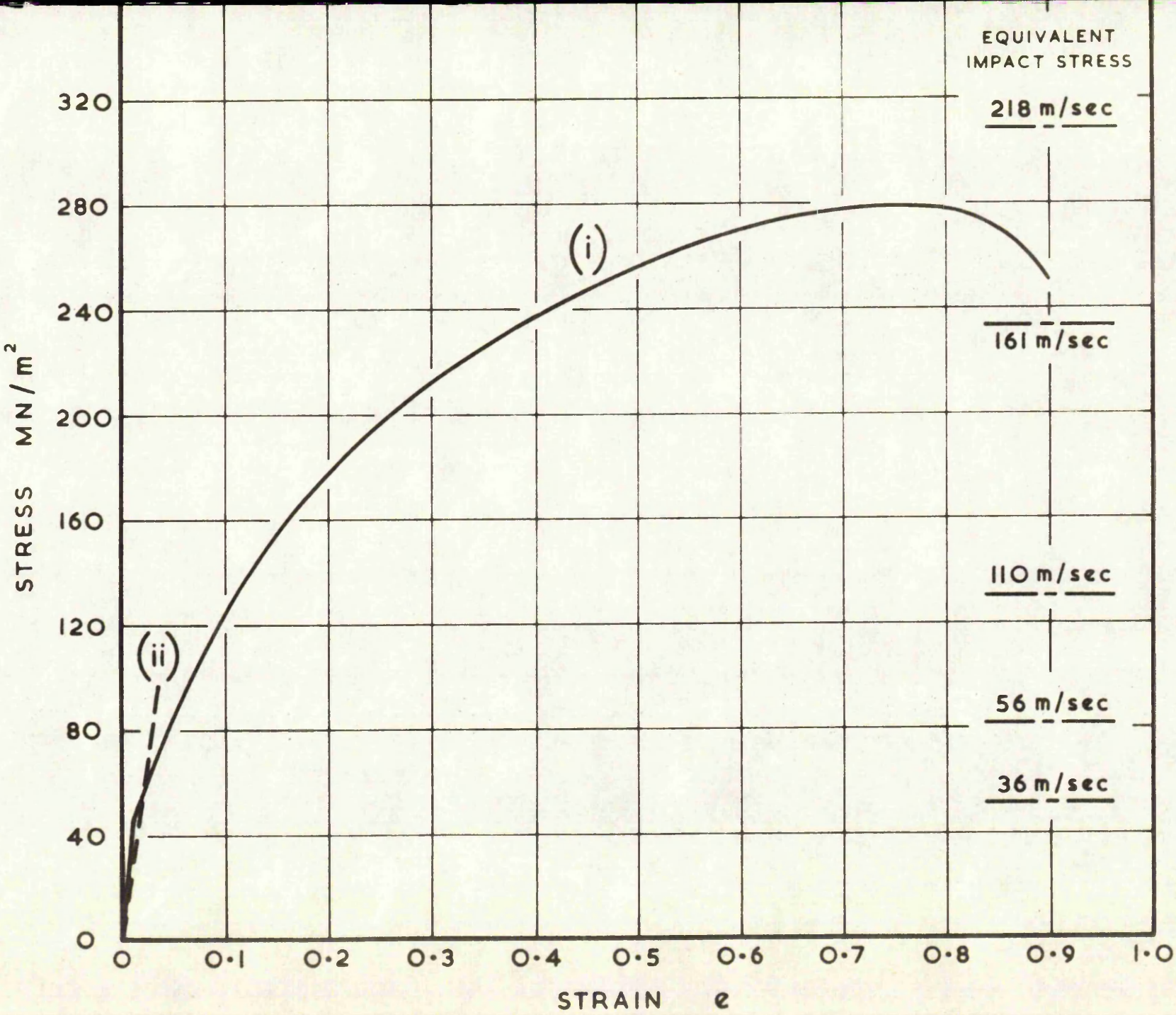

FIG. 3·1 STRESS VERSUS STRAIN FOR (i) α-BRASS
(ii) PERSPEX

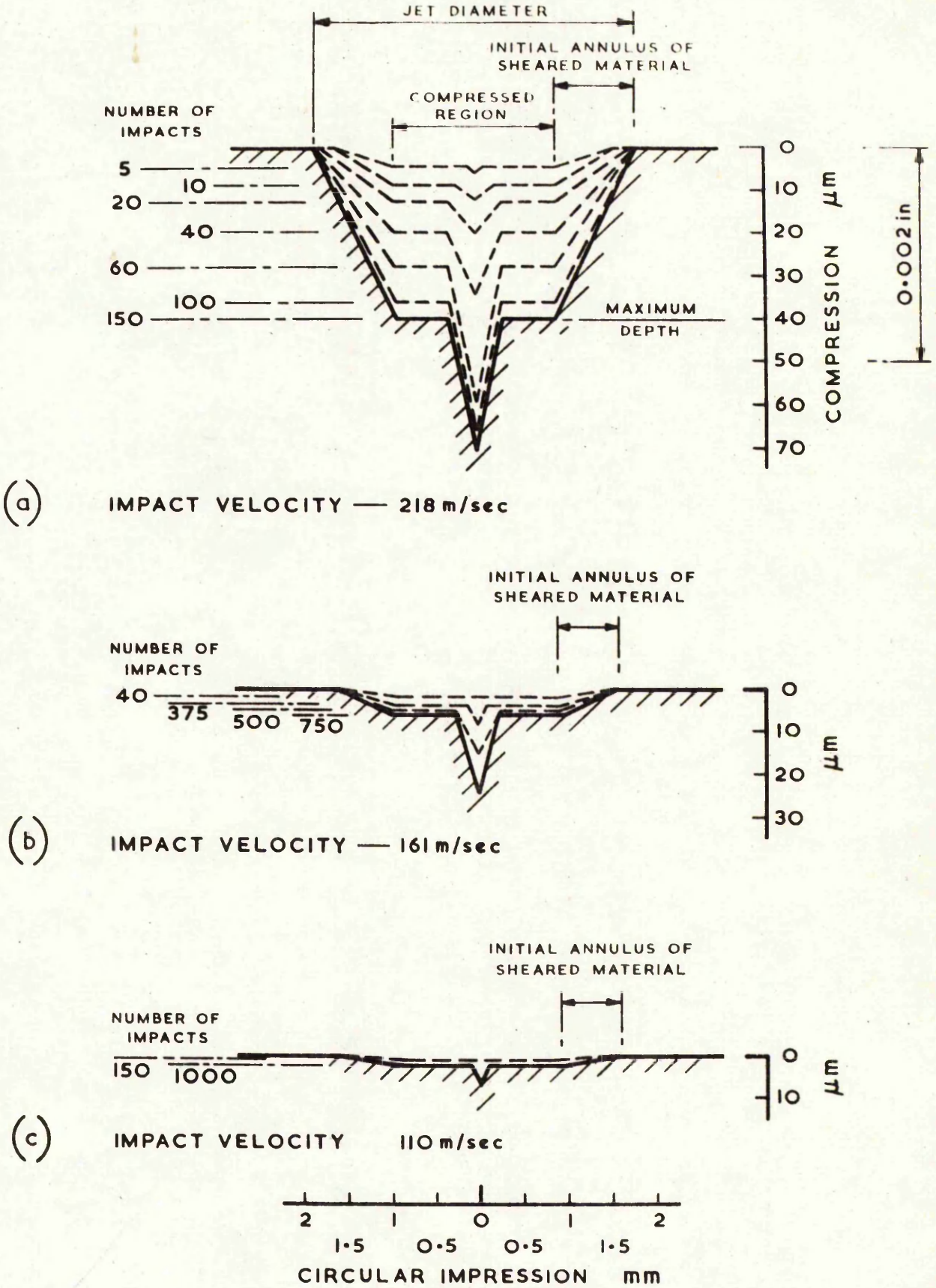

FIG. 3·2 DEVELOPMENT OF IMPRESSION IN ∝ - BRASS

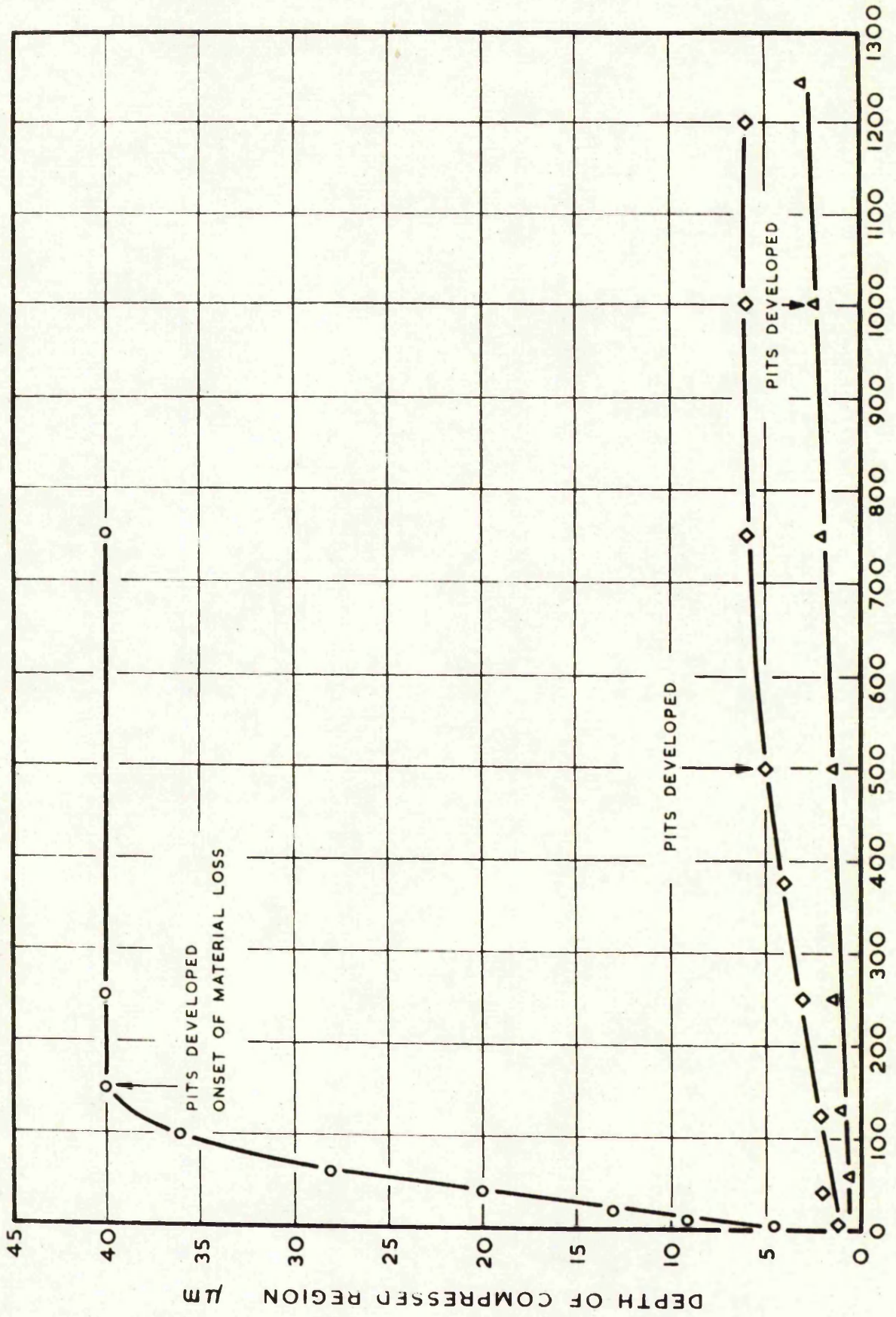

FIG.3·3 DEPTH OF IMPRESSION VERSUS NUMBER OF IMPACTS IN α - BRASS (SYMBOLS AS FIG. 3·9)

(i) IMPACT IMPRESSION

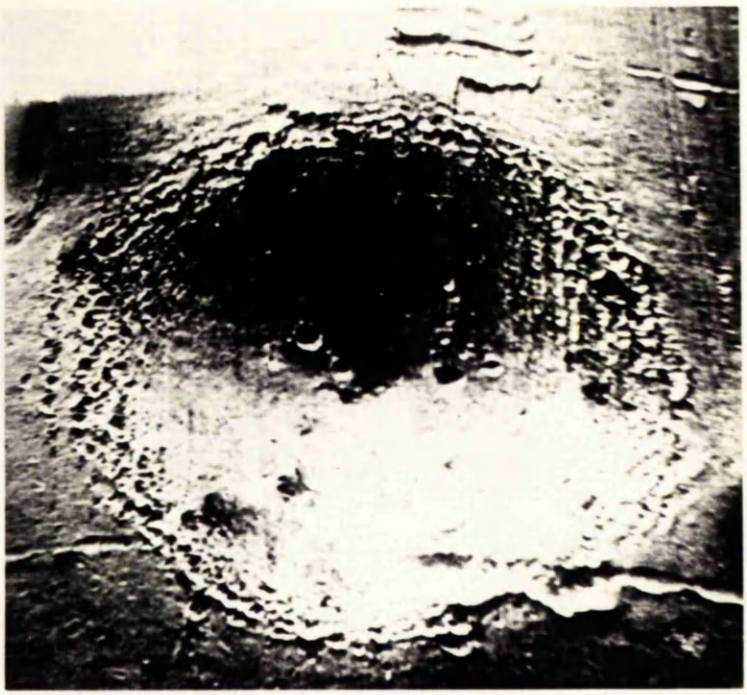

x 20

(ii) CENTRAL REGION

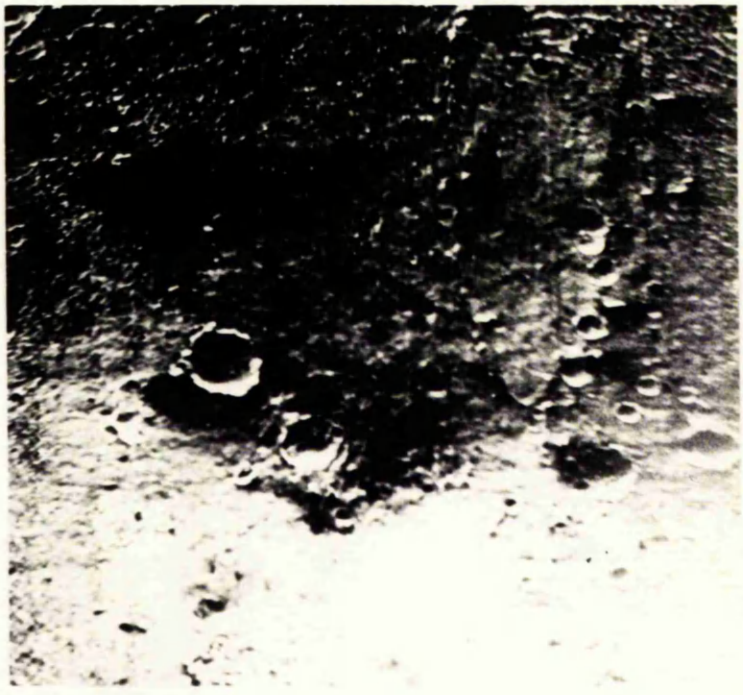

x 60

FIG. 3·4 ELECTRON SCANNING MICROGRAPH OF LEAD TARGET (I IMPACT)

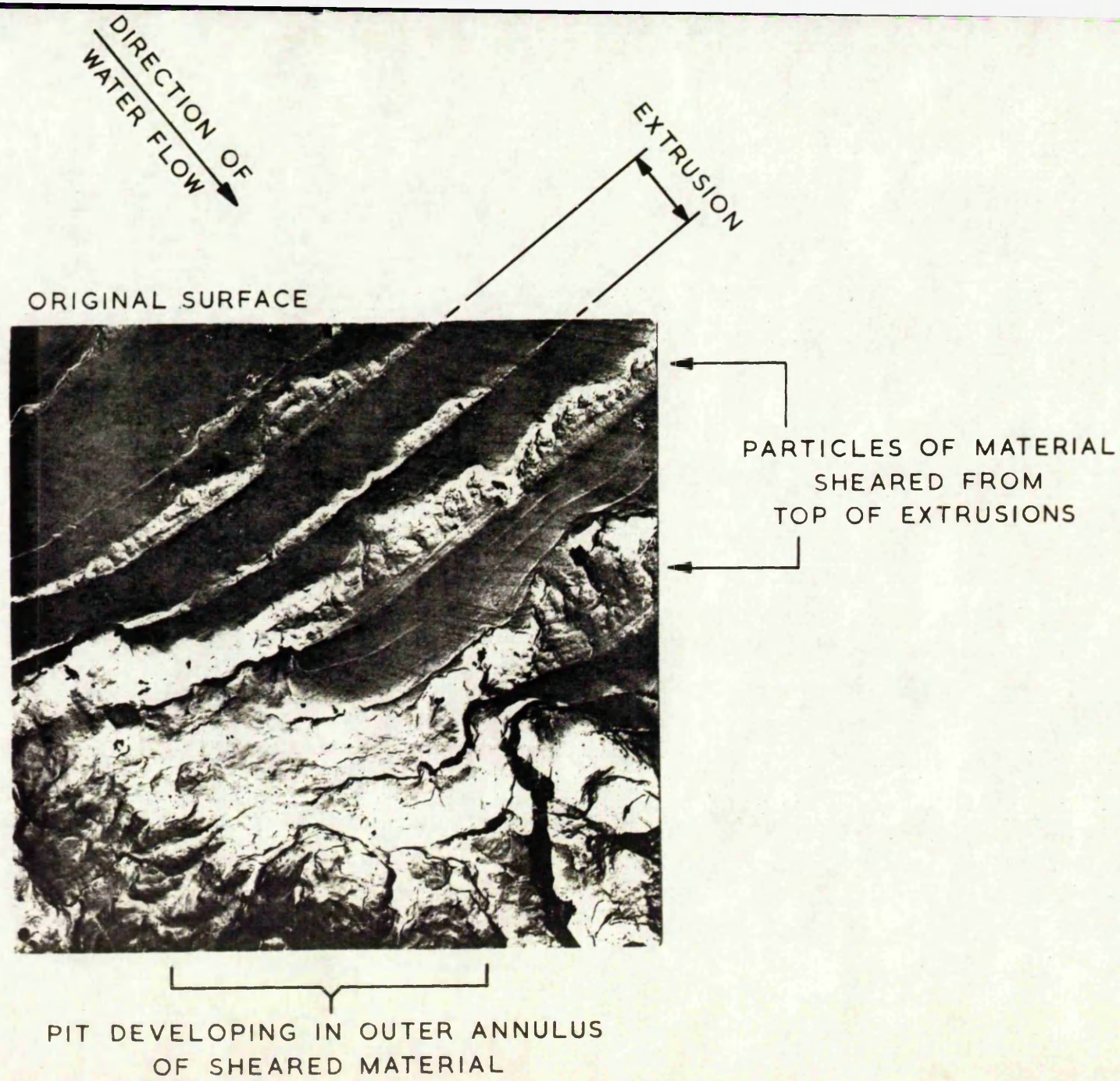

FIG.3·5 MICROGRAPH OF ∝ - BRASS SURFACE

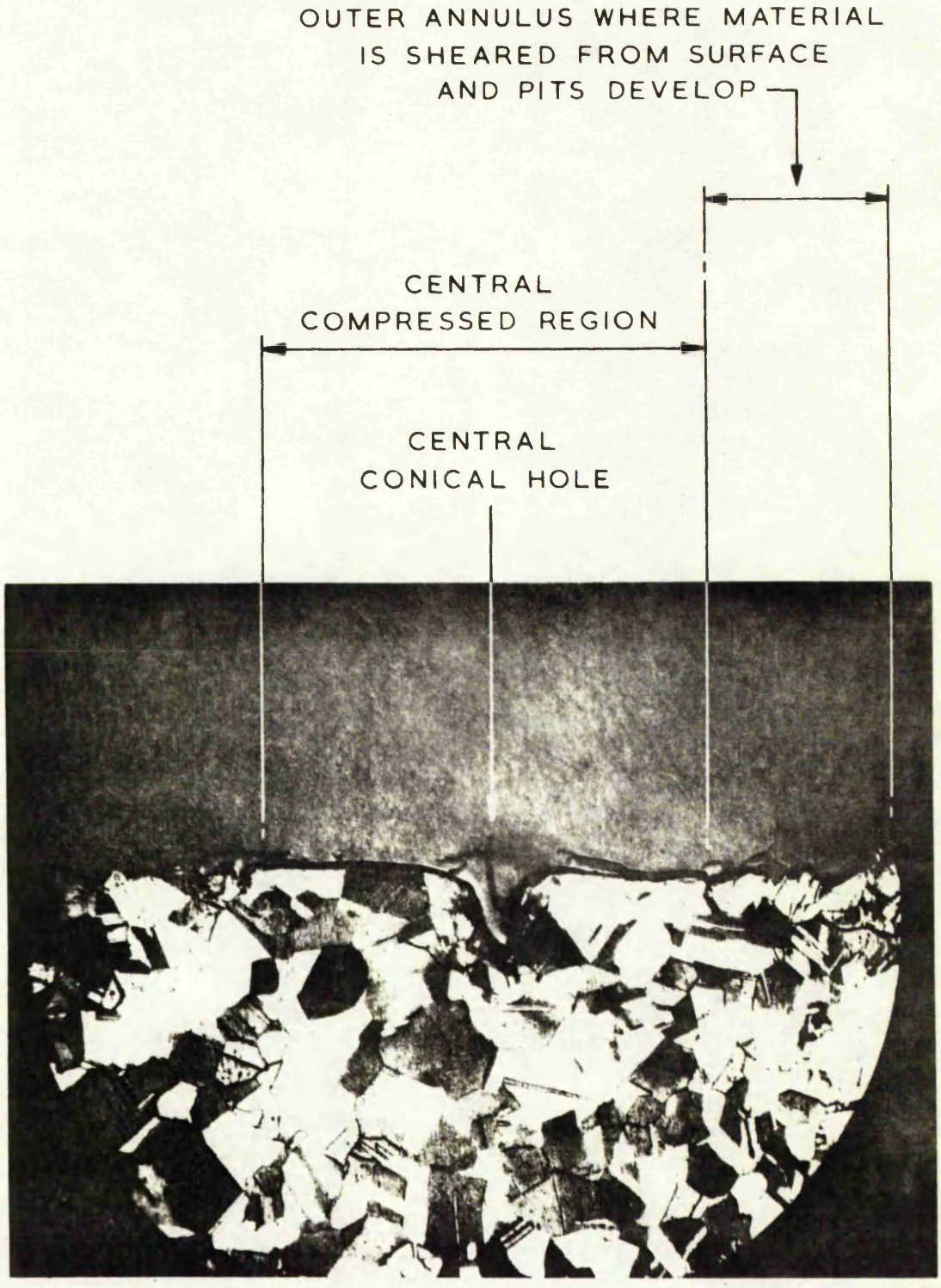

FIG. 3·6 SECTION OF α - BRASS TARGET

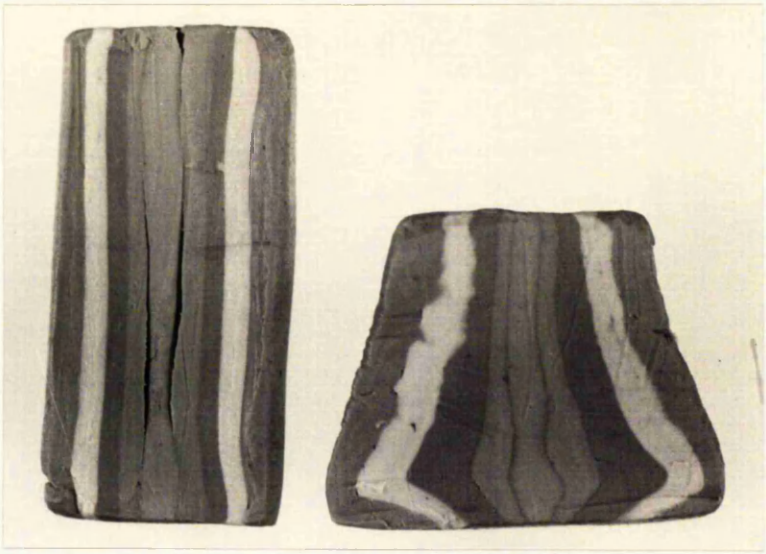

FIG. 3.7 SECTIONED PLASTICINE PROJECTILE
(BEFORE AND AFTER IMPACT)

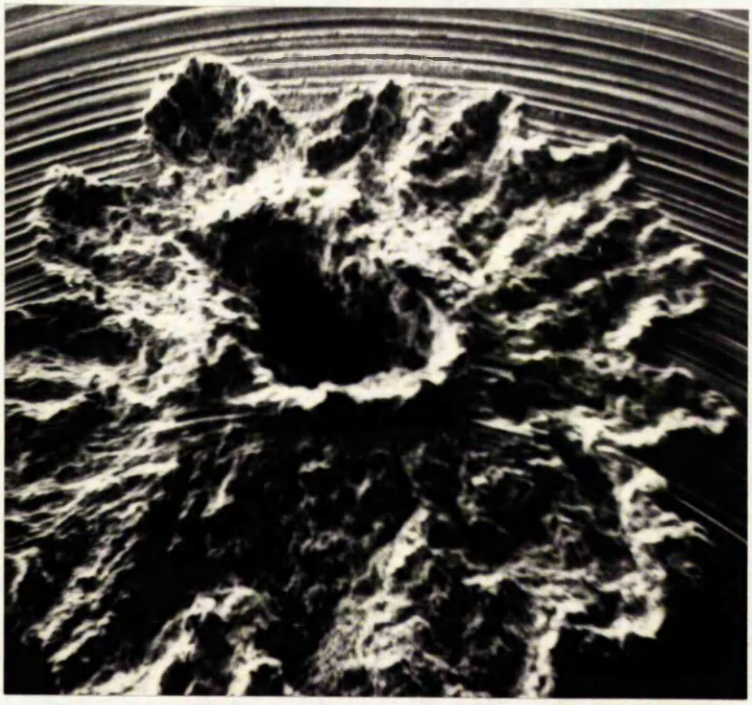

FIG. 3.8 EROSION CRATER IN α-BRASS

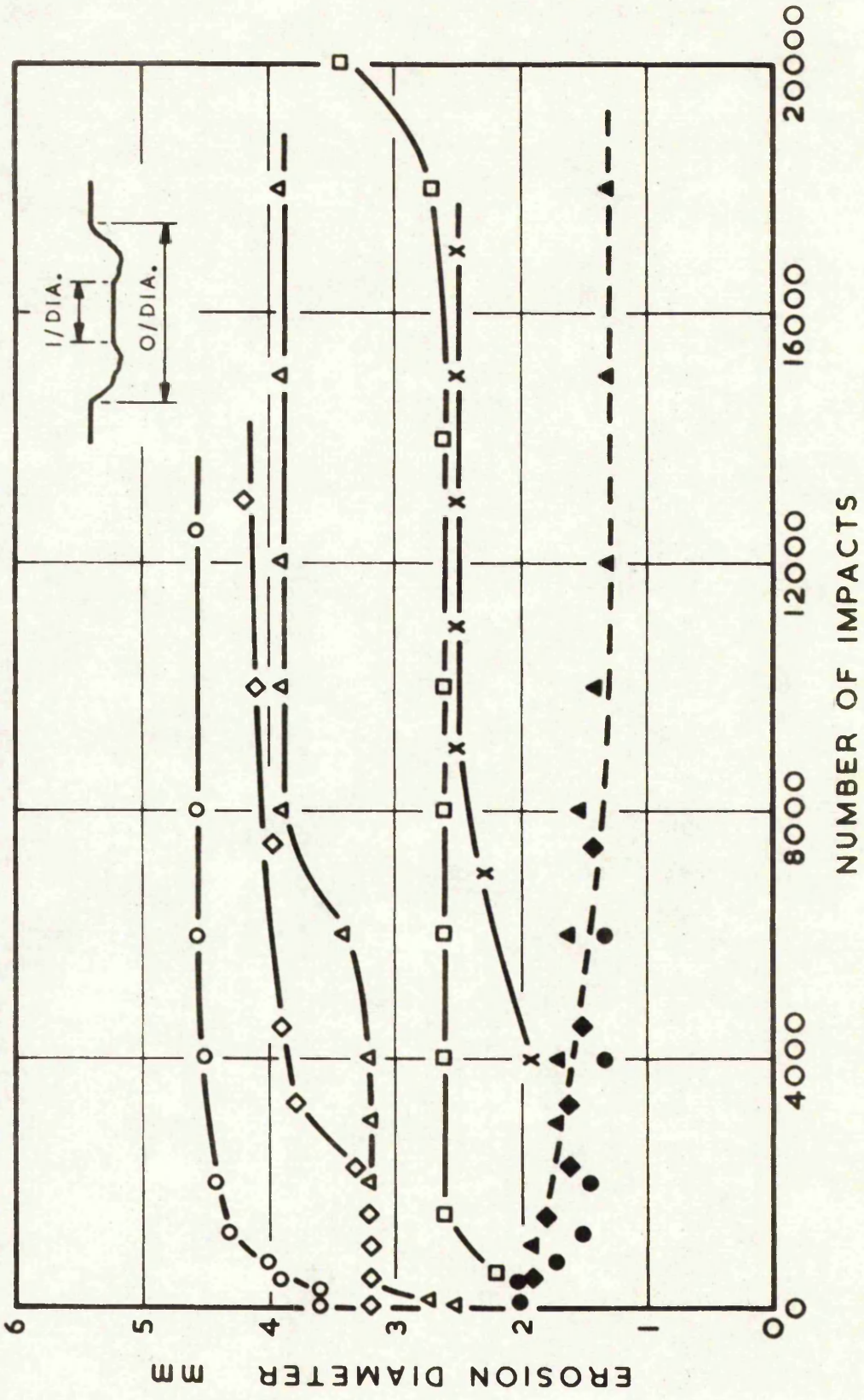

FIG. 3·9 CRATER SIZE VERSUS NO. IMPACTS

OUTER DIA. ○ - 220, ◇ - 160, △ - 110, □ - 56, x - 36 m/sec

INNER " ● - " , ◆ - " , ▲ - " , ■ - " ,

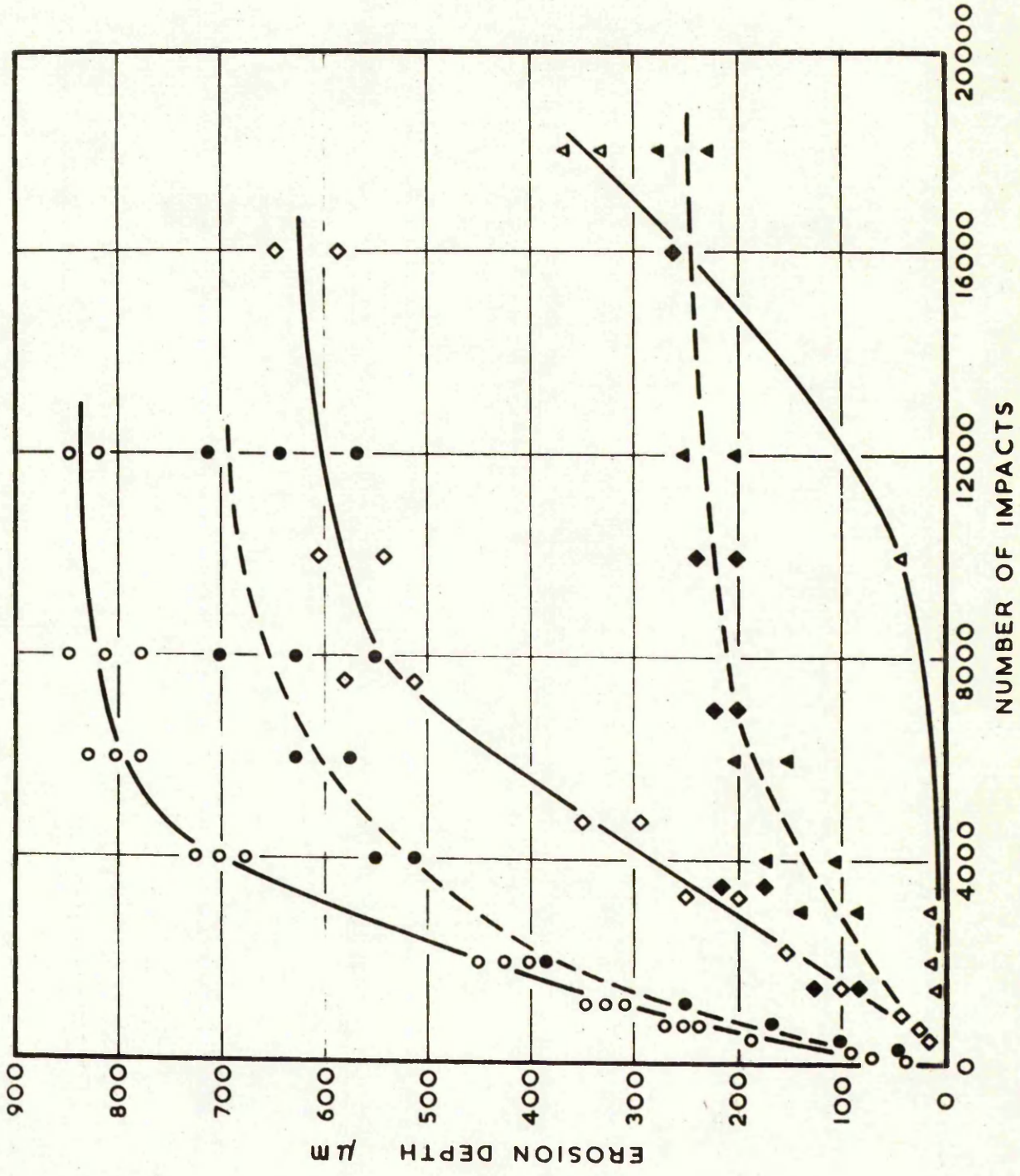

FIG.3·10 DEPTH OF, CENTRAL HOLE (——), AND SHEARED RING (---), WITH NUMBER OF IMPACTS (SYMBOLS AS FIG.3·9

FIG. 3.11 EROSION CRATER IN PERSPEX

FIG. 3.12 SCANNING ELECTRON MICROGRAPH OF OPENED CRACK

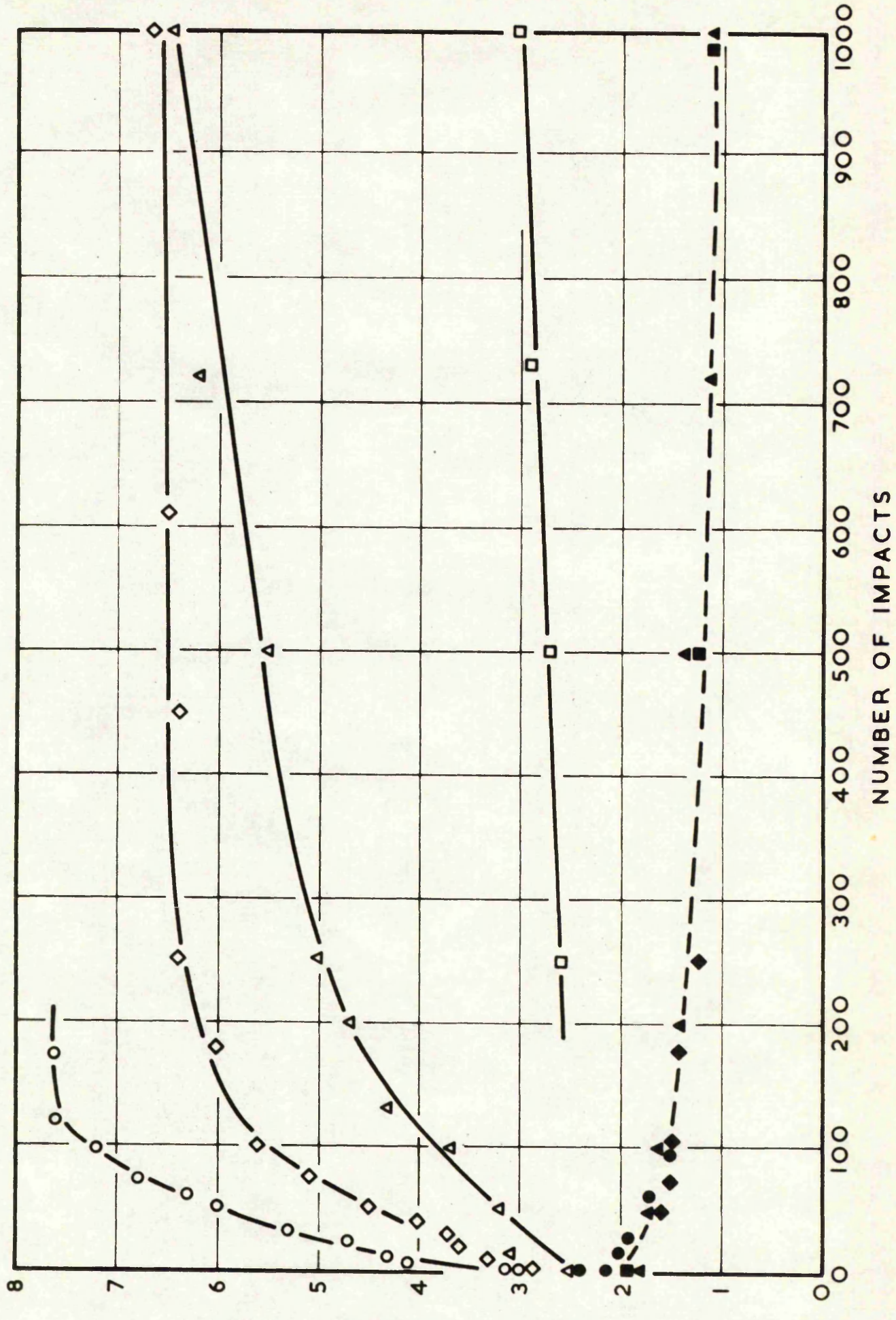

FIG. 3·13 CRATER SIZE VERSUS NO. IMPACTS
(SEE FIG.3·9 CAPTION)

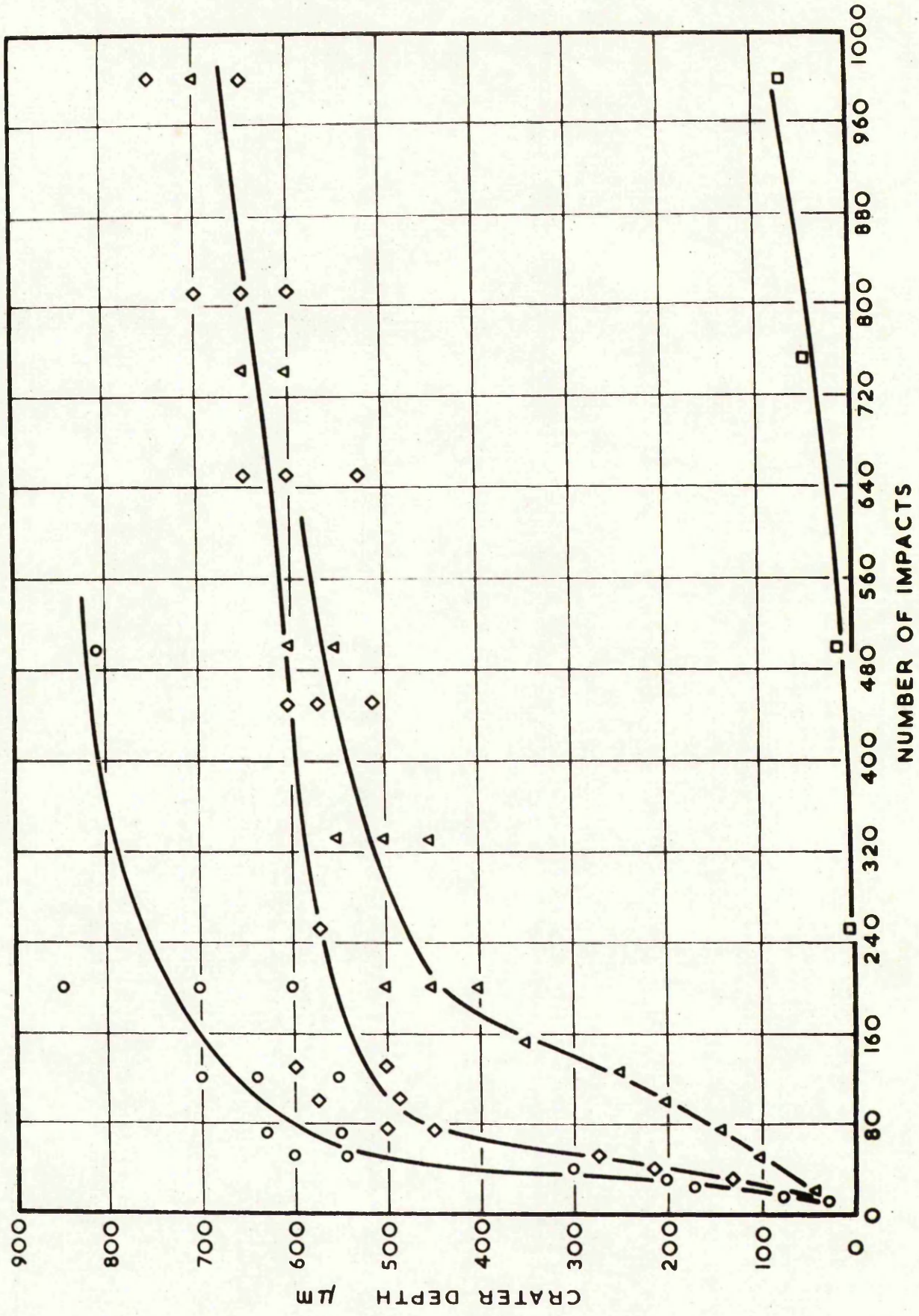

FIG. 3·14 CRATER DEPTH IN PERSPEX WITH NO. IMPACTS

(SYMBOLS AS FIG. 3·9)

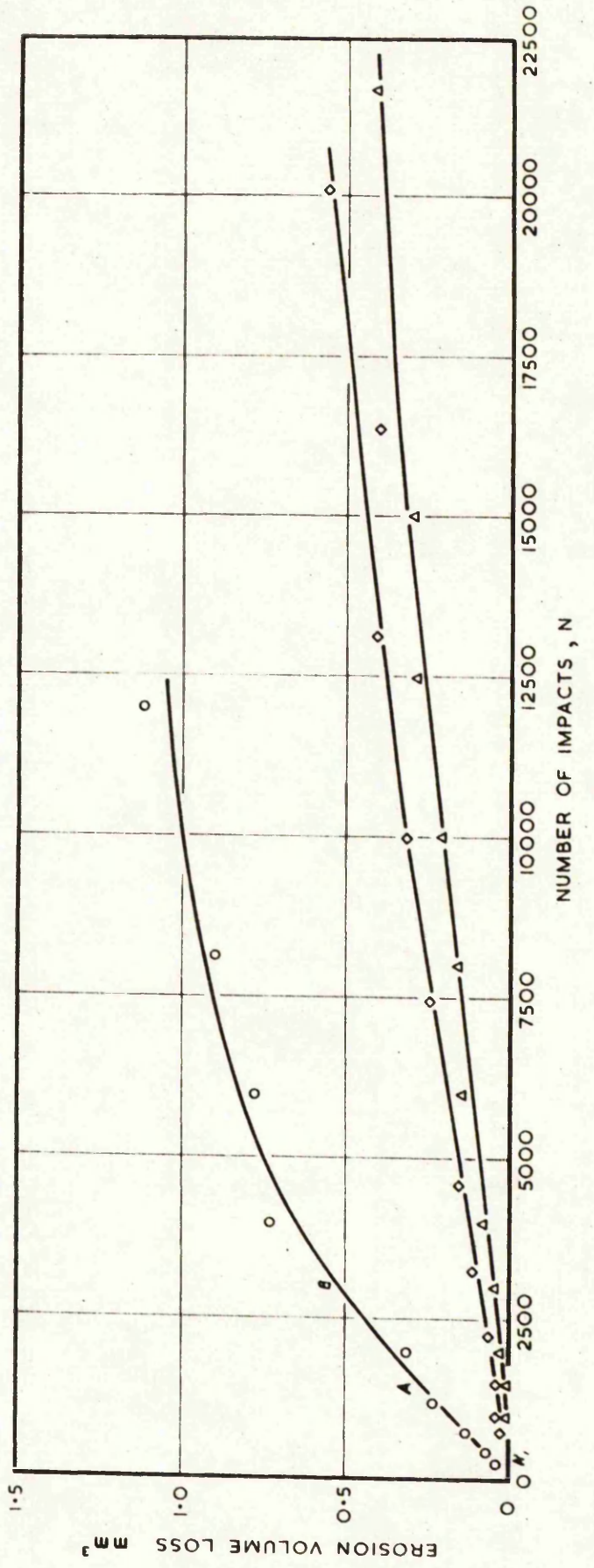

FIG. 3·15 VOLUME LOSS VERSUS NUMBER OF IMPACTS IN ∝- BRASS

(SYMBOLS AS FIG. 3·9)

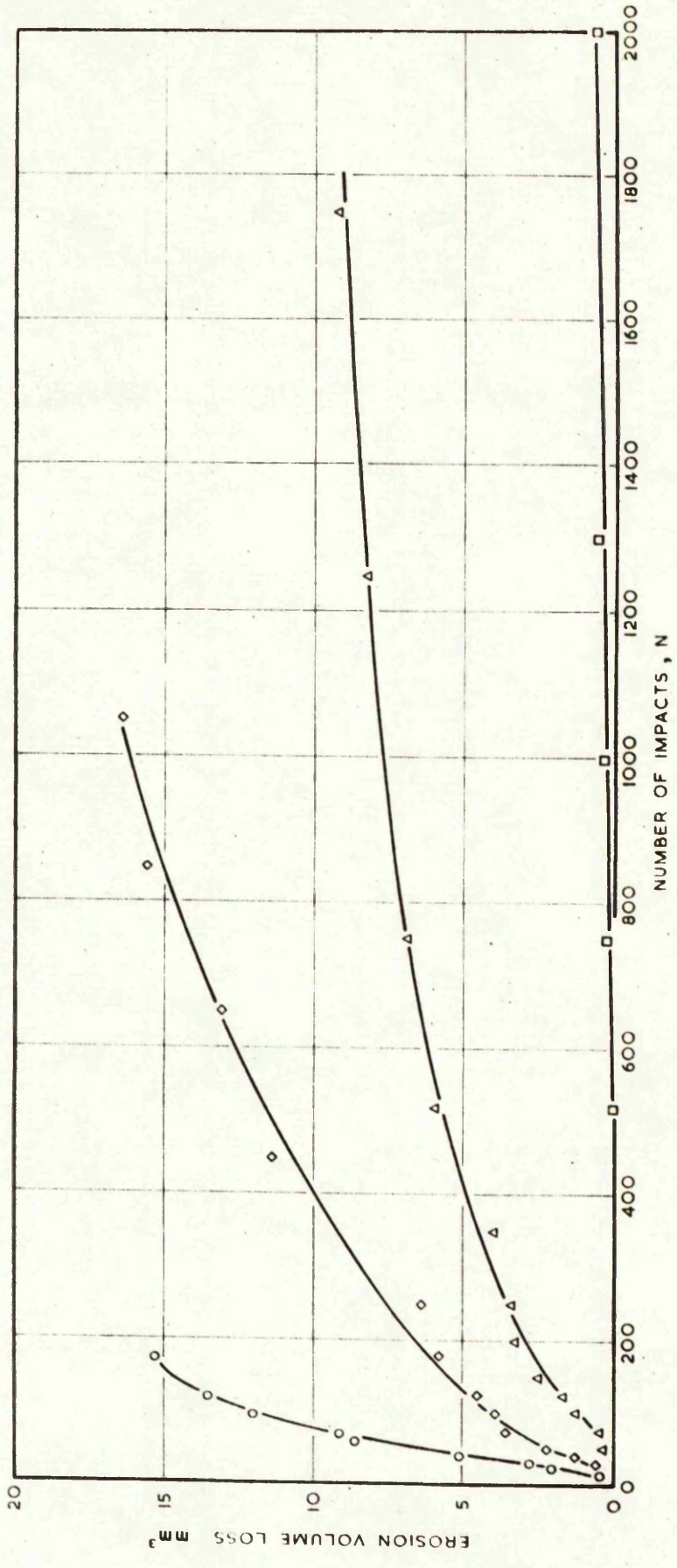

FIG.3·16 VOLUME LOSS VERSUS NUMBER OF IMPACTS IN PERSPEX

(SYMBOLS AS FIG.3·9)

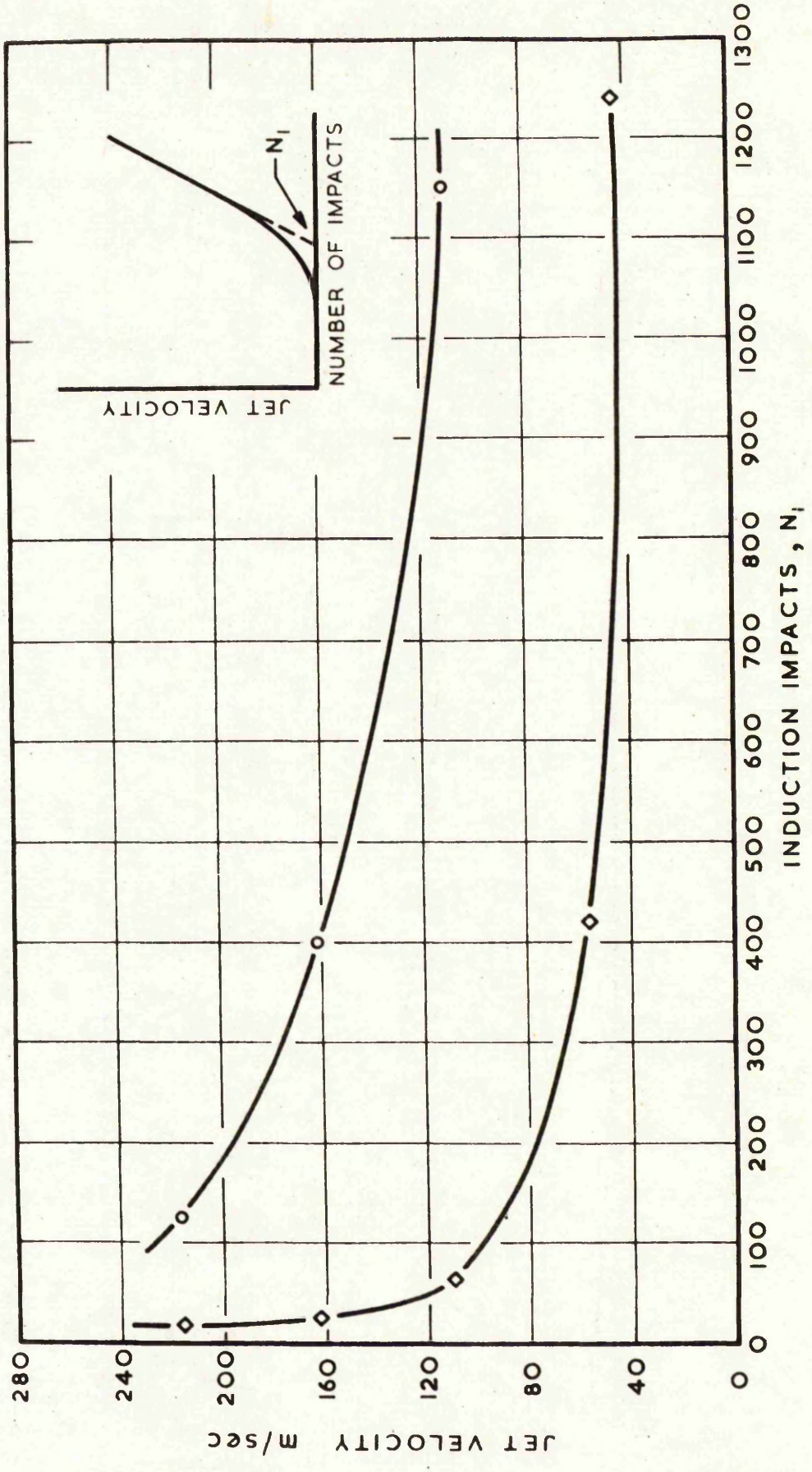

FIG. 3·17 INDUCTION PERIOD VERSUS NUMBER OF IMPACTS FOR ∝- BRASS (o) AND PERSPEX (◇)

CHAPTER FOUR

CHAPTER FOUR

SURFACE CONDITION

4.1 INTRODUCTION

Some aspects of surface condition and its influence on erosion are examined below. Partly this was planned as consolidating background work and it has served to confirm previous results and extended them.

Surface finish has been previously shown to affect the commencement of erosion in certain materials and also affect the rate of mass loss during erosion because the surface becomes very irregular. Honnegger [79] was one of the first to notice the diminution of erosion rate with time, and surface roughness, and attributed it to a protective liquid held in surface depressions. Since then many workers, including Plessett and Divine, [104] Hamitt [64] and Heymann, [69] have examined this effect.

Initial surface roughness has been examined by Smith et al [116] who found with artificially roughened turbine blade shield material that mass loss is significantly lower due to break-up of droplets striking the peaks and also cushioning by water in the craters. In Engle's [40] explanation of this phenomenon it is attributed to the reduced angle of attack afforded by the slanting walls of the roughened surface. It has also been shown [16] that liquid is deflected by surface protrusions tending to intensify damage in depressions. Hancox and Brunton [66] determined, with 60 m/sec water jets impinging on Perspex targets, that surfaces prepared with 1μm particles needed 3.3 times as many impacts to produce pitting as surfaces abraded with 14 and 30μm particles; a similar conclusion was reached for stainless-steel targets. Further experimental evidence was supplied by Field [46] who found that changes in surface profile of 1000 A^{o} could be significant in acting as sites for erosion damage. An apparently contradictory result was given by Hobbs, [74] for high

tensile brass who found surface roughness to make little difference to erosion, although in the case of manganese bronze the induction period was extended with very smooth specimen.

The topic of protective materials has been fairly well researched [42] particularly with regard to the protection of vulnerable aircraft components and also turbine blades. For instance Lichtman [97] found that some polyurethane coatings give better erosion protection than even highly resistant materials such as Stellite 6B. Schmitt [111,112] subjected polyurethane coatings to 2 inches per hour of simulated rainfall at speeds of 500 m.p.h. and found they lasted twenty times as long as some neoprene coatings. Nickel plating on non-conducting substrates such as epoxy or polyester can also be a very effective barrier [134]. With thin elastomeric coatings a primary cause of failure is adhesion [24] due to tensile reflection from the coating adhesive interface.

In this work the effect that suface finish has on induction period and rate of mass loss, with brass, stainless-steel and Perspex is investigated in the absence of entrapped surface liquid. The protective nature of chromium plating on mild steel is examined, particuarly at low speed from the viewpoint of car bumpers or high-speed train components. Also anodic films on aluminium and the effects of shot penning are briefly examined.

4.2 SURFACE FINISH

4.2.1 Experimental procedure

Six brass specimens were produced with target surfaces finished by rough flycutting, smooth shaping, surface grinding, fine emerying, rough and smooth polishing. Surface finishes ranged from 0.005 to 7.5μm cla measured using a Talysurf 4, on K setting, with 0.03 meter cut-off. Eight targets of stainless-steel and Perspex were similarly produced with surface finishes ranging from 0.0005 to 0.41μm cla.

Erosion was caused by water jets of 220 m/sec and during the course of the tests the specimens were carefully cleaned, weighed on a micro-balance to record the mass loss and examined under a microscope. Further tests were conducted on brass targets with water jet speeds of 110 m/sec and with Perspex targets at 56 m/sec; the examination in these cases was purely visual.

4.2.2 Results and discussion

(i) Brass targets

It can be seen from Fig.4.1(i) which shows volume loss with number of impacts that surface finish has little bearing on the onset or rate of erosion. This is probably due to the surfaces being quickly damaged by viscous shearing and thus eradicating possible differences. Tests with lower speed water jets exhibited similar tendencies with pits forming and developing at corresponding times. However, these comparisons were limited by the difficulty of visually examining damage on different reflective surfaces.

One distinct difference in the formation of erosion damage with surface finish is the distribution of pits. With rough surfaces, pits form on the inward faces and crests of surface protrusions(relative to the outward radial flow) while the reverse faces of these protrusions are protected from fierce liquid flow. Also with directional surfaces, such as shaping or flycutting a preferred erosion takes place across the lay of the surface. With smooth targets pits form randomly.

(ii) Stainless-steel targets

Many similarities were evident as between stainless-steel and brass specimens i.e. material was removed across the surface lay and all pits developed on the inward face of surface furrows. However, polished stainless steel surfaces needed three to four times the number of impacts that rougher

surfaces (shaped or emery finishes) needed to cause pitting. Very rough surfaces did not extend further the induction period. Also it was noticeable that any minute scratches intoduced initially on polished surfaces were sites for pitting and had induction periods similar to those of rough surfaces.

If surface scratches are assumed triangular and scratch depth is taken as four times the cla.value then these results confirm the work described in reference 11.

(iii) Perspex targets

Volumes of eroded material versus number of impacts is given in Fig. 4.1 (ii) and shows the induction period to be much the same for all four specimens. Mass loss can be seen to be eratic and has no significant relationship with surface finish. From experimental observations mass loss depends on flakes of material being levered off the target at infrequent intervals and making sudden differences in weight. This variability is independent of surface finish as the cracks, which form during the first impact, propagate under the surface possibly be pressurized leverage within the crack. The rate of crack propagation and hence mass loss is not a function of surface finish.

The tests on Perspex with water jet speeds of 56 m/sec where damage does not occur during the first impact did not follow the above trend. Here the formation of ring cracks were subjectively assessed as necessitating two or three times the number of impacts than required on the smoothest and roughest surfaces compared with the two intermediate roughness specimens. Again, assessment is not precise when comparing fine hairline cracks on finely polished and coarse surfaces but the trend was distinctly present.

4.2.3 Conclusions

On relatively low strength ductile materials, such as brass, surface finish has little effect on induction period or rate of mass loss as the

original surface is quickly eradicated. With polished stainless steel the induction period is extended. Surface finish distinctly changes the formation of erosion pits.

Brittle materials are only affected by surface finish with low velocity impact where damage does not commence immediately.

In all cases the rate of mass loss once erosion has commenced is not influenced by surface roughness. This casts doubts on attributing the diminution of erosion with surface roughness to break up of droplets and reduced angle of attack and strengthens the belief that protective liquid held in depressions is the true cause.

4.3 CHROMIUM PLATED MILD STEEL

Normally when mild steel (En la) targets, are subjected to water jet impacts of 220 m/sec, a central hole forms after 30 impacts which increases linearly in depth with number of impacts to a maximum of 1.3 mm at approximately 17,000 impacts. Pits develop at about 800 impacts: an example of radial pit growth is given in Fig. 4.2 showing a pit after 4,000, 5,000, 9,500 and 12,500 impacts.

With good quality chromium plating (flashes of copper, nickel and 0.0015 in thickness of chromium) the formation of the central hole is retarded and requires 1000 impacts more until penetration of the plating has occurred; thereafter the depth increases with number of impacts up to a maximum at 18,000. Pitting is eliminated even after 40,000 impacts and as pitting causes mass loss the plating gives a significant protection.

At lower impact velocities minute local depressions form around the stagnation point as shown in Fig. 4.3 but do not develop to form a central hole. Protection is thus afforded to the mild steel substrate although the minute depressions could form sites for subsequent corrosion particularly with very thin flashes of chromium. Evidence of damage is clearly visible

at velocities as low as 56 m/sec (120 mph).

4.4 ANODISED ALUMINIUM

The possible protective effect of an anodic ceramic film on aluminium was investigated and it was found that with repetitive water impact that even a hand anodic film 150μm thick quickly cracked and large particles were chipped from the surface. A micrograph of the surface, see Fig. 4.4, after 60 impacts shows bad pitting of the anodic film. For comparison a normal aluminium specimen at this stage had negligible damage with a central hole 20μm deep and only a slight suggestion of pitting. After 200 impacts much of the anodised film was chipped away to a depth of 150μm revealing the substrate; the central hole developed to a depth of 270μm.

A decorative anodic film 25μm thick, behaved similarly affording no protection to the surface and indeed rendering the surface susceptible to damage. After 60 impacts an annulus on the target subject to shearing was completely devoid of any anodised film and the central hole was nearly four times as deep as an untreated target.

At 800 m/sec impact speed a single jet penetrated less into a thickly anodised target, than a polished target, although the target became crazed with fine hair line cracks and was of little further protective value.

4.5 SHOT PEENING

Targets of mild steel (En 1a) and aluminium alloy (Al, Zn, Mg) were shot peened using a medium sand shot which induced compressive stresses in the surfaces, although visually they remained relatively undamaged.

The formation and growth of pits during erosion in both materials, was markedly assisted by shot peening. The shot peened specimens needed only half the number of impacts that polished specimens did to produce small pits. Also the growth of pits progressed at approximately twice the rate on

shot peened surfaces. This result is consistent with work by Mathieson and Hobbs [99] and may be explained as in Chapter five where pre-compressive stress is shown to lead to an increase in the erosion of ductile materials. However, as shot peening is known to improve fatigue life this result seems contrary to the current popular belief that erosion is a fatigue initiated mechanism.

(i) 60-40 BRASS - 220 m/sec vel.

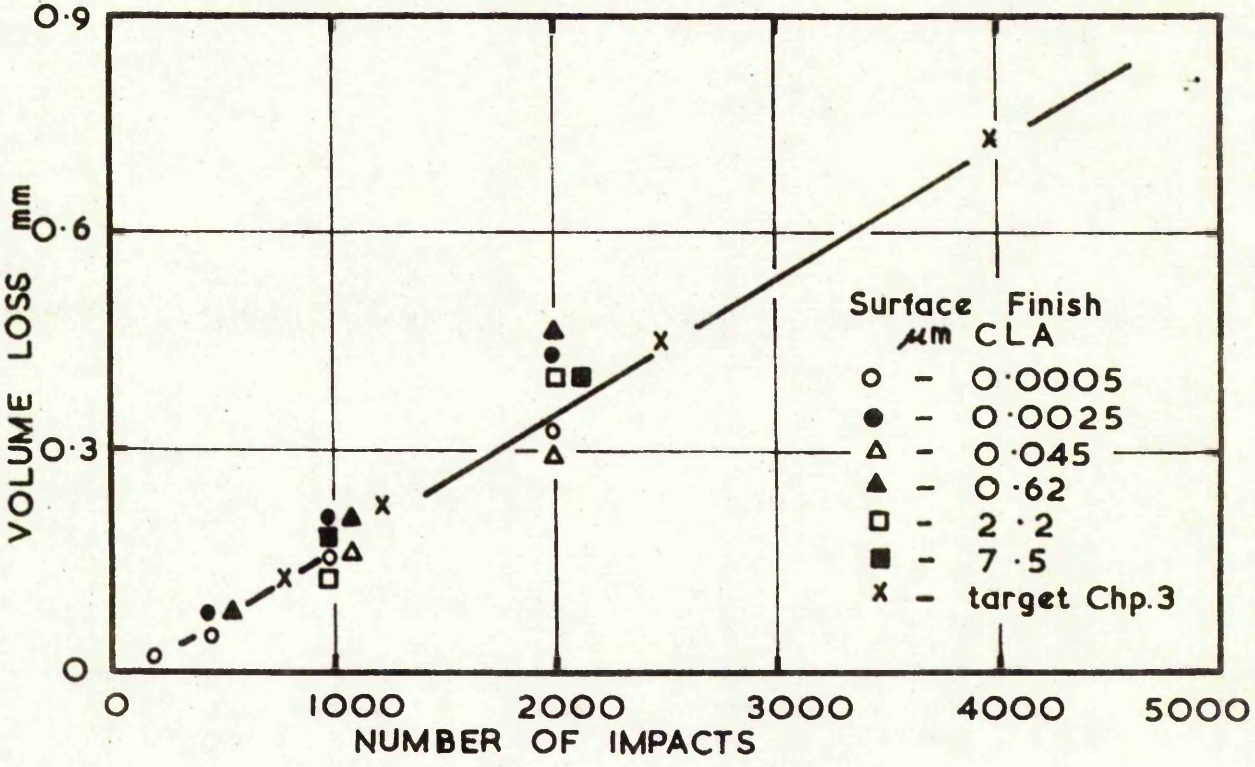

(ii) PERSPEX - 220 m/sec vel.

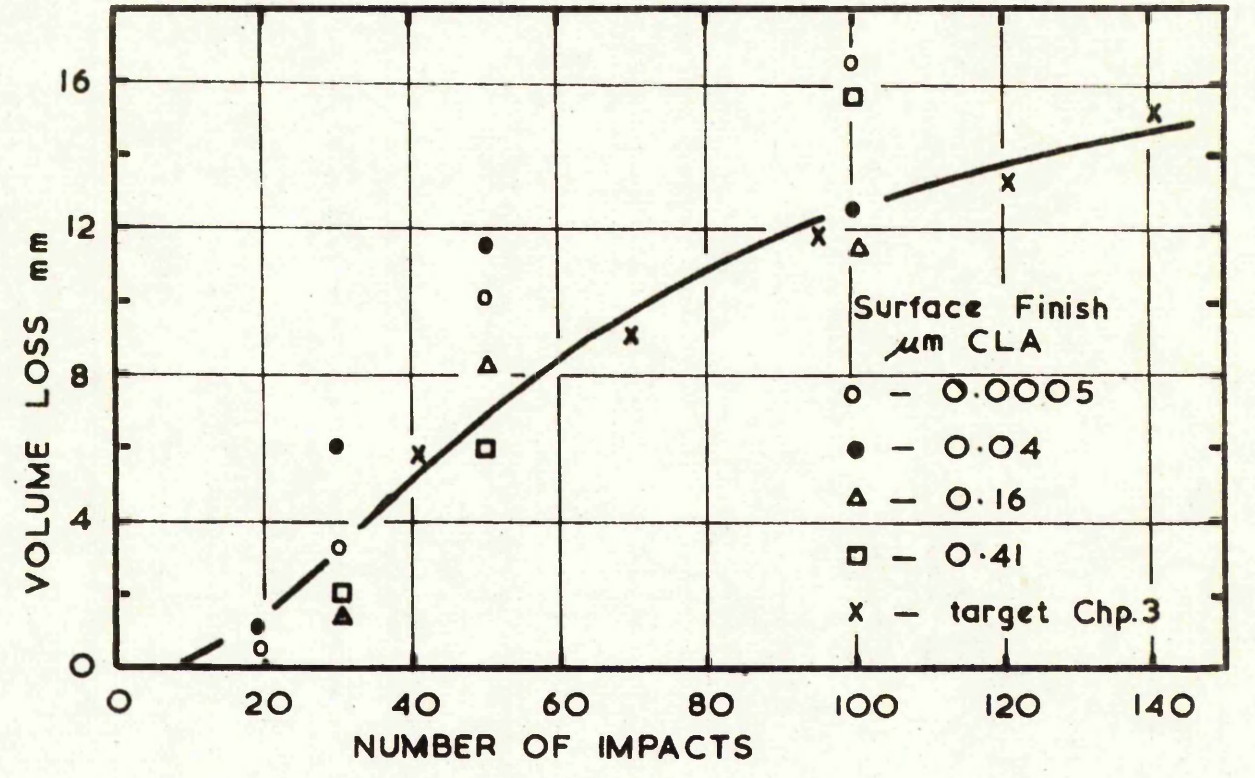

FIG. 4·1 VARIATION OF MASS LOSS WITH SURFACE FINISH

(i) 4,000 IMPACTS

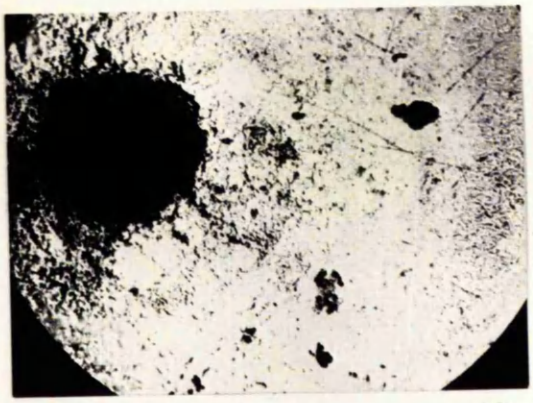

(ii) 4,000 IMPACTS

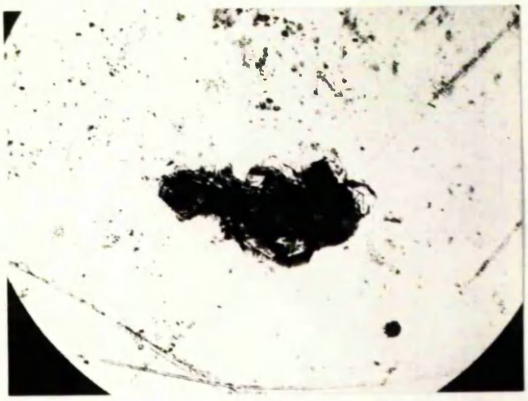

(iii) 6,000 IMPACTS

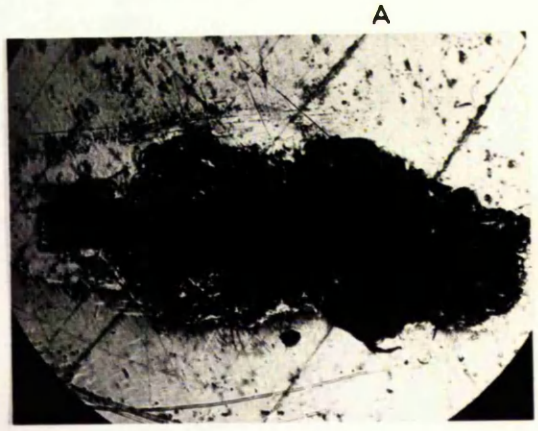

(iv) 9,500 IMPACTS

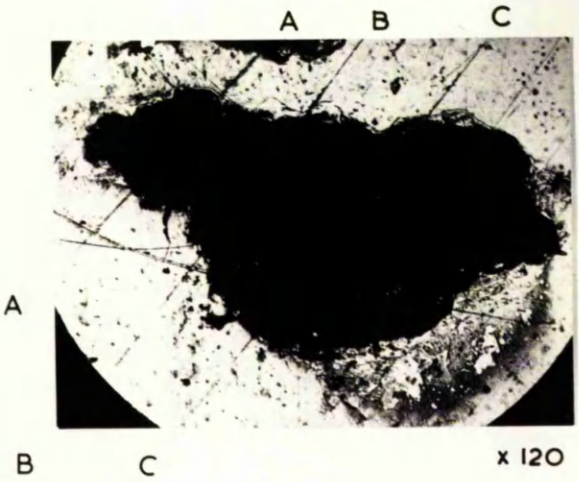

(v) 12,500 IMPACTS

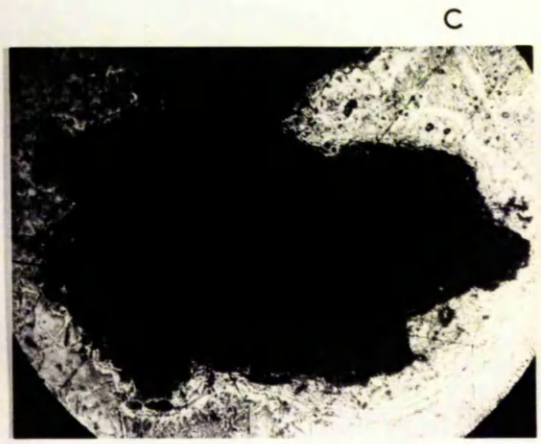

FIG. 4·2 PITS DEVELOPMENT IN En.1a STEEL

220 m/sec JET VEL.

(i) CENTRAL IMPACT REGION
6,000 IMPACTS

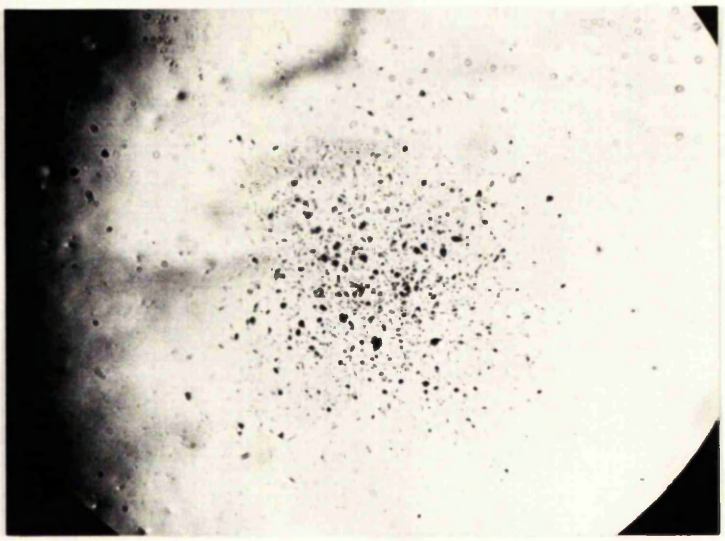

x 60

(ii) VIEW OF DEPRESSIONS
13,000 IMPACTS

x 1,200

FIG.4·3 CHROMIUM PLATED MILD STEEL
110 m/sec JET VEL.

(i) 60 IMPACTS

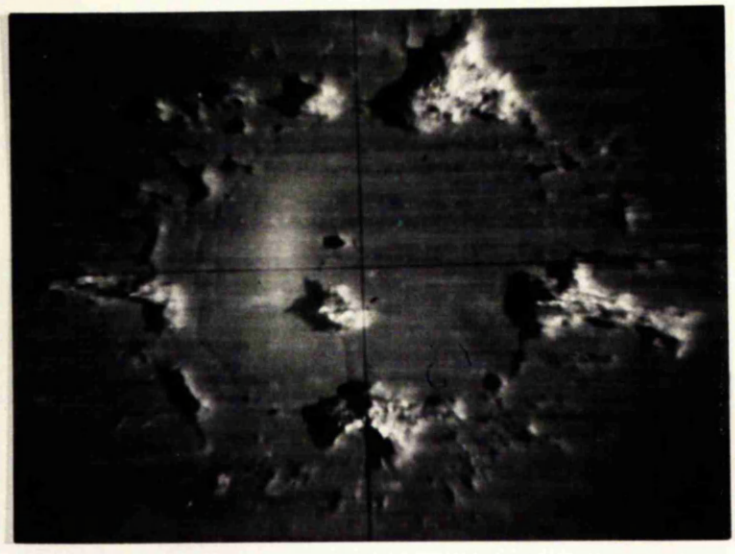

x 20

(ii) 200 IMPACTS

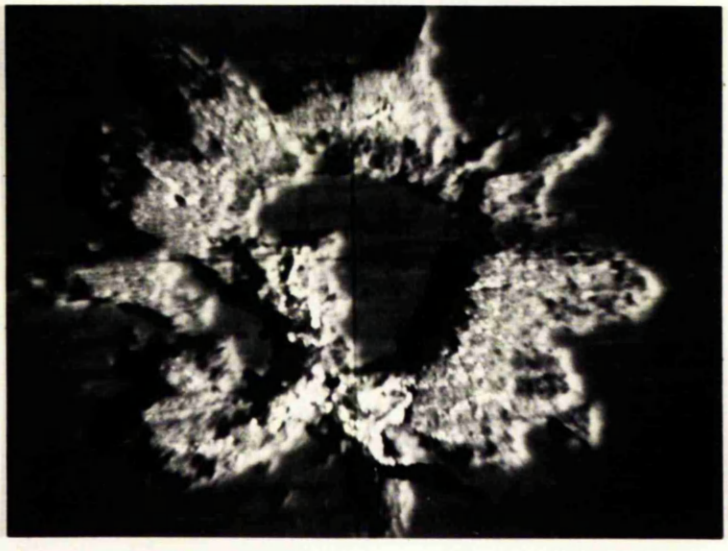

x 20

FIG.4·4 ANODISED ALUMINIUM (Al. Zn. Mg.)

220 m/sec JET VEL.

CHAPTER FIVE

CHAPTER FIVE

PRE-STRESS AND PRE-STRAIN

Erosion experiments on targets subjected to uniaxial and biaxial tensile and compressive stresses are described. The erosion was produced by means of repetitive water jets at impact speeds of 30 to 220 m/sec.

5.1 EQUIPMENT

5.1.1 Uniaxial loading fixture

To apply uniaxial tension or compression to a specimen during erosion a small loading fixture was used as shown in Fig. 5.1. It comprised two brass blocks whose relative position was changed by rotation of a square threaded rod with an integral collar having a 0.001 in. movement of the blocks per division of the handwheel. Rotation of the blocks about the axis of the thread is prevented by two hardened steel slide rods.

Toughened steel studs screwed into the top machined surfaces of the brass blocks are used to apply pre-load to the erosion specimen.

The fixture was located on a repetitive water jet gun with the specimen 16 mm above the die orifice. Water jet impact occurs midway between the two locating holes, which is also on a line connecting the two loading studs.

The specimen resembles a flat tensile test piece with a parallel portion 11 mm wide where impact occurs, broadening out to 20 mm at either end. A specimen thickness of 3 mm was selected as being unlikely to influence the erosion process yet thick enough to allow substantial stress to be applied. It was later confirmed that the erosion of Perspex and α-brass specimens of this design gave mass loss characteristics identical with those of conventional cylindical specimens subject to no pre-stress.

To ascertain the stress level applied to specimens, longitudinal and lateral strain gauges were attached at the impact position and in addition a Huggenburger extensometer of 12 mm gauge length was fitted to the specimen in situ on the loading fixture. A load was applied to the specimen by rotating the handwheel and apparent strain from the extensometer and from the handwheel dial were recorded and plotted against the strain gauge readings. The extensometer was found to give close agreement with the longitudinal strain gauge and was therefore used with all specimens to initially measure the applied strain. At intervals during the tests the specimens were removed from the loading fixture for examination and weighing; the correct pre-stresses were restored to the specimens by returning the handwheel to its initial positions.

The applied specimen stress was limited to 90 MN/m^2 (6 $tonf/in^2$) with a specimen cross-sectional area of $(33 \times 10^{-3})m^2$.

5.1.2 Biaxial loading

To subject a specimen to biaxial compression, a well lubricated cylindrical billet of target material was pressed by a plunger into a one half degree tapered steel tube, as shown in Fig. 5.2. As the billet began to emerge from the parallel portion of the tube the process was terminated, thus achieving a compressive stress on the target material. Before erosion tests were carried out the parallel portion of the tube was parted off, faced, polished and a location pin fitted.

Two strain gauges attached circumferentially to the parallel portion of the tube before extrusion gave an average value of hoop strain. Using the Lamé equations the radial compression, σ_r , within the target material was calculated. The value of compressive stress in the target was cross-checked by calculation of the interference fit of the billet together with the relevant stress equivalent strain diagram of the target material.

To allow for possible creep of the Perspex specimen after extrusion, strain gauge readings were taken intermittently over a period of days until no significant change occurred. It was noted that the most deformed Perspex specimen, the largest initial billet diameter, crept by a greater amount and hence resulted in a lower pre-stress on the target.

The work-hardening of the ∝-brass as a consequence of pre-straining by both methods, and as measured by Vickers Hardness Number, is given in Table 1.

5.2 EXPERIMENTAL PROCEDURE

Pre-stressed specimens were prepared as follows:

(i) For tests with water jets of speed 220 m/sec

1 ∝-brass specimen subjected to 7.5 MN/m^2 biaxial compression

1 " " " " 90 " " "

1 " " " " 180 " " "

1 " " " " 67 " uniaxial "

1 " " " " 67 " " tension

(ii) For tests with water jets of speeds 160, 110 and 56 m/sec

3 ∝-brass specimens subjected to zero stress

3 " " " " 180 MN/m^2 biaxial compression

1 " " " " 67 " uniaxial tension

(iii) For tests with water jets of speeds 220, 160, 110, 56 and 30 m/sec

5 Perspex specimens subjected to zero stress

5 " " " " 60 MN/m^2 biaxial compression

5 " " " " 67 " uniaxial tension

The specimens were mounted on the repetitive water gun and water jet impact velocities adjusted to the corresponding values. At intervals during the erosion process the specimens were thoroughly cleaned and weighed on a micro-balance, and the depth and diameter of the developing

impression recorded.

5.3 EXPERIMENTAL RESULTS AND DISCUSSION

5.3.1 Erosion of ∝-brass specimens

(i) Experimental observations

Erosion, in ductile materials, normally occurs with progressive plastic indentation of the surface, followed by gross shearing in an annulus surrounding an undamaged central area.

The erosion characteristics of ∝-brass, as experimentally determined, are given in Fig. 5.3 and show that the rate of mass loss with number of impacts is substantially influenced by the externally applied stress system.

Of the five specimens impacted with water jets travelling at 220 m/sec, four showed a general scatter of points with little apparent difference in the rate of mass loss. However, the target with the smallest applied pre-stress gave marginally less resistance to erosion than the others. Thus within these tests the introduction of externally applied stresses transverse to the jet axis slightly reduces the rate of mass loss. This result is not unexpected as Hoff [77] et al with beryllium copper alloys, and Brunton and Hobbs [18] with a wide range of non-ferrous materials, have shown that erosion resistivity increases with target hardness and hence the work hardening associated with pre-stressing may be expected to similarly affect erosion.

Results shown in Fig. 5.3 for the tests with 160 and 110 m/sec impact speeds are contrary to those described above. They show that the pre-loaded specimens have significantly higher rates of mass loss with number of impacts than the stress free specimens. Similarly, in tests with water jets of 56 m/sec the erosion resistivity is reduced with both tensile and compressive pre-loaded specimens. Micrographs, given in Fig. 5.4, illustrate the deeper and more extensive pitting in the biaxially compressed specimen after only 14,000 impacts as compared with the stress free specimen after 20,000 impacts.

(ii) Discussion of results

A qualitative assessment of the behaviour of the pre-stressed targets is obtained by considering an element of surface material within the annulus subjected to shearing, as shown in Fig. 5.5(a). Stresses acting on the element, shown in Fig. 5.5(b), comprise the externally applied biaxial stress system, σ_r, and σ_θ, a vertical pressure σ_p, together with radially outward surface viscous shear stress τ and complementary shear stress τ', resulting from the water jet impact. It is probable that σ_p, τ and τ' will vary with radius r, depth d and time t, but identically positioned elements, in terms of 'r' and 'd' in comparable specimens will be subject to similar erosion stresses. The only variable with these elements is that due to the externally applied pre-stress.

A Mohr's circle diagram[82] representing the stresses acting on an element is given in Fig. 5.5(b). From experimental observation of ductile material erosion characteristics a maximum shear stress criteria was believed to be most likely for 'pitting' and material loss. The maximum shear stress τ max, is given by

$$\tau_{max} = \sqrt{\tau^2 + \frac{(\sigma_r - \sigma_p)^2}{4}} \qquad (5.1)$$

As τ may be considered constant for similarly positioned elements a graphical representation of equation 5.1(i) i.e. $\tau^2 max / \sigma_p^2$ versus the ratio of σ_r / σ_p, given in Fig. 5.6 shows a marginal reduction of erosion when

$$0 < \sigma_r(\text{compressive}) / \sigma_p < 2$$

but increase in erosion when

$$\sigma_r(\text{compressive}) / \sigma_p > 2$$

Similarly, with biaxial tension applied to an erosion target, the stresses acting on an element are given in Fig. 5.5(c). Maximum shear stress is given by

$$\tau_{max} = \sqrt{\tau^2 + \frac{(\sigma_r + \sigma_p)^2}{4}} \qquad (5.2)$$

Equation (5.2) is also plotted in graphical form in Fig. 5.6 and predicts an increase in erosion when

$$\sigma_r \text{ (tension)} / \sigma_p > 0$$

The true values of σ_p on any element during the shearing stage of erosion is as yet unknown. However, initial impact pressure is shown by Cook [25] to be represented by the water hammer equation

$$p = \rho . c . v \qquad (5.3)$$

where c is the speed of compression waves in the liquid. This pressure decays very rapidly with time to approximately five per cent (for water impact on brass at these jet speeds) of its initial value. If a typical value of σ_p is taken as half the initial impact pressure then the experimental results can be related to those in Fig. 5.6.

In experiments with water jets of 220 m/sec σ_p is assumed to be 150 MN/m^2 and the value of σ_r ranges from 60 to 225 MN/m^2. Thus all erosion tests under these conditions occur within the region in Fig. 5.6 of

$$0 < \sigma_r \text{ (comp.)} / \sigma_p < 2$$

which indicates that erosion is marginally alleviated.

With water jet speeds of 160, 110, 60 m/sec σ_p is taken as 110, 75, 41 MN/m^2 and with σ_r of 225 MN/m^2 all the $\sigma_r \text{ (comp)} / \sigma_p$ ratios are above 2. Thus erosion in these tests is likely to be intensified, which is in fact borne out by experiment.

(iii) Initial indentation phase

In the erosion of ductile materials there is an initial progressive plastic indentation phase before loss of material occurs. The development of the depth of this compressed region is given in Fig. 5.7 for a water jet impinging on targets with various levels of applied biaxial compression. An increase of transverse compressive pre-stress can be seen to cause a reduction in the degree of surface indentation. This is due to the increase in hydrostatic component of stress (i.e. $[2\sigma_r + \sigma_p]/3$ and hence a reduction in the deviatoric stress ($2[\sigma_p - \sigma_r]/3$).

The indentation depth may be compared with the depth of plastic penetration achieved by a rigid indenter at a stress level ($\rho c v - \sigma_r$). Table II shows that the final depth of the compressed area is less with water impact than with a rigid indenter.

5.3.2 Erosion of Perspex specimens

Perspex, as with other brittle materials, erodes by the formation of a series of discrete cracks forming an annulus of damaged material surrounding a central area of undamaged material of approximately two-thirds the impinging jet diameter [21].

Fig. 5.8 shows the mass loss characteristics of Perspex when impacted by water jets travelling at 220, 160 and 110 m/sec. The targets for all three speeds of water jet are either stress free or subjected to 60 MN/m^2 biaxial compression.

In all cases the targets subjected to compression eroded significantly less than the stress free specimens. The compressive stress has little effect on the occurrence of cracks and the mode of failure but inhibits crack growth into the material. As mass loss is accomplished by the cracks propagating into and undermining the surface of the material, rate of mass loss is necessarily reduced. Also the outer diameter of the area subject to

cracking is substantially reduced; the inner diameter, however, remains unchanged.

Other tests with slower water jets of 60 and 30 m/sec impinging on similar specimens also show a reduction in rate of erosion with compressive stress. However, the induction period, (number of impacts required for cracks to first appear in the target surface) and the threshold level (velocity below which erosion ceases) appears to be unaffected by the application of pre-stress to the targets.

Erosion tests on Perspex specimens subjected to 60 MN/m^2 uniaxial tension with water impingement speeds of 220, 160, 110, 56 and 30 m/sec indicate an increase of mass loss as compared with stress free specimens at these impact speeds. The discrete erosion cracks penetrate deep into the pre-stressed target material. However, cracks once initiated at the erosion crater propagate rapidly across the width of the target - in a direction perpendicular to the maximum principal stress - thus splitting it before further mass loss occurs. A micrograph of such a specimen is given in Fig. 5.9.

5.4 CONCLUSIONS

The influence of pre-stress on erosion is dependent on the damage mechanism of the material, (i.e. ductile or brittle fracture) the type of applied stress and the relative values of pre-stress to impact stress.

With α-brass, tensile or compressive pre-stress generally increases erosion by inducing a higher level of shear stress in the impact zone. However, there exists a range of impact situations with high impact speeds and low compressive pre-stresses that marginally reduces erosion. From an analysis of the stresses this has been shown to occur when

$$0 < \sigma_r \text{(compressive)} / \sigma_p < 2.$$

In Perspex, subject to compressive stress, the rate of erosion is reduced because cracks formed during impact are inhibited from spreading into and undermining the material to as great an extent as in stress free targets. The contrary is also true, that tensile pre-stress increases erosion.

5.5. PRE-STRAIN

Erosion experiments on super-pure aluminium showed that tensile and compressive pre-strain (i.e. plastic deformation of targets prior to erosion tests) of 16.5 to 29% had only a minimal effect: unlike the previous work with pre-stressed targets. The results, given in Fig. 5.10, show a slight reduction in crater depth and slight increase in the rate of mass loss with pre-strain. The type of pre-strain (i.e. tensile or compressive) made no difference to the result.

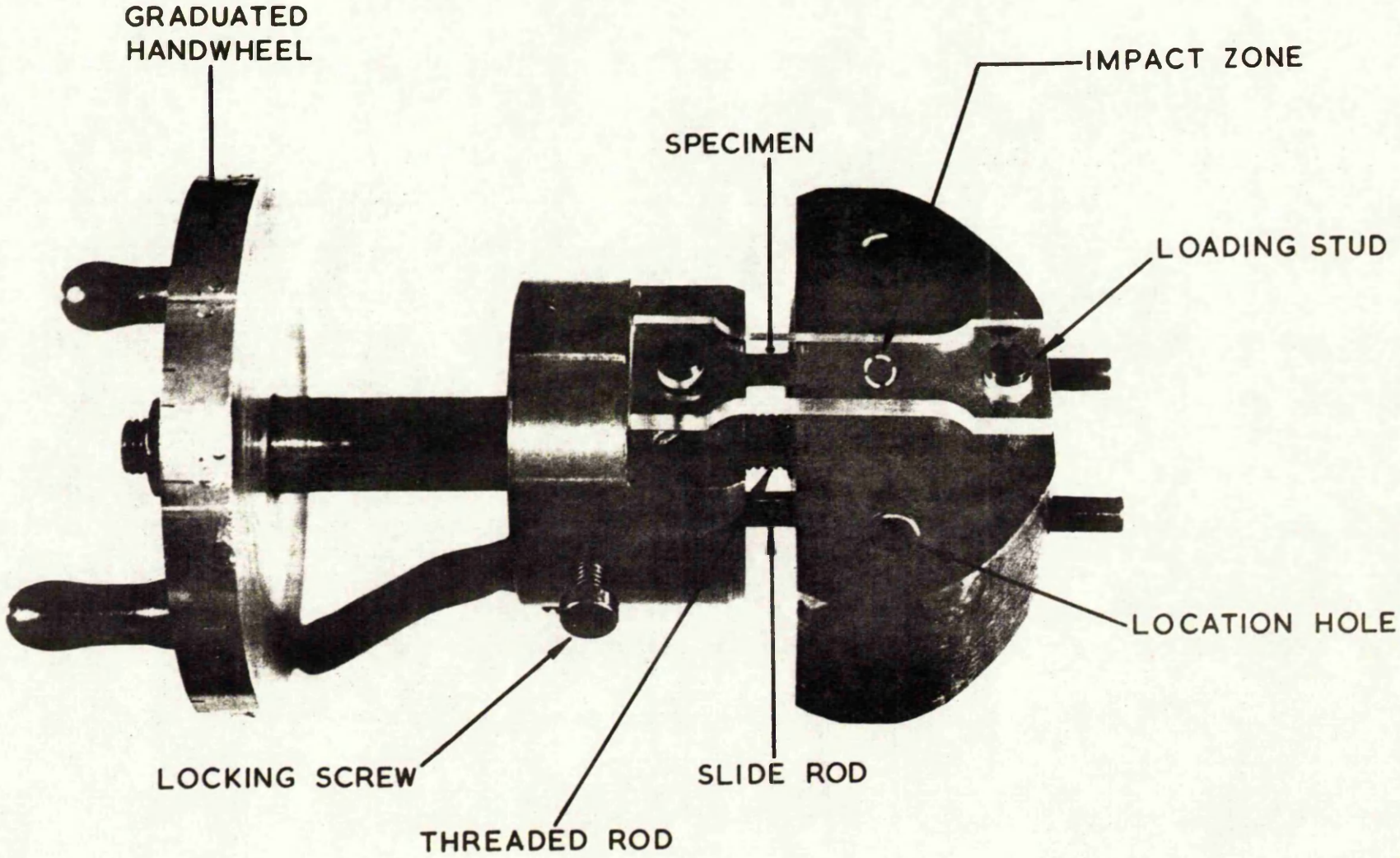

FIG. 5.1 LOADING FIXTURE

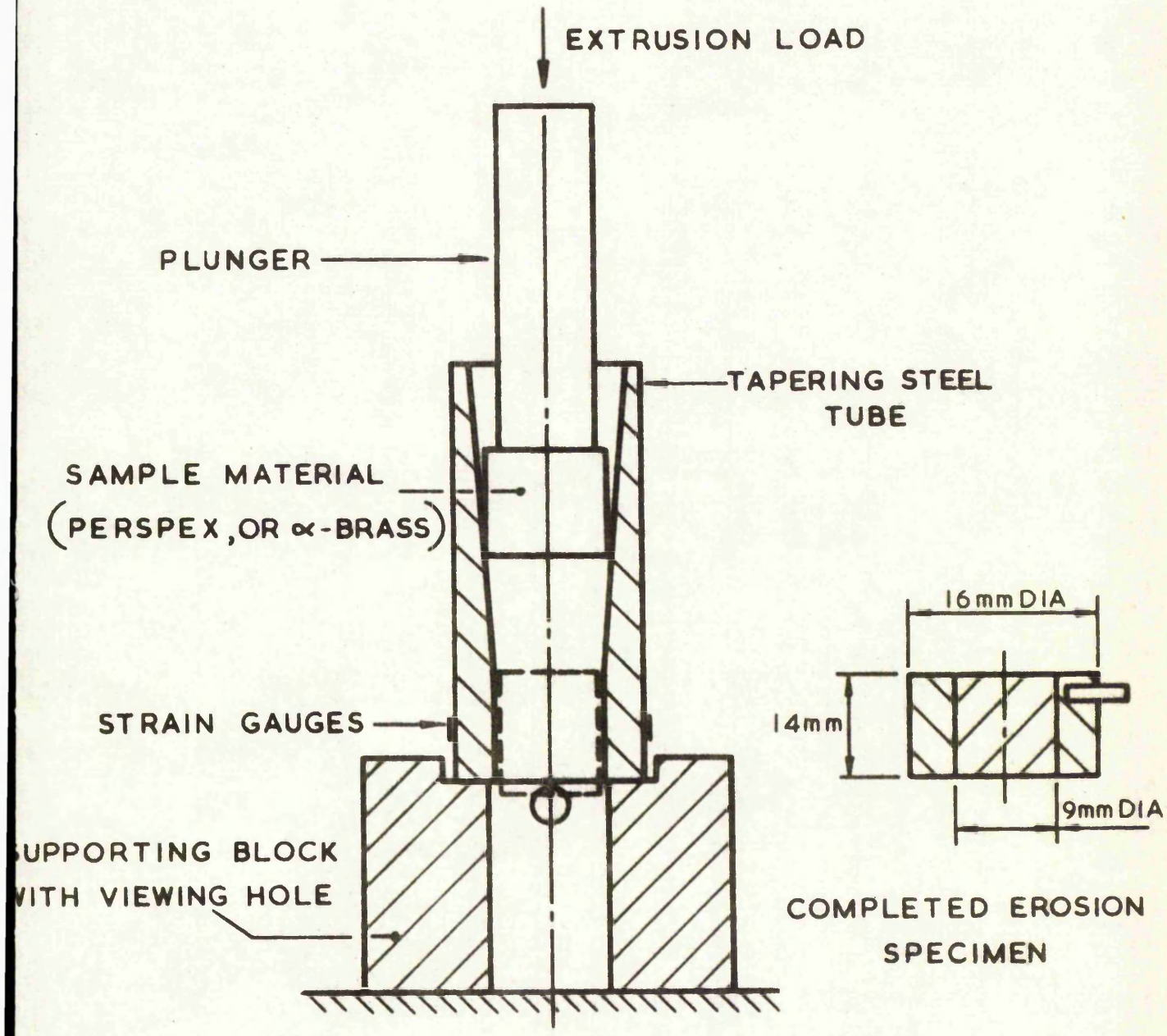

FIG. 5.2 ARRANGEMENT FOR SUBJECTING SPECIMENS TO BIAXIAL COMPRESSION

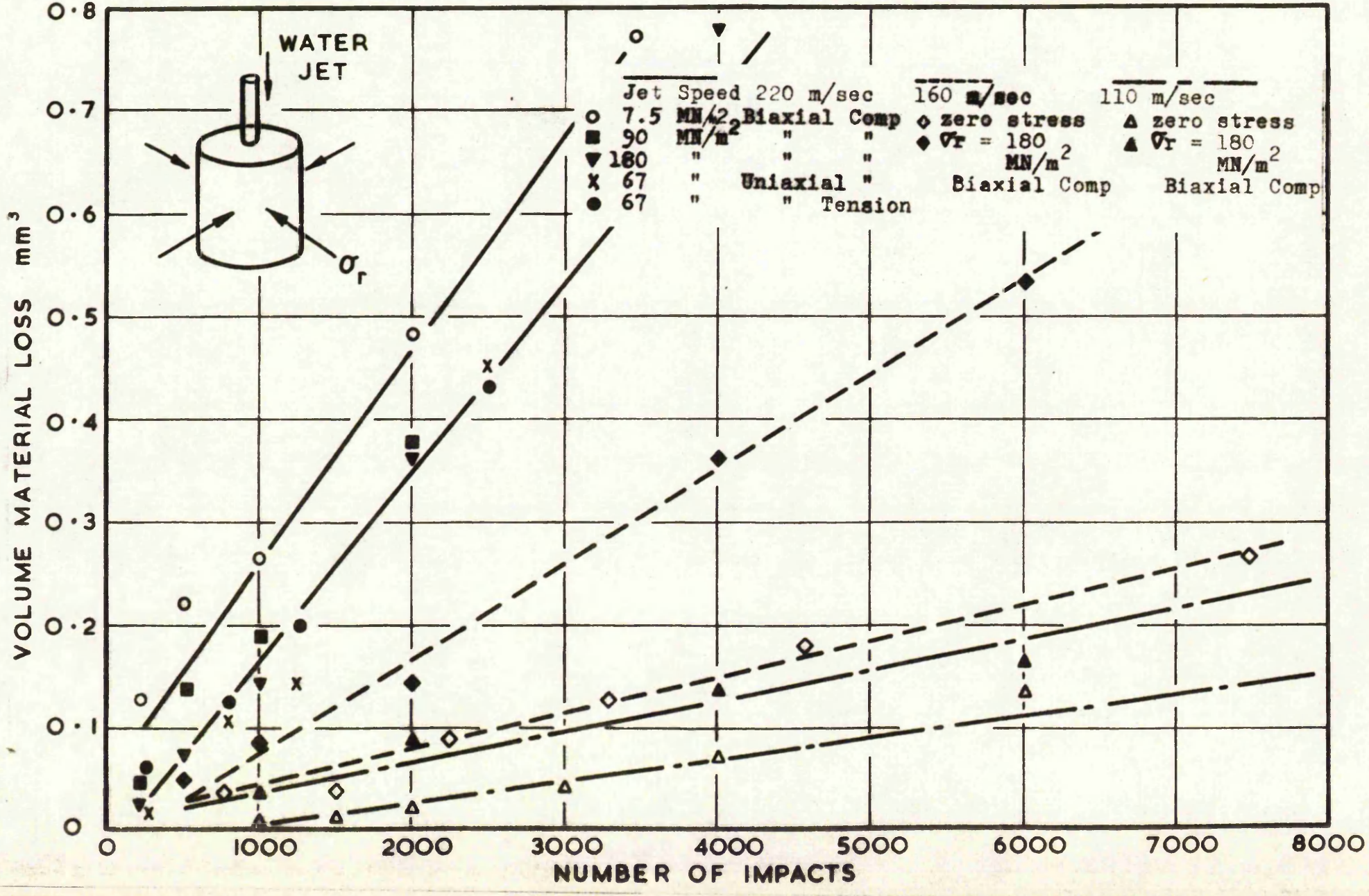

Fig. 53 - Brass Erosion Versus Number of Impacts

(i) IMPACT IMPRESSION

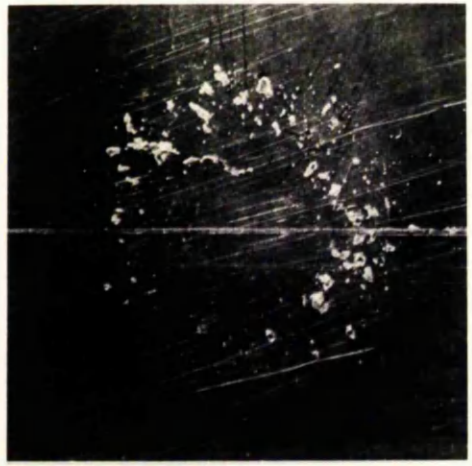

x 20

(ii) ZERO PRE-STRESS (20,000)

x60

(iii) 225 MN/mm² BIAXIAL COMP. (14,000)

x60

DIRECTION WATER FLOW

FIG. 5·4 COMPARISON OF PIT SIZE, WITH TARGET PRE-STRESS. 60 m/sec JET VEL.

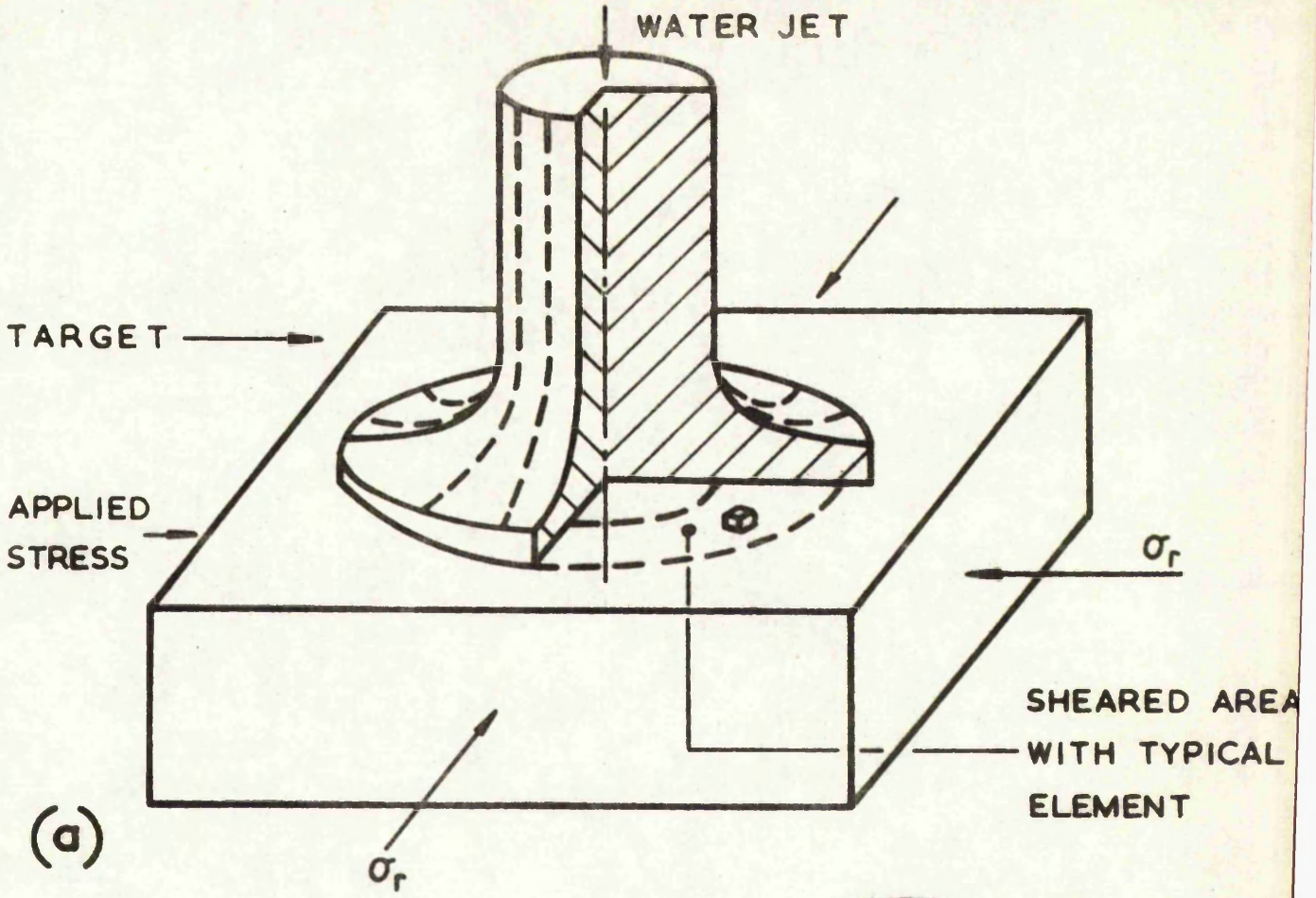

(a)

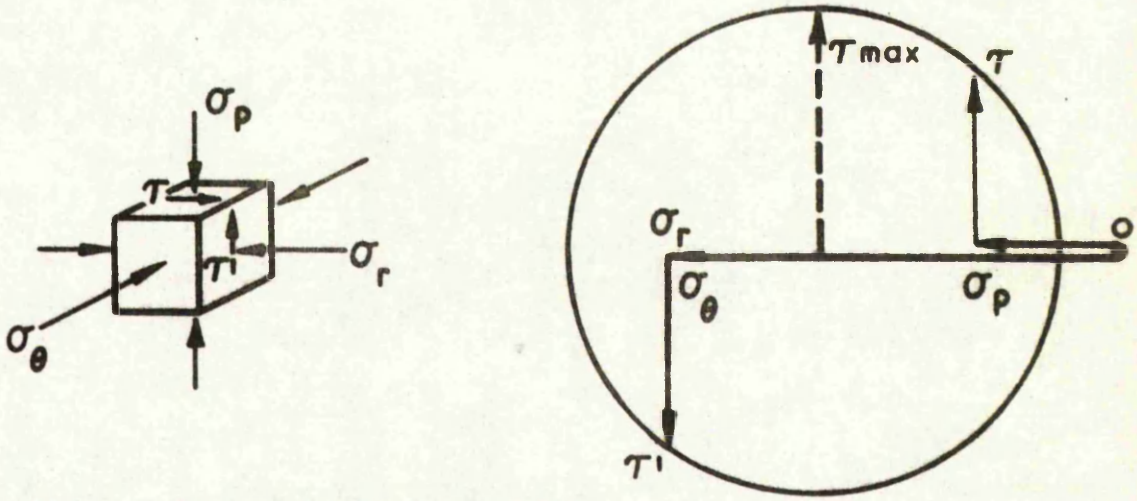

(b) TARGET SUBJECT TO BIAXIAL COMP

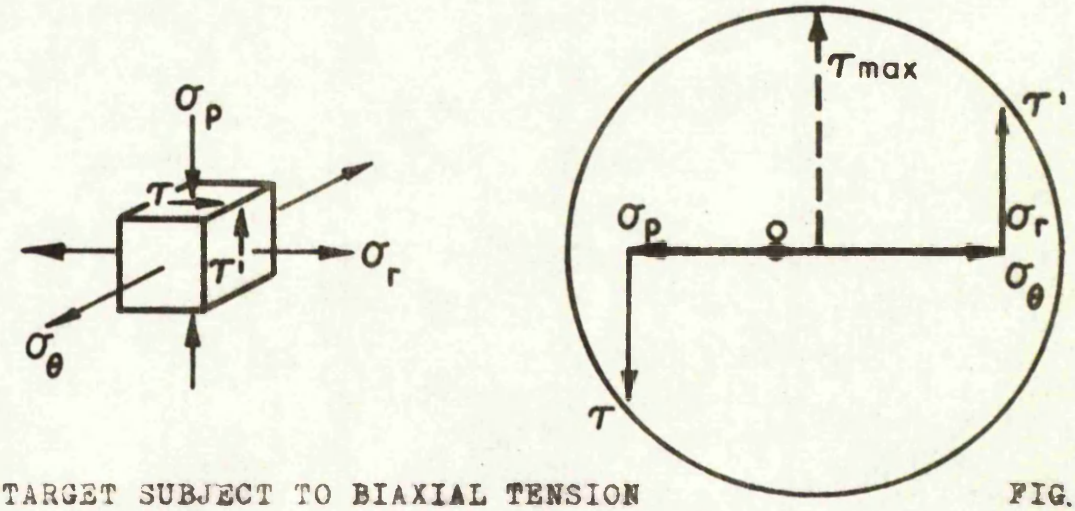

(c) TARGET SUBJECT TO BIAXIAL TENSION

FIG. 5-5

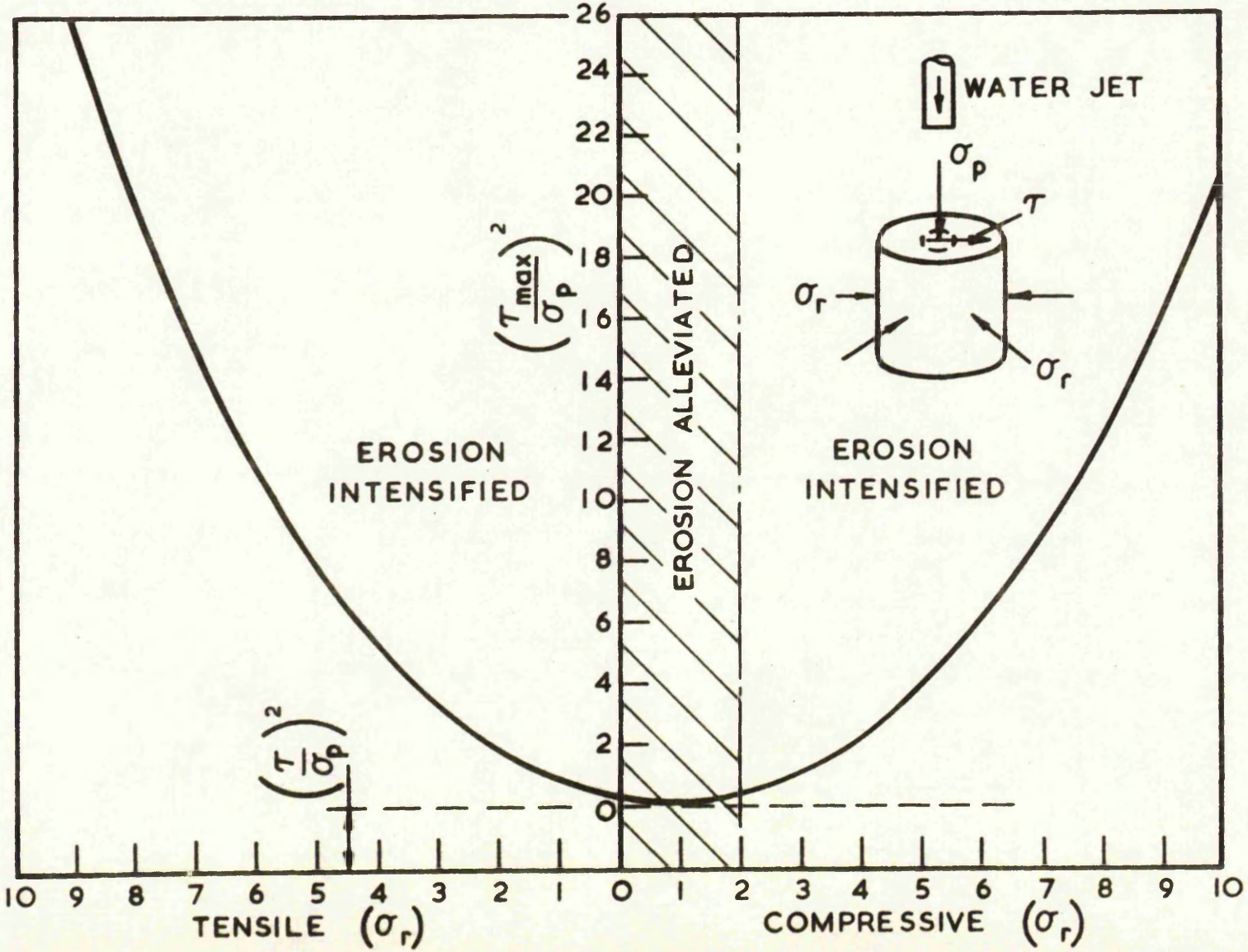

FIG. 5.6 SHEAR STRESS VERSUS RATIO σ_r/σ_p

FIG. 5.7 ∝ - BRASS INDENTATION VERSUS NUMBER OF IMPACTS

JET SPEED 220 m/sec; ○ - zero, ● - 75, ■ - 90

▼ - 180 MN/m^2 COMPRESSIVE STRESS

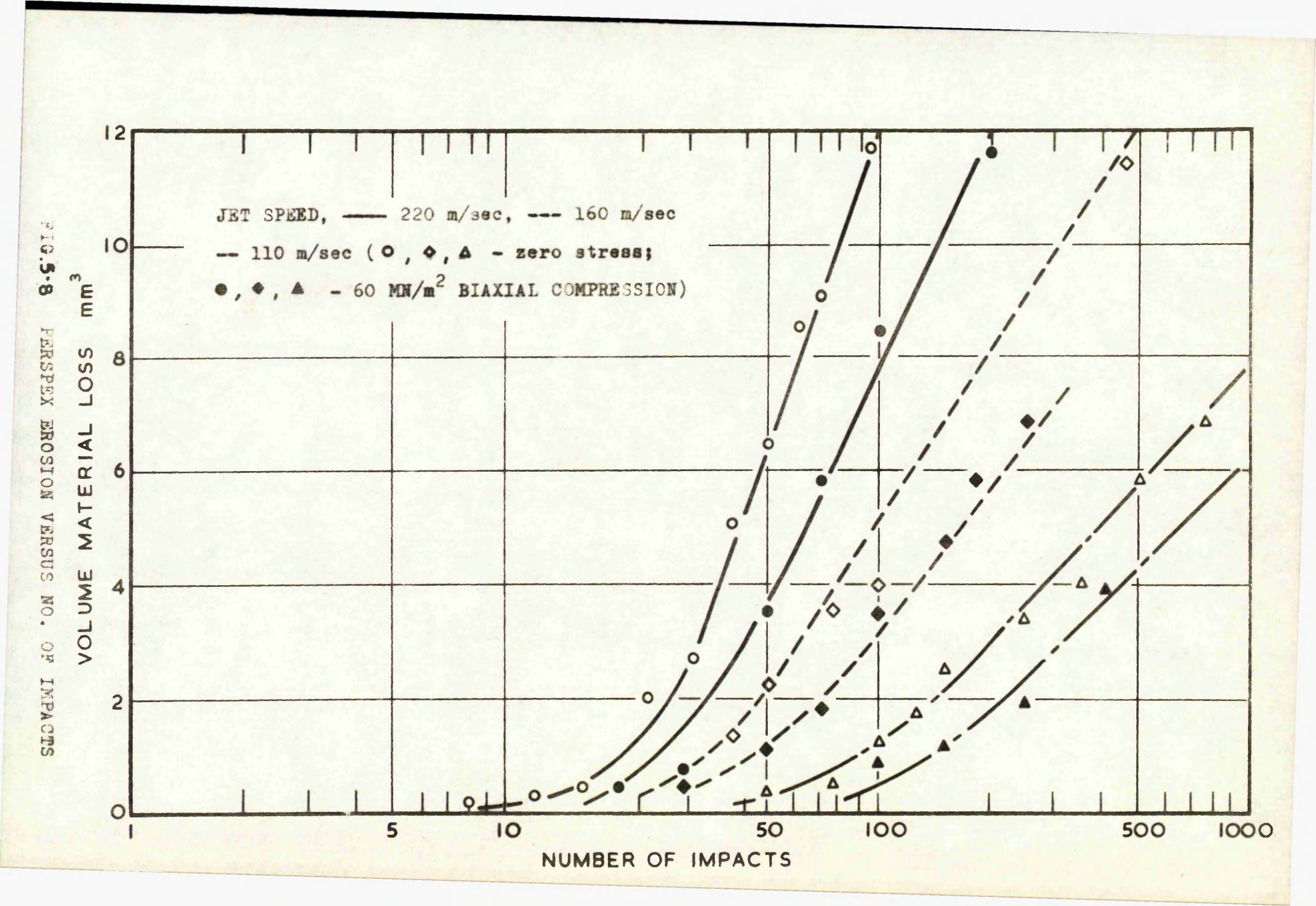

FIG 5.8 PERSPEX EROSION VERSUS NO. OF IMPACTS

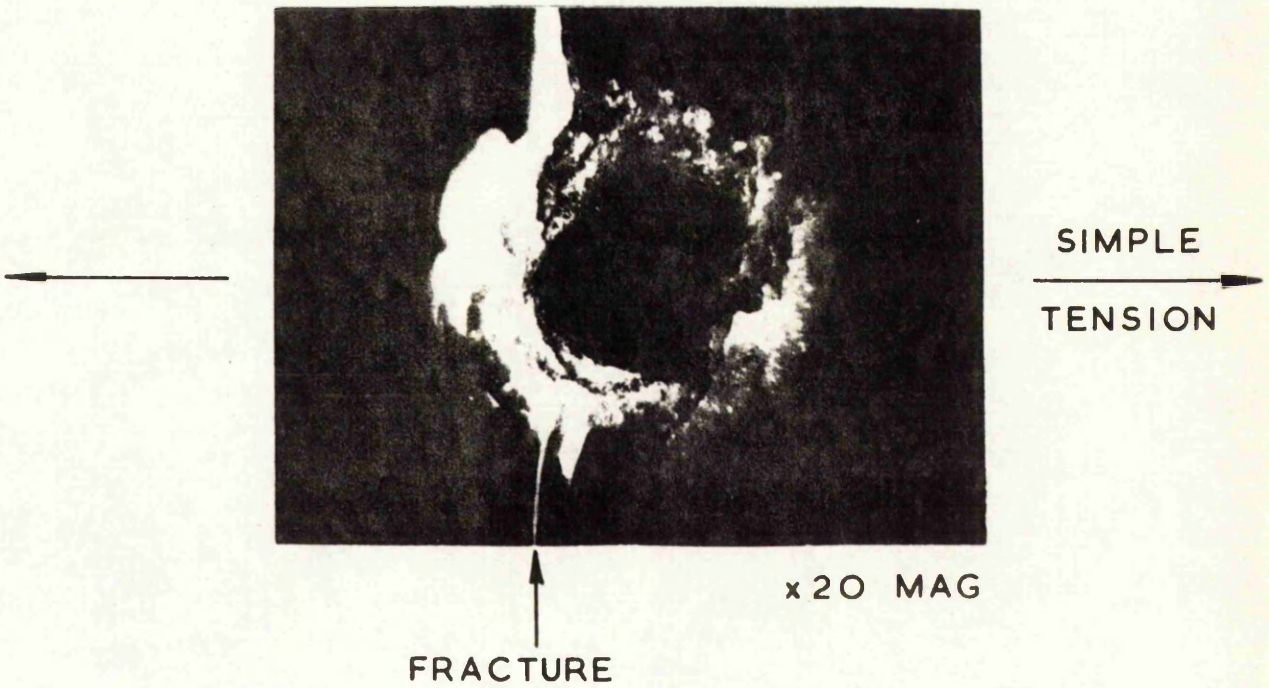

FIG. 5.9 PERSPEX TENSION TARGET, JET SPEED 110 m/sec

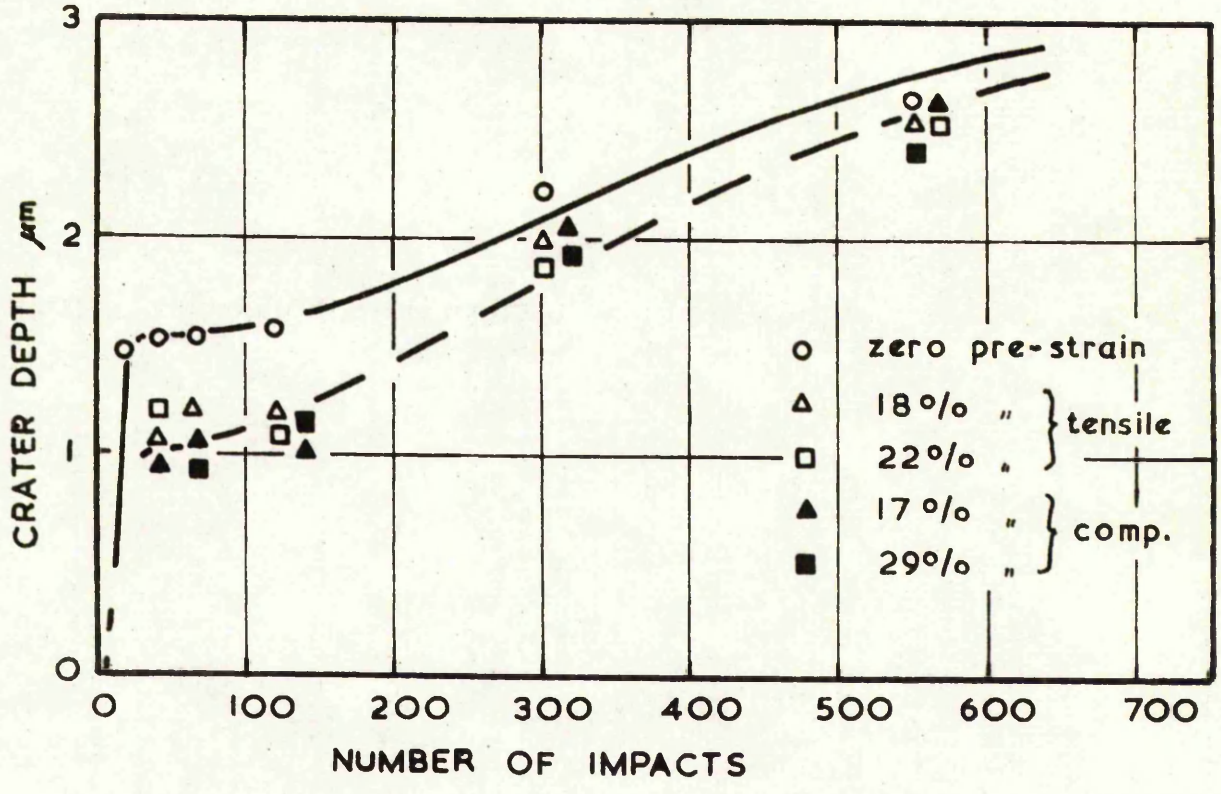

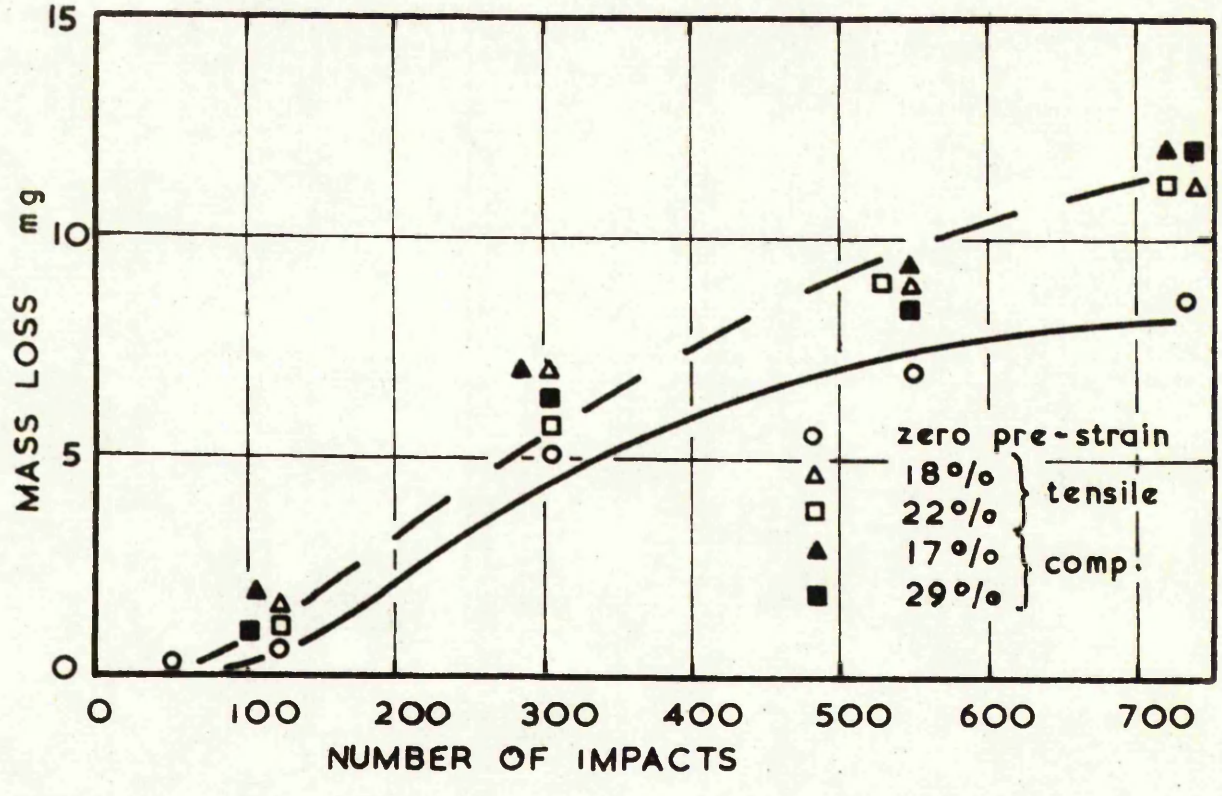

FIG.5·10 VARIATION OF MASS LOSS AND CRATER DEPTH WITH PRE-STRAIN

CHAPTER SIX

CHAPTER SIX

JET FLOW AGAINST CONVEX, CONCAVE AND FLAT INCLINED SURFACES

The damage resulting from water jet impact on convex, concave and flat inclined Perspex targets is reported as below. The direction and distribution of surface cracks and pits within the zone of impact are related to liquid flow during impact and the essential features of such impact damage are analysed in terms of stress wave phenomena.

6.1 INTRODUCTION

A hard polymer, or other brittle material, when subject to normal impact by a liquid drop or jet forms an annulus of discrete cracks surrounding an undamaged central area. Liquid flowing radially outwards removes projecting material from the zone of ring fracture. Examination of the shear pits thus formed shows the direction of liquid flow as material is removed from the outer part of the cracks as discussed in Chapter three. The distribution of shear pits also indicates that liquid flow across the surface does not occur, to any marked degree, within a central area bounded by the inner diameter of ring cracks and indeed flow increases rapidly outside this area.

The diameter and distribution of surface cracks and shear pits gives a good insight into the impact situation. Bowden and Field [12] have considered the case of a spherical drop, radius, r, colliding normally at velocity, v, with a flat rigid solid. On impact the circular area of contact spreads out more rapidly than the compression wave in the droplet and outward flow is prevented. As the drop advances, the expansion of contact area becomes progressively slower and a point is reached where flow at the periphery of contact becomes possible. From simple geometry the radius, x_o, of this region is given by

$$x_o \simeq r.v/c \qquad (6.1)$$

where c is the speed of compressive waves in the liquid.

Experiments by Hancox and Brunton [66] concerned with the impact between a flat specimen and the side of a cylindrical jet identified a central undamaged band. The width of this band, which they expressed in terms of, β, the angle subtended at the centre of the jet between the line of first contact and line along which appreciable flow begins, was shown to be larger than 2 x_o from equation (6.1) by almost an order of magnitude. The experiments were conducted with specimens of Perspex and aluminium striking water jets of 0.42, 1.35 and 2.54 mm diameter at impact velocities of 30 to 80 m/sec. Also a mercury jet of 1 mm diameter was struck at velocities from 152 to 183 m/sec. The error in results was attributed to neglect of viscosity in the analysis so that at very small values of β the liquid fails to flow.

An extension of the above theoretical treatment was given by Thomas [128] in which he asserts using Bernoulli's theorem, that flow would not start until some time after the compression wave had first reached the free surface of the liquid. The resulting expression is given as

$$x_o = r\sqrt{v/2c} \qquad (6.2)$$

Using equation (6.2) agreement with the observed values from Hancox and Brunton's work is much improved.

This chapter describes experiments with approximately flat topped water jets impinging at 220 and 110 m/sec on convex, concave and flat inclined surfaces. The dissimilar flow patterns, as indicated by surface pitting, are examined and a comparison made of theoretical and observed values of 2 x_o over a wide range of target curvature. Also an analysis substantiated by experimental work is given for flat inclined surfaces.

6.2 THEORETICAL JET IMPACT

6.2.1 Jet impact on convex surfaces

As a flat topped water jet of diameter d, impinges at velocity v, on a cylindrically convex solid surface of radius r, a point P at the junction of the curved surface of the target and the jet moves radially outward with speed $\dot{x}$, see Fig. 6.1(i). Now

$$\dot{x} = \frac{d}{dt}(r \sin\theta) = r.\cos\theta \,.\, \dot{\theta}$$

and

$$v = \frac{d}{dt}(r \cos\theta) = r.\sin\theta \,.\, \dot{\theta}$$

so that

$$\dot{x} = v \cot\theta \qquad (6.3)$$

From equation (6.3) it can be seen that on initial contact the point P moves more rapidly than the compression waves in the liquid and flow does not occur. As the jet advances $\dot{x}$ falls below c and liquid flow starts before the colliding surface arrives and incompressible flow is possible. The limiting case, as defined by length of contact $2x_o$ is, from equation (6.3)

$$\dot{x} = c = v \cot\beta \simeq v.\frac{r}{x_o}$$

or

$$\frac{2x_o}{d} = \frac{2v.}{c}\,\frac{r}{d} \qquad (6.4)$$

6.2.2 Jet impact on concave surfaces

When a cylindrical colum of liquid impinges on a concave solid surface of large radius of curvature r, the concave surface fills with liquid in time t, which is determined by the leading edge of the jet travelling a distance y, at velocity v, as shown in Fig. 6.1 (ii). The time is given by

$$t = y/v = r\,(1 - \cos\phi\,)/v \qquad (6.5)$$

where $\phi = d/2r$

During this time the liquid travels outwards from the initial jet contact point at velocity w. Thus the entrapped liquid defined by a distance

$2\,x_o$ is

$$2.x_o = d + 2.w.t \qquad (6.6)$$

Substituting for time in equation (6.6) and rearranging gives

$$\frac{2\,x_o}{d} = 1 + 2\,\frac{r}{d}\,\frac{w}{v}\,(1 - \cos\phi) \qquad (6.7)$$

The steady state value of w along the surface for a two dimensional jet can be shown, from momentum considerations, to be the same as the jet velocity. However, Bowden and Brunton [11] found the tangential flow along the surface immediately following impact to be two to three times the jet velocity and it is related with the profile geometry of the jet head and target by

$$w = v \cot \alpha/2 \qquad (6.8)$$

where α is the wedge angle which the sloping face of the jet makes with the target.

As the jet used in the experiments is not cylindrical but has a flat topped mushroomed-shaped head an estimate of α may be obtained from enlarged shadowgraphs of the jet profile. With concave surfaces of $\frac{1}{4}$ in, $\frac{1}{2}$ in, and infinite radius, values of w become 14, 8 and 5 times the jet velocity. It can be shown that as α tends to zero the mass and momentum of the liquid flowing from under the wedge also tends to zero and thus the above theoretical values of w are probably an over-estimate; this is particularly so as Levin and Hobbs [96] show radial flow of water drops on slightly convex surfaces as being only approximately six times greater than the impact speed. This latter value is selected as the most likely value of w appertaining to a shrouded tipped jet.

If compression waves in the jet reach the jet axis before the leading edge of the jet impinges on the bottom of the convex surface i.e. when

$$d/2c > r\,\frac{(1 - \cos\beta)}{v}$$

then a micro-jet forms travelling in advance of the main jet. The micro-jet impact will probably damage the target apex and incompressible sideways flow will take place before impact from the main jet. Thus with convex surfaces, inward flow of liquid occurs when

$$r \leqslant \frac{d.v}{2c(1-\cos\beta)} \qquad (6.9)$$

The speed of inward movement of a point P at the junction of the target and jet is given by equation (6.3). For the case where inward incompressible liquid flow commences, then as given in equation (6.9), the value of $\dot{x}$ at a radius of d/2 is

$$\dot{x} = \frac{v^2}{c(1-\cos\beta)} \qquad (6.10)$$

It is clear that if the speed of the compression waves in the liquid, c, is greater than $\dot{x}$ at radius d/2 there will be a limited inward motion until the two are equal at a distance from the jet axis defined by equation (6.4). The radius of curvature of a convex surface at which $c = \dot{x}$ at distance d/2 from the jet axis and hence at which there is no inward fluid motion is given, from equation (6.3) as

$$r = \frac{dc}{2v} \qquad (6.11)$$

6.2.3 Jet impact on flat inclined surfaces

As a liquid jet impinges obliquely, at velocity v, on a flat surface a compression wave propagates, at velocity c, from the initial contact point, A, into the body of the jet. On encountering a free surface at the rear of the jet a tensile release is formed which disrupts the jet and enables liquid to flow away from the surface before impact with the target occurs. Thus the position of the release wave at B given in Fig. 6.1 (iii) when contact occurs between B and D, determines the length of impression AD or $2x_o$.

The time taken, t, for the compression wave to travel from A to C and for the release wave to return back to B is given by,

$$t = \frac{d + \delta}{c} = \frac{(d - \delta)\tan\alpha}{v}$$

or

$$d\left(1 - \frac{v}{c}\cot\alpha\right) = \left(1 + \frac{v}{c}\cot\alpha\right),$$

so that

$$\delta = \frac{d\,(1 - v\cot\alpha/c)}{(1 + v\cot\alpha/c)} \qquad (6.12)$$

Now

$$d = 2x_o\cos\alpha + \delta$$

which upon substitution into equation (6.12) gives

$$2x_o = d\sec\alpha\left[1 - \frac{(1 - v\cot\alpha/c)}{(1 + v\cot\alpha/c)}\right]$$

and hence

$$\frac{2x_o}{d} = \frac{2}{c.\sin\alpha/v + \cos\alpha} \qquad (6.13)$$

If the speed of contact between the leading edge of the jet and the target is faster than the speed of travel of the compression wave then flow is restricted to that of normal impact. The limit of this condition occurs when $\zeta = o$ and by substitution in equation (6.12) we have

$$\frac{v}{c} \cot \alpha - 1 = o$$

Hence normal impact occurs when

$$o \leqslant \alpha \leqslant \cot^{-1} c/v \qquad (6.14)$$

If

$$\alpha > \cot^{-1} c/v$$

disruption of part of the jet occurs prior to impact and the limits of incompressible liquid flow are defined by equation (6.13).

6.3 EXPERIMENTAL RESULTS AND DISCUSSION

Water jets, produced by the repetitive gun described in Chapter 2, were fired at a series of convex, concave and flat incline Perspex specimens at speeds of 110 and 220 m/sec. A sufficient number of impacts were made to give clear, measurable target damage whilst this varied with target shape, was typically 20 to 50 impacts. The impression thus formed consists of an oval annulus of finite cracks as shown in Fig. 6.3. The extent of the impression measured in a transverse direction across the incline, or the curved surface, is similar to the diameter of a normal impact impression. However, the length of undamaged target, in the $2x_o$ direction, becomes extended with concave, and reduced with convex and inclined surfaces. In all cases the $2x_o$ dimension was measured using a travelling microscope with vernier attachment.

6.3.1 Convex and concave surfaces

Results of tests with water jets impinging at 110 m/sec on Perspex rods of 0.35 mm to 25.4 mm radius are given in Fig. 6.2. Also shown are the theoretical curves from equations (6.1) and (6.2) and the experimental

results of Hancox and Brunton [66] using water and mercury jets.

These show that the distance $2x_o$ across the impression is represented reasonably by equation (6.1) for large curvature surfaces. When 1/r becomes greater than one mm^{-1} equation (6.2) gives a better approximation and the effect of viscosity may be significant at small radii as suggested by Thomas [127]. A scanning electron micrograph of a small radii target is shown in Fig. 6.3 (iii) .

Some disparity exists between the present results and those given by Hancox and Brunton [66]. Differences in experimental techniques may account for this and may be summarised as

(i) the target and not the liquid is convex;

(ii) the impact is three and not two-dimensional;

(iii) the jet speeds are 110 and 220 m/sec and not 30 to 80 m/sec.

Other tests were conducted on convex and concave surfaces of 0.4 mm to infinite radius with water jet speeds of 110 and 220 m/sec. Variation of undamaged central area with radius, expressed in dimensionless form, is given in Figs. 6.4 and 6.5. Size of jet head diameter was estimated from enlarged shadowgraphs as 2.6 mm and 2.2 mm for 220 and 110 m/sec jets respectively; these values were not precisely measurable as water spray obscured the leading edge. The results show clearly that equation (6.4) gives a better estimate of $2x_o/d$ on large curvature convex surfaces than equation (6.2). With large curvature concave surfaces the $2x_o$ dimension becomes the major axis of the oval impression and is adequately represented by equation (6.7), with $w = 6.v$.

Onset of inward flow with increased target concavity is in close agreement with the radius indicated by equation (6.9). The different flow patterns are clearly shown by the scanning electron micrographs in Fig. 6.3

where (i) gives an oval pattern formed by outward liquid flow on a large radius of curvature concave target while (ii) gives cracks along the surface trough and damage due to inward flow on small radius concave targets. With 110 m/sec jets the critical radius of 8.5 mm (from equation 6.9) falls between the two specimens of 9.5 and 6.4 mm radius where change of flow, from outward to inwards, occurs. Similarly, with 220 m/sec jets the theoretical radius of 5.7 mm lies between the two specimen where change of flow occurs.

A crack is formed along the trough of the concave surface and always appears when the water flow is inward it becomes more clearly defined at faster speeds, and is due to two streams of liquid converging at the centre of the target in a way similar to that of explosive welding[3]. Fig. 6.3(ii) also shows a band of negligible damage enclosed between the inward flow cracks. This band occurs where $\dot{x} > c$ and may be represented by equation (6.3). Results for the slower jets are given in Fig. 6.4 but with faster jets the band is not measurable as extensive central crack damage obscures this region.

In the experiments, no cracking was evident due to the limited inward flow between radii defined by equations (6.9) and (6.11). This would seem to indicate that further water flow is necessary before cracking occurs.

6.3.2 Flat inclined surfaces

Water jets travelling at 110 and 220 m/sec were allowed to impinge on flat Perspex targets at angles of incidence of 0^{o} to 60^{o}. Increase in impact angle shortened the undamaged central area, defined by $2\,x_{o}$. The results which are shown in Figs. 5.6 and 5.7 and show satisfactory agreement with the theoretical values defined by equation (6.13).

The validity of this model is further substantiated by a central jet impact on the apex of two flat inclined surfaces; half the jet flows down each

surface. Equation (6.13) is still true for this case and agreement exists in Fig. 6.12 for 10^{o} inclined surfaces or 160^{o} included apex angle.

6.4 CONCLUSIONS

Experiments show clearly that stress wave phenomena may be successfully employed to predict occurrences in liquid-solid impact situation with respect to the direction and position of appreciable liquid flow within the impact zone. A detailed discussion has been presented of the damage resulting from water jet impact on concave, convex and flat inclined surfaces.

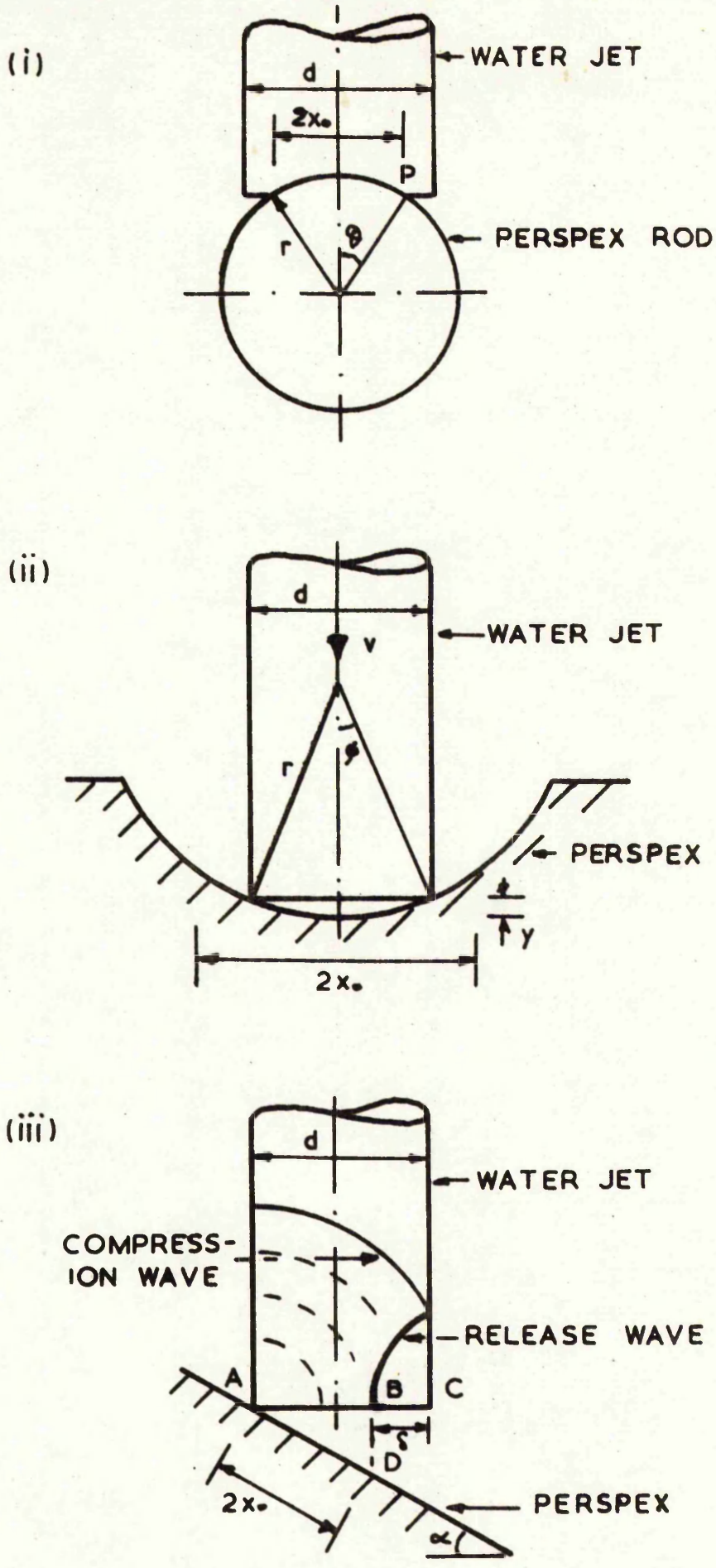

FIG. 6·1 DIAGRAM OF JET IMPACTS

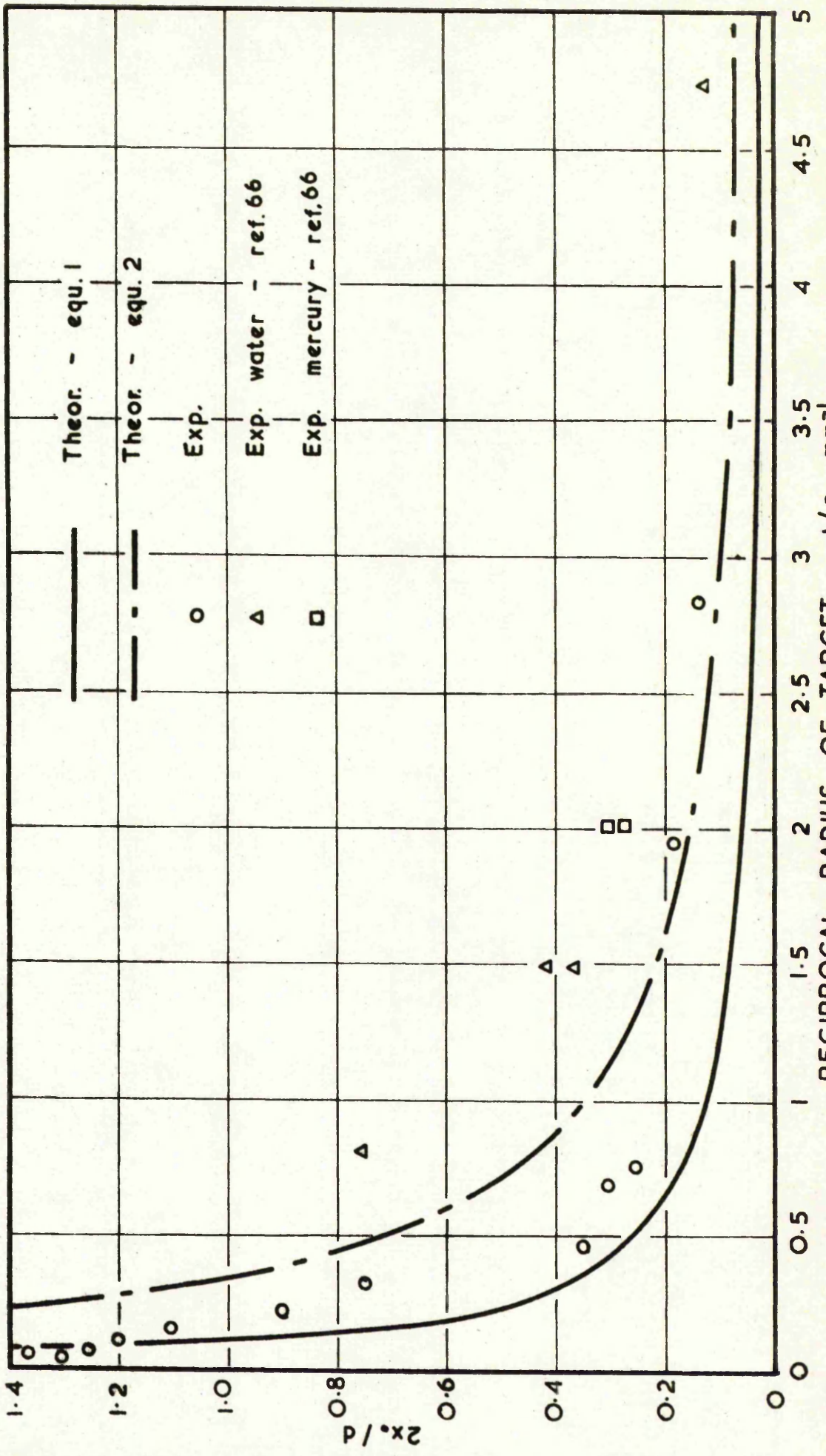

FIG.6·2 IMPRESSION SIZE VERSUS TARGET RADIUS
110m/sec VELOCITY

(i)

Concave surface

d = 19 mm

110 m/sec jet

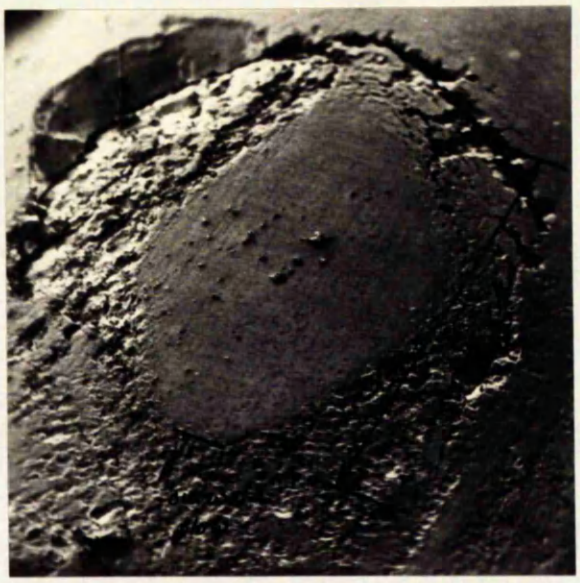

(ii)

Concave surface

d = 7.8 mm

220 m/sec jet

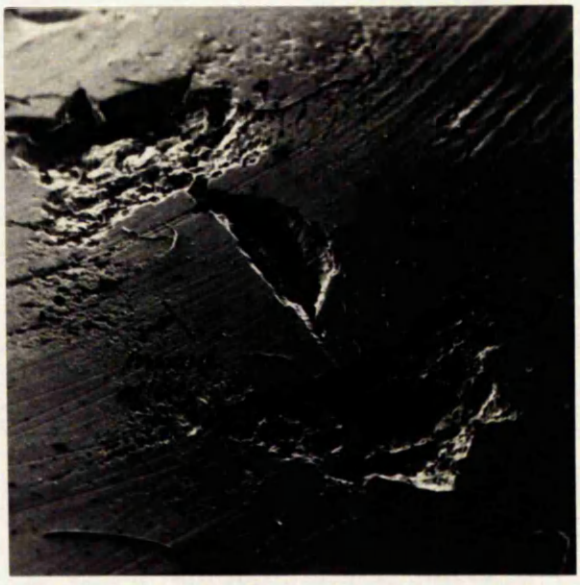

(iii)

Convex surface

d = 1 mm

110 m/sec jet

FIG. 6.3 SCANNING ELECTRON MICROGRAPH OF EROSION CRATERS

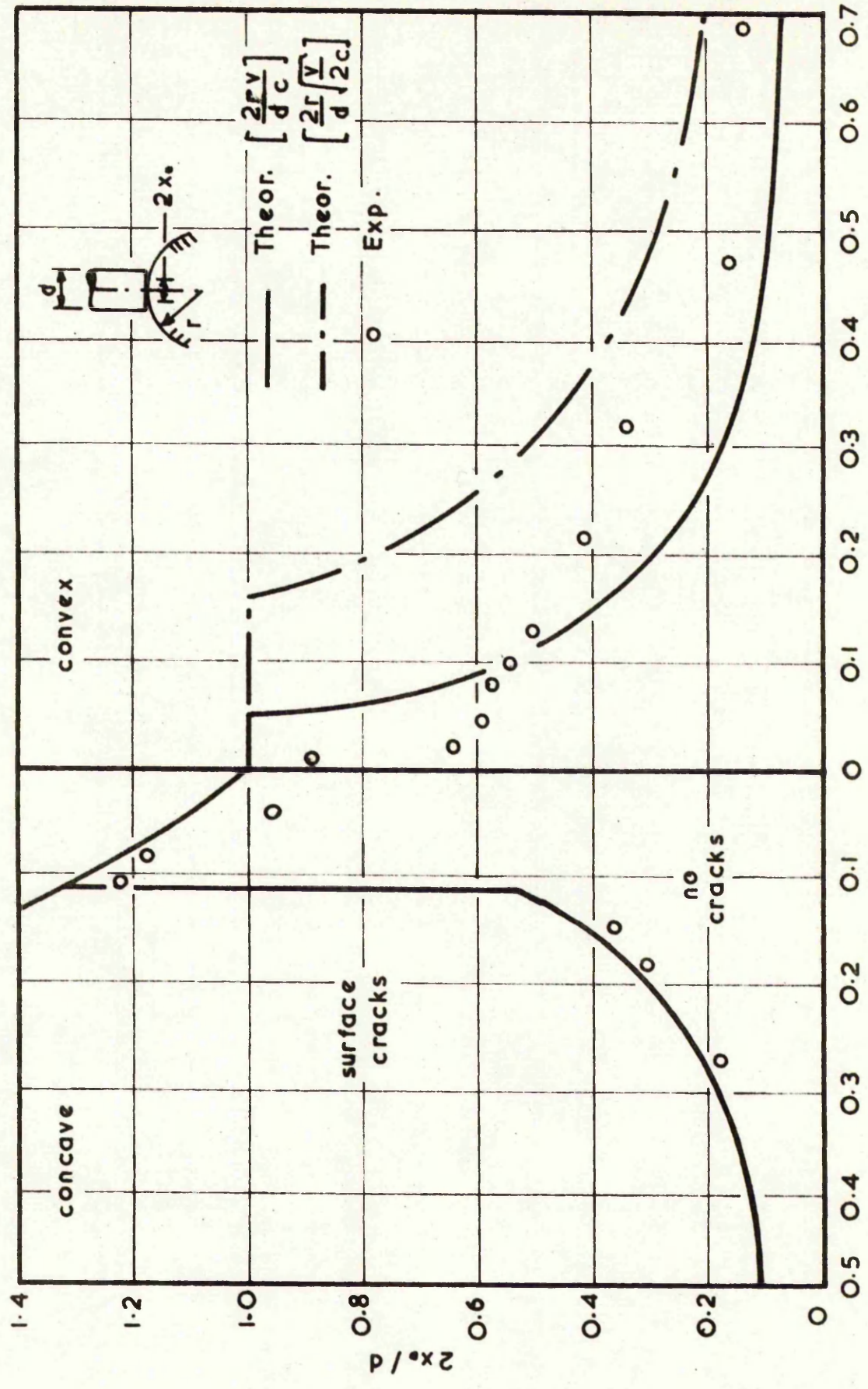

FIG. 6·4 IMPRESSION SIZE VERSUS TARGET RADIUS
110 m/sec VELOCITY

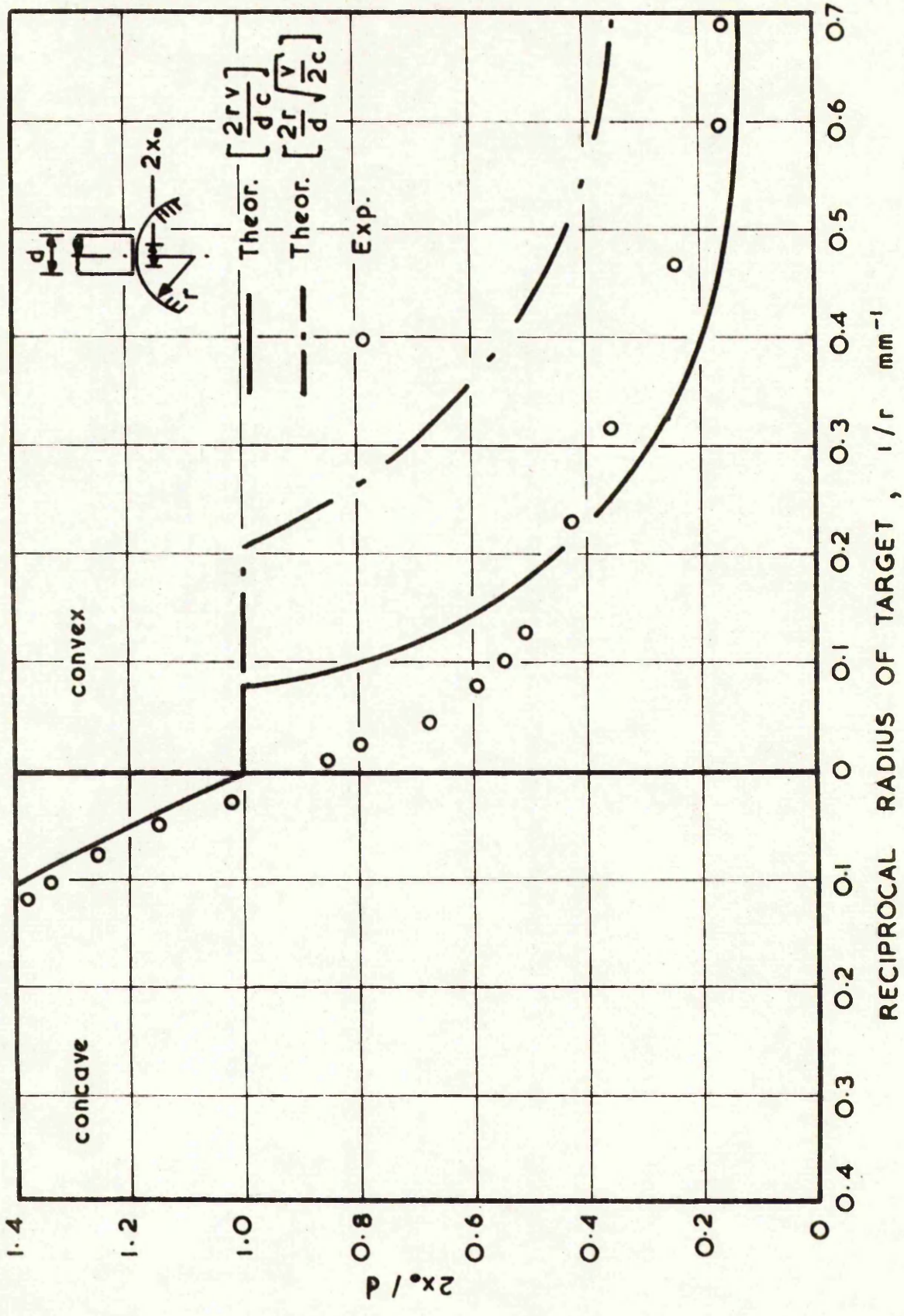

FIG.6·5 IMPRESSION SIZE VERSUS TARGET RADIUS

220 m/sec VELOCITY

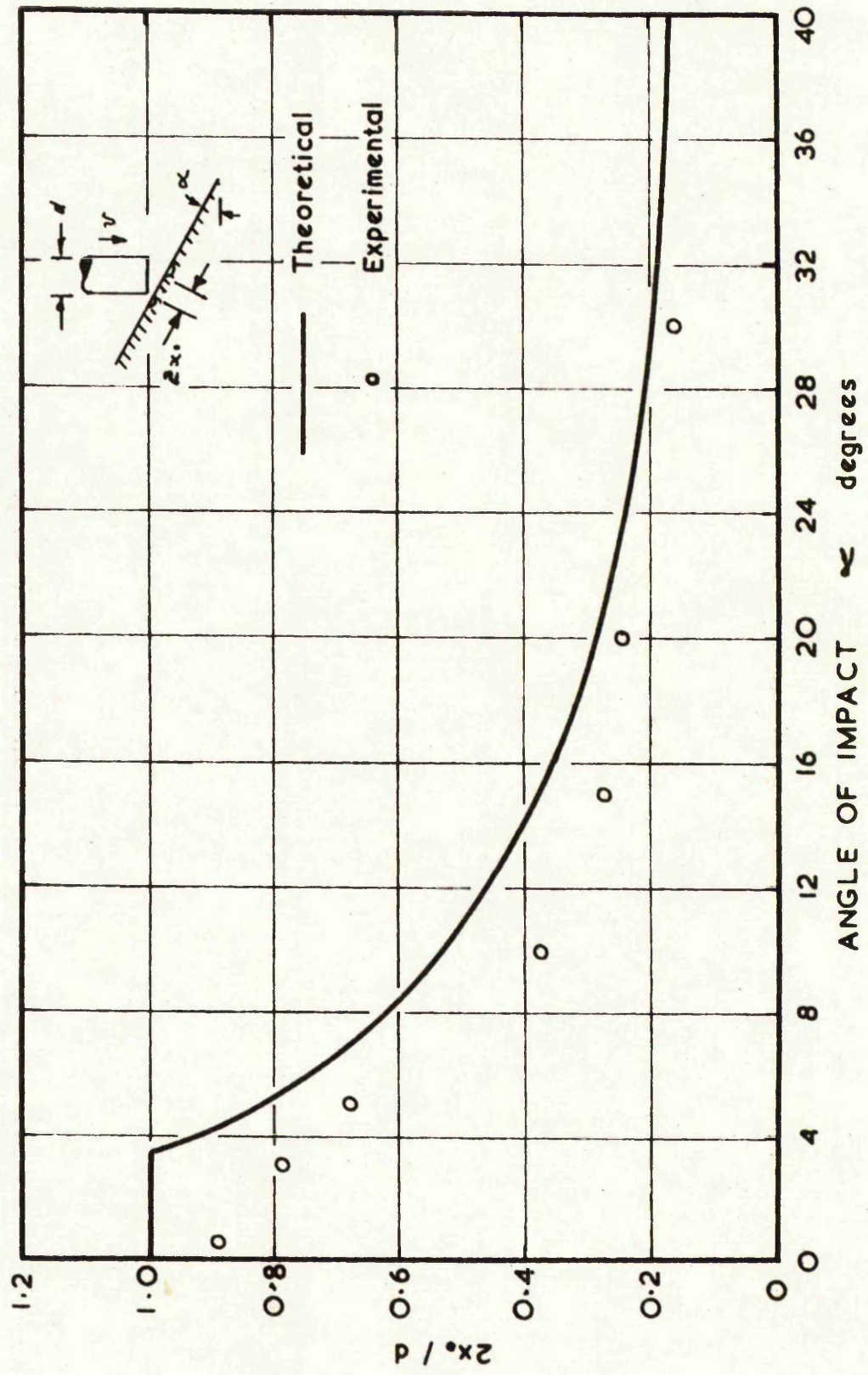

FIG.6·6 IMPRESSION SIZE VERSUS NUMBER IMPACTS
110 m/sec VELOCITY

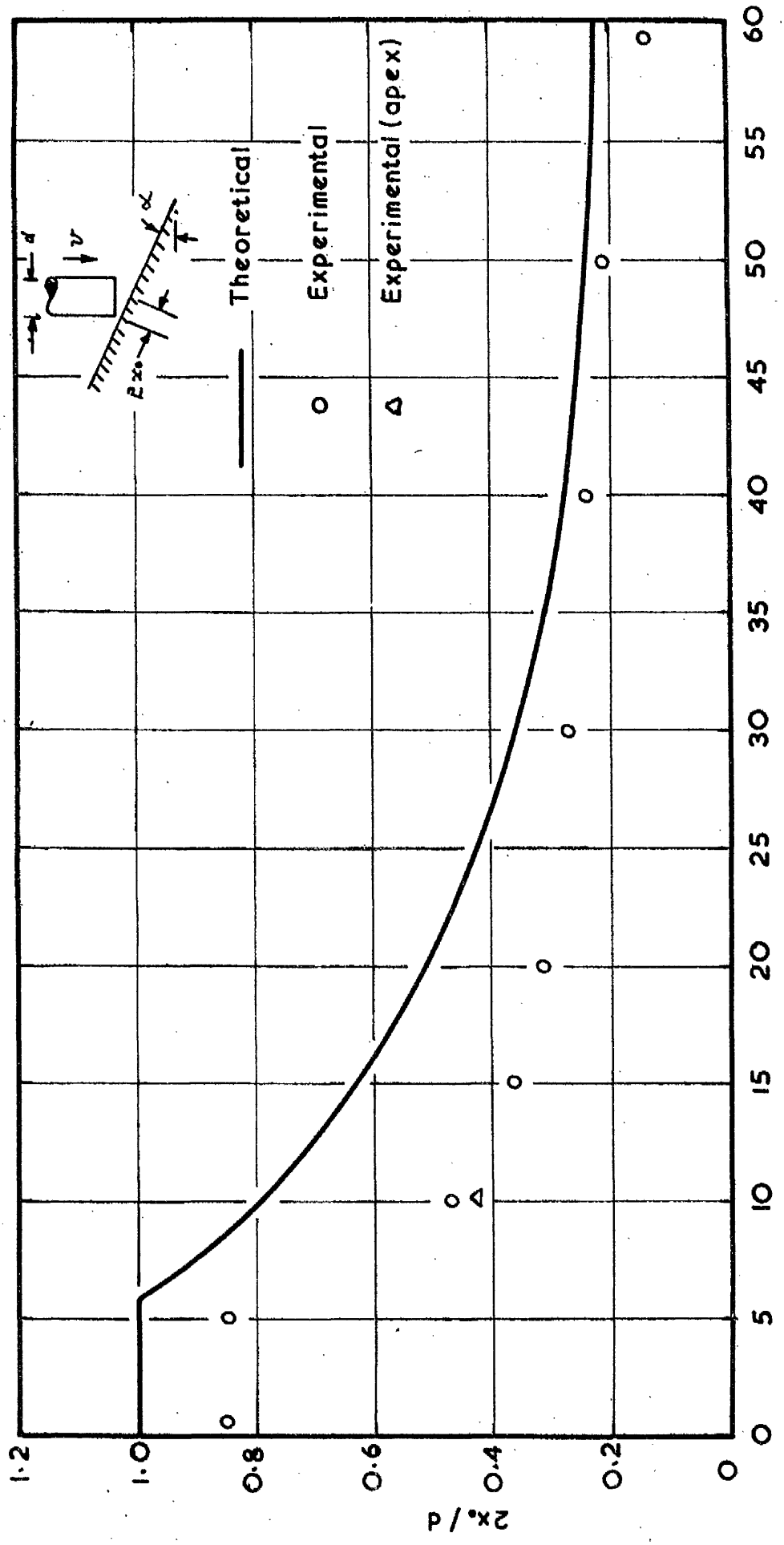

FIG. 6·7 IMPRESSION SIZE VERSUS NUMBER IMPACTS

220 m/sec VELOCITY

CHAPTER SEVEN

CHAPTER SEVEN

PENETRATION AND PERFORATION

7.1 INTRODUCTION

This Chapter deals with some aspects of the penetration of relatively large blocks of material - nominally semi-infinite masses - and the perforation of thin plates, by water jets.

An early penetration equation assumed that resistance to penetration was constant, but a more general form used by Allen [1] assumes the resisting force to be a function of projectile mass and velocity. Taylor [8] and later Rostoker [108] assumed that solid materials may be considered as incompressible fluids at sufficiently high speeds of impact and derived an expression for penetration in terms of target and projectile densities and projectile length. The hydrodynamic model considers a projectile of density, ρ_p, travelling at velocity, v, striking a semi-infinite target of density ρ_t and penetrating at velocity u. By applying Bernoulli's theorem to the pressure, p, on both sides of the stationary interface we have

$$p = \tfrac{1}{2}\rho_t u^2 = \tfrac{1}{2}\rho_p (v - u)^2 \qquad (7.1)$$

By neglecting the target resistance, which is justified when the velocity of impact is very high (i.e. in the regime indicated by 'damage number' [84] $\rho . v^2/\bar{Y}$ of 10^3) it can be shown that

$$P = L\sqrt{\frac{\rho_p}{\rho_t}} \qquad (7.2)$$

where P is the penetration and L is the length of jet.

Continuing this approach it has been shown in ref. 26 that the cross sectional area of the hole A' produced in the target by the projectile, area A_o, is given by

$$A' = \frac{A_o}{2\bar{Y}} \cdot \rho_p (v - u)^2 \qquad (7.3)$$

This assumes that the momentum transferred to the target results effectively only in lateral flow. Thus the ratio of the diameter of the crater, D, to the diameter of the projectile, d, when the target and projectile are of the same material, is given by

$$\frac{D}{d} = 0.35\, v \sqrt{\frac{\rho_t}{\bar{Y}}} \qquad (7.4)$$

Perforation of thin plates by conical ended indentors has also been analysed by Taylor [120], each element of the deformed plate material being assumed to form into a lip, on the reverse side of the plate, by 'hoop stretching' and 'rotation'. The analysis, assuming constancy of volume and strains of equal magnitude in both transverse directions (i.e. subject only to hoop stress), results in,

$$H = \frac{2}{3} R_o \qquad (7.5)$$

where H is the height of lip R_o is the radius of the cylindrical indenter.

7.2 EXPERIMENTS AND DISCUSSION

Water and mercury jets were projected at speeds of 100 to 800 m/sec at blocks of plasticine, and thin plates of lead and aluminium. Jets of two different diameter were used and in some tests the angle of impact and length of jet was varied. The ensuing deformations were recorded and are discussed below.

7.2.1 Penetration of plasticine

(i) Crater shape

Liquid jets produce well defined conical craters which do not resemble the hemispherical craters formed by other low strength projectiles, i.e.

plasticine projectiles against plasticine targets. The deformation is closely akin to that produced by short metal projectiles in clay or plasticine where the projectiles are undamaged and cause a hole of reducing diameter, or of conical shape, the diameter of the hole reducing as the speed of penetration decreases. With water jets the conical shape may reflect a reduction of jet speed or a diminishing jet diameter. It is interesting to note that lead projectiles fired into lead targets produce conical craters below a critical transition projectile velocity of 700 to 800 ft/sec but hemispherical above this velocity. As the transition occurs at a damage number of 350 and the water jet on plasticine condition has a greater damage number of 450, it is doubtful if the transition occurs in this case.

(ii) Depth of penetration

The depth of water jet penetration into semi-infinite blocks of plasticine increases with velocity as shown in Fig. 7.1. Carrell found a similar relationship with plasticine projectiles where depth of penetration became a maximum, equal to the length of the projectile. The damage number for maximum penetration with plasticine projectiles was 300 to 400 and with water jets 450 - a similar figure which seems to define a lower limit to the applicability of Taylors [8] hydrodynamic model.

Jet length estimated from the volume of liquid in the die was 63 mm which from equation (7.2) predicts a penetration of 44 mm into black plasticine of specific gravity of 2.1. This is similar to the 35 to 37 mm actual penetration. However, further experiments with only half the volume of liquid made no difference to penetration, indicating a fortuitous result above. It eventually transpired that there was ample liquid in the die but the jet length was determined by the length of the lead projectile which

extrudes the liquid jet. When this was reduced from $\frac{1}{2}$ in to $\frac{1}{4}$ in long, penetration dropped to 25 mm and with $\frac{3}{4}$ in and 1 in long lead projectiles, penetration increased to between 44 and 48 mm respectively. Projectiles longer than 1 in made no significant difference to penetration as all the liquid was extruded at maximum speed. Thus the 44 mm maximum theoretical penetration is comparable with 48 mm actual penetration. The fact that the shortest lead projectile gave the greatest error (15 mm estimated and 25 mm actual penetration) suggests that the length of water jet is not related linearly to the length of the projectile.

Experiments with small diameter water jets of equivalent length ($\frac{1}{2}$ in long lead projectile) resulted in slightly less penetration i.e. 34 mm. Mercury jets, however, produced a conical hole much slimmer (10 mm diameter) and deeper (64 mm) than water jets. The densities of mercury and water indicate, from equation (7.2) a penetration ratio of 3.4 to 1. Actually the ratio was much less at 1.8 to 1 but this may be due to the reduced jet length of mercury as a given length of lead projectile is unlikely to extrude as much mercury as water.

The normal stand-off distance for these experiments was 12 mm; variation from 6 to 56 mm made no difference to the depth of penetration.

(iii) Crater diameter

With water jets of 5 mm and 3.5 mm diameter at speeds of 800 m/sec craters were formed which measured 15 mm and 8 mm at their widest point. These values are two to three times less than the diameters indicated by equation (7.4). Carrell [22], also noticed considerable error in this equation when firing short plasticine projectiles into plasticine targets.

The ratio of penetration to crater diameter when firing water jets into plasticine is approximately three which is typical where conical craters form, i.e. lead projectiles on lead targets below the transition velocity.

Obviously when hemispherical craters form this ratio is only a half [83].

(iv) Angle of impact

A series of tests with different angles of impact such that the angle of incidence varied from 0 to 80 resulted in almost the same depth of penetration measured along the axis of symmetry of the jet. A few examples are given in Fig. 7.1. Perpendicular penetration, P_p, is given by

$$P_p = P \cos \theta$$

7.2.2 Perforation of lead and aluminium plates

(i) Size and shape of hole

Thin plates perforated by high speed water jets show a mode of deformation which conforms to the model given by Taylor [120] and which a lip of metal forms around the hole on the reverse side of the plate. Fig. 7.1 shows a perforated lead plate with typical lip and an aluminium specimen with localised perforation deformation combined with bending terminating at the support.

Variation of nominal perforation diameter with thickness of lead and aluminium plates for two diameters of water jet is given in Fig. 7.2. It can be seen, particularly with lead plates over the middle ranges that the perforation diameters approximate to the projected water jet diameters of 5 mm and 3 mm. Stronger aluminium plates have smaller perforation diameters than lead plates. Shadowgraphs of water jets before and after perforation of 3 mm lead plates show that the retardation occurred in only a few micro-seconds, also, the jet head regained its supersonic velocity in air immediately after perforation. The lip height, H, in lead and aluminium plates is compared in Fig. 7.2 with that predicted height from equation (7.5) using the actual perforation diameters. The measurement of H, is by no means accurate when bending and perforation profiles are superimposed as with aluminium specimens. In all cases the actual lip

height is significantly greater than the theoretical height. Apparent agreement in Fig. 7.2 when the plates are thin is misleading as constancy of plate material during impact is not maintained.

Haji-Ibrahim [61] apparently found good agreement between theoretical and experimental values of lip height with brass plates; the inconsistency is difficult to explain.

(ii) Perforation thickness

The maximum thickness at which perforation occurs is very much less than indicated by Taylor's [120] theory; this is perhaps not surprising as the regime indicated by $\rho v^2/\bar{Y}$ is only 12 for aluminium and 35 for lead. Carrell also found with lead projectiles at slower velocities that the hydrodynamic theory no longer held and gave limiting penetration target thickness to projectile diameter ratios of between 1 and 4. With water jets this ratio is between 0.6 and 1.5. A close approximation to the maximum thickness of penetration is achieved by considering a punch, loaded at equivalent pressure, blanking a slug from the plate. The transient impact stress (many times the steady state stress) does not have any influence, probably because of its short duration.

7.3 CONCLUSIONS

1. A conical crater is formed by water and mercury jets impinging on large blocks of plasticine. The depth of penetration is predicted by Taylor's hydrodynamic model, equation (7.2) when the damage number ($\rho v^2/\bar{Y}$) is equal to or greater than 450. The ratio of depth of penetration to hole diameter is higher than that for other low strength projectiles which form hemispherical craters. Penetration of inclined jets is related to normal penetration by the cosine of the angle of incidence.

2. A lip of metal forms on the reverse side of thin plates when perforated by water jets, the height of the lip being greater than that predicted by equation (7.5). Taylor's hydrodynamic model at damage numbers of 12 - 35 is not applicable.

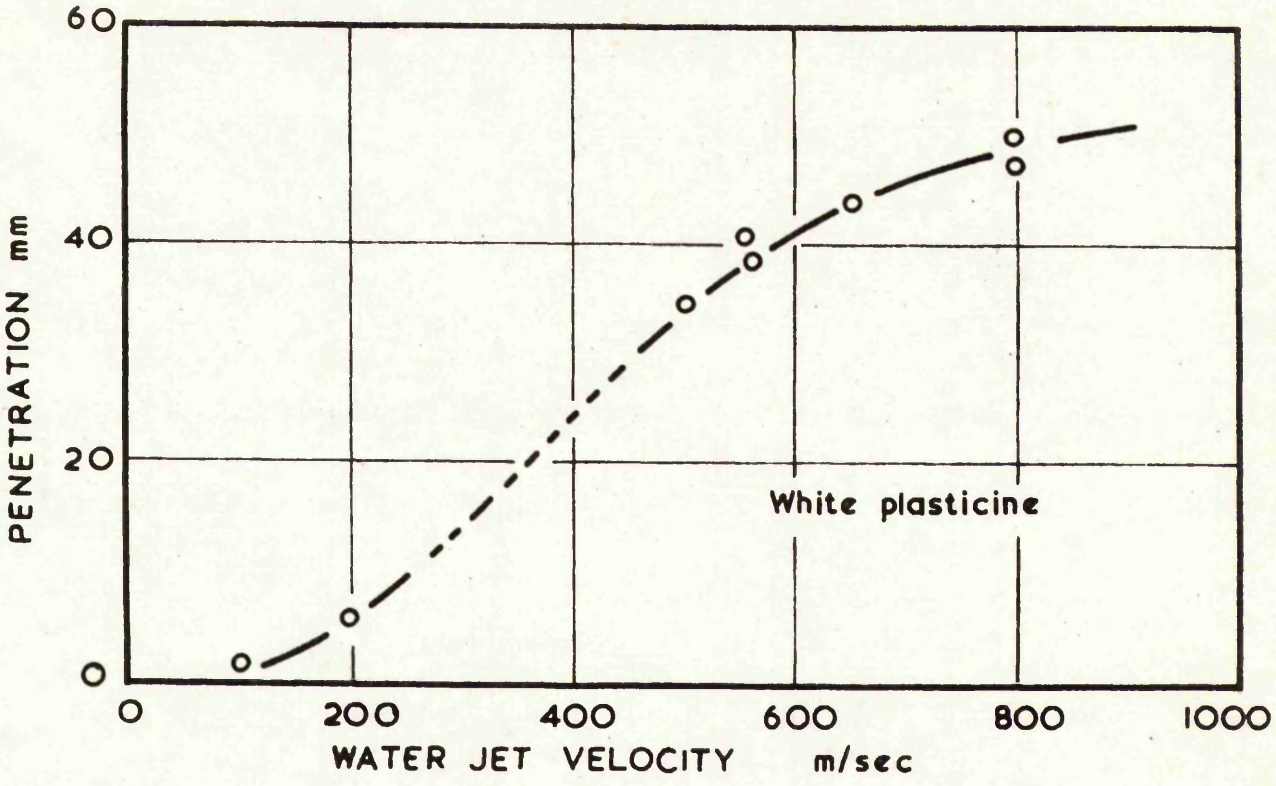

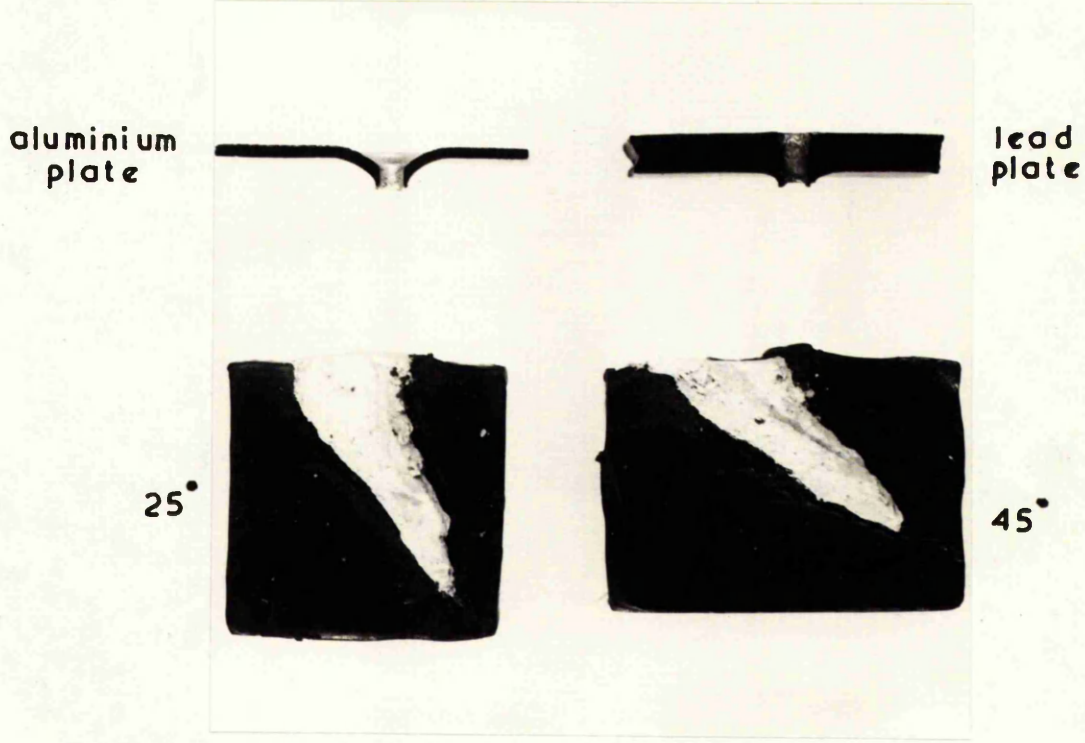

FIG. 7·1 PENETRATION OF PLASTICINE BY SINGLE WATER JETS

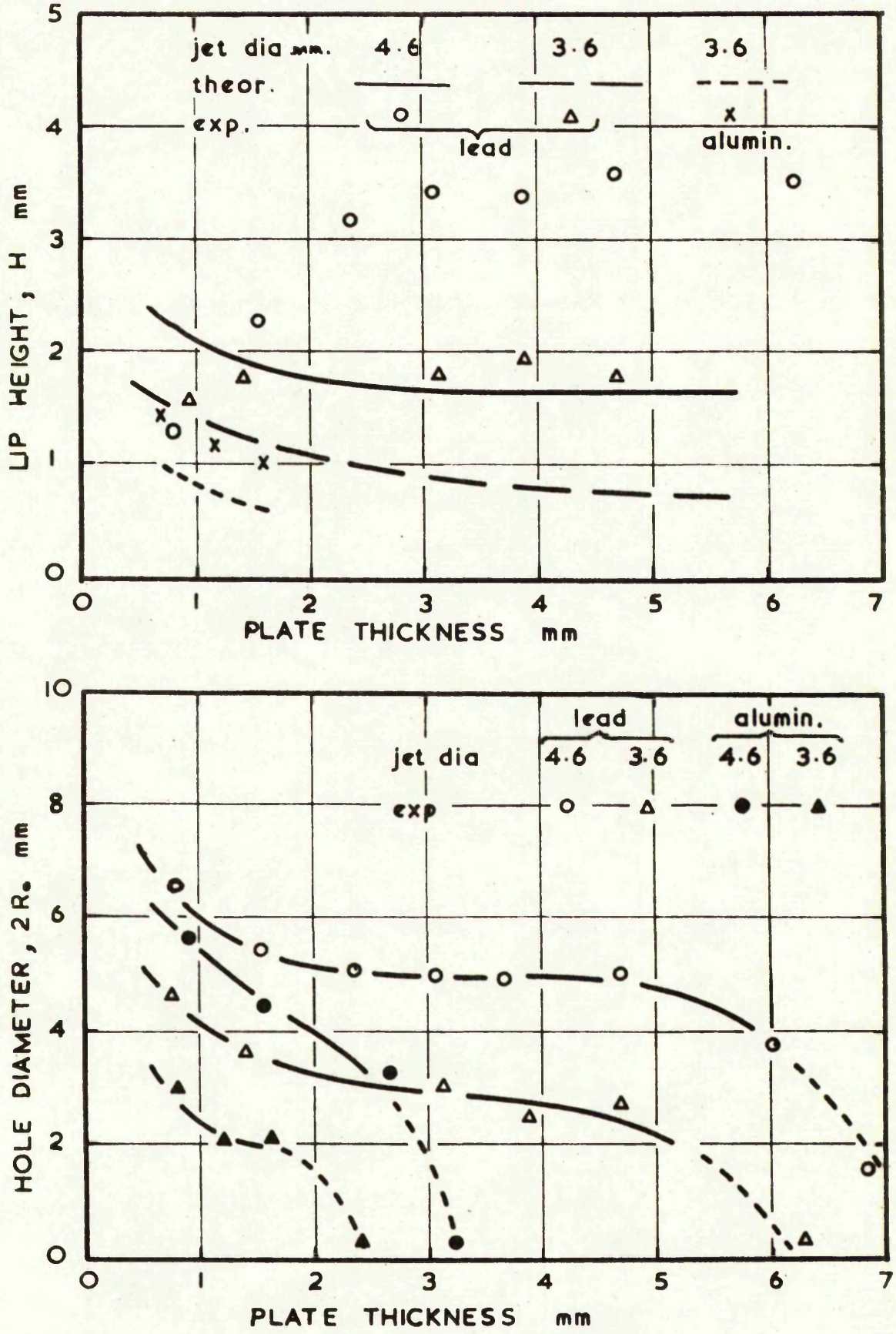

FIG. 7·2 HOLE DIAMETER AND LIP HEIGHT VERSUS PLATE THICKNESS

CHAPTER EIGHT

CHAPTER EIGHT

IMPACT STRESSES

During the course of this work it seemed that in order to dispense with uncertain ad hoc criteria for assessing liquid impact and erosion damage it was necessary to quantify the impact stresses with regard to their distribution and variation with time. This chapter is concerned with the measurement of such stresses.

8.1 INTRODUCTION

(i) Impact pressure

As we have already seen a liquid drop or jet, at impact, produces a very high compressive stress in the vicinity of the area of contact and this is followed by outward radial flow of liquid at very high speed. The initial, momentary high compressive stress on impact supposedly arises because the liquid remains 'in place' until release waves from the circumference of the water jet reach the centre of the jet. Once a steady state flow of water across the impact surface has been achieved, the pressure, P, at the stagnation point becomes

$$P = \tfrac{1}{2} \rho V^2 \qquad (8.1)$$

where ρ is the density of the impinging liquid and V the impact speed of the jet.

One of the first investigations concerning initial impact pressure is due to Cook [25] who showed (though in a slightly different form) that it can be represented by the water hammer equation

$$P = \rho c V \qquad (8.2)$$

where c is the speed of compressive waves in the liquid. Later, de Haller [31], taking account of the compressibility of the solid under

impact as well as the properties of the impinging liquid, showed that the equation which should apply in place of (8.2) is,

$$P = \frac{\rho c V}{\left[1 + \frac{\rho c}{\rho_m c_m}\right]} \qquad (8.3)$$

where ρ_m is the density of impacted medium and c_m is the speed of compressive waves in the solid.

The validity of (8.3) has since been verified by Engel [37], and Bowden and Brunton [11] and indeed the latter determined, by impact against a barium titanate crystal, that this initial pressure could be reached in a time of 1μs and fell to zero in 2 to 3μs. Also Jolliffe [85] using a dislocation etching technique to study liquid impacts supported these findings.

(ii) Hemispherical pressure distribution

The above work gives no indication of pressure distribution and its decay with time for liquid drop impact. Brunton [15] has suggested that a good approximation to the stresses present in the target is given by a hemispherical distribution

$$P_r = P\left(1 - (r/a)^2\right)^{\frac{1}{2}} \qquad (8.4)$$

where P_r is pressure at radius, r, and a is the jet radius.

The principal stresses resulting from such a pressure distribution were determined by Morton and Close [100] using an extension of Hertz's [68] theory. Inside the area of contact the three principal stresses are of comparable magnitude whilst outside this area the normal stress disappears and a small radial tension equal in magnitude to the hoop compression decays rapidly with radius.

(iii) Hertzian pressure distribution

Work by Skalak and Felt [115] using known analogous solutions of linearized supersonic airfoil theory for rigid wedges impacting a semi-infinite fluid indicates maximum pressure near the edges of the contact area and minimum at the centre, i.e. a ring of high pressure contact. A similar pressure distribution is provided by Sneddon [117] and later Mucki when considering the Hertzian stress caused by a flat ended cylindrical indenter elastically penetrating the surface of a semi-infinite mass. The direct pressure varies with radius and becomes infinite at the circumference of the flat ended indenter. By using their formulae for direct stress and punch load and assuming that the punch load of the indenter is, at the instant of impact, equal to the water hammer pressure, given by equation 8.2, multiplied by the jet cross-sectional area it may be shown

$$P_r = \frac{0.5 \rho c V}{\left[1 - (r/a)^2\right]^{\frac{1}{2}}} \qquad (8.5)$$

(iv) Surface friction

Another seemingly dissimilar, but relevant, solution results from the measurement of surface friction in the impact zone of axially symmetrical drowned jets (i.e. air jets in air). Much of this work is related to cooling surfaces, such as glass, with single or multiple air jets and rate of heat loss is measured by hot wire probes or thermo-couples. As it may be shown [67] using Reynold's analogy, that rate of heat loss is analogous to shear stress, the rate of heat loss distributions [58,101,109] being indicative of surface shearing. Gardon and Cobouque [59,60] have shown that surface friction has a double peak distribution which is maximum typically at $r/a = 0.5$ and 2 and is a function of Reynolds Number, nozzle

to plate spacing and turbulence in the jet. They conclude that this partially results from a transition from a laminar boundary layer around the stagnation point to a turbulent boundary layer in the wall jet as radially outward velocity increases.

An exact solution for the boundary layer thickness in the stagnation region of a two dimensional laminar flow jet against an infinite plate is given by Schlichting [110]. Adapting this treatment to air jets of finite size, Schrader [114] has shown that a boundary layer of constant thickness covers the stagnation region having a radius of approximately 1.1 nozzle diameters.

The limitations of applicability of this work to erosion are that it covers mainly drowned jets which are in a steady state and not in a transient impact situation.

8.2 EXPERIMENTAL PROCEDURE

Using the jumbo jet apparatus, described in Chapter 2, jets of liquid were projected at the pressure cell. Adjacent pairs of strain gauges in the pressure cell were connected to opposite sides of a Wheatstone bridge and the change of bridge potential resulting from liquid impact was recorded on a differential amplifier storage oscilloscope. A series of strain traces were thus obtained at 6 mm increments across the impact zone. At least two traces were made from each pair of vertical and inclined strain gauges at every position (i.e. at least six traces per position) and an allowance was made for the spread of gauges within the rosette so that all results, at each position, were taken in exactly the same place. Alignment was facilitated using a pointer sliding centrally in a boss that fitted into the die orifice.

Before each test the platen face was cleaned with carbon-tetrachloride to provide consistant conditions, although some later tests were made with

films of oil, grease and P.T.F.E. on the surface of the pressure cell as well as 5 mm thick layers of water. Other tests were conducted with the platen face inclined at $12\frac{1}{2}^{o}$ and 21^{o} to the normal position.

The storage oscilloscope used in these tests enabled the displays to be accurately traced on transparent paper and generally they showed a remarkable degree of repeatability and clarity. A few typical traces were photographed and are shown in Fig 8 1.

As a working note it might be worth recalling that with such high signal amplification 50 c.p.s. 'pick-up' proved an initial problem even using a differential amplifier. The problem was overcome by reducing the length of all wires to a minimum, screening, and even earthing all nearby conduit piping which contained live wires.

8.3 EXPERIMENTAL RESULTS AND DISCUSSIONS

8.3.1 Direct impact stress

The strain experienced by inclined and vertical gauges at two positions in the impact zone are shown in Figs. 8.2 and 8.3. Surprisingly they show an initial tensile pulse whose duration increases with radius. This is thought to be due to a compression wave from the point of first jet contact on the jet axis being transmitted through the pressure cell and encountering the strain gauges (subjecting gauges perpendicular to the surface to tensile strains) before direct impact of the liquid jet.

Qualitatively the strain relationships appear correct as Q_3 is only compressive when Q_2 is compressive and when Q_1 decays to Q_3 their value is approximately half Q_2. The magnitudes and durations of these and other strain traces were used with equations (2.7) and (2.8) to build up the impact stress distribution.

The maximum direct impact stress distribution resulting from normal impact is given in Fig. 8.4. It shows a stress at the stagnation point two thirds of the water hammer pressure as given by equation (8.2) rising sharply to 1.5 times this pressure at the circumference of the jet. It is remarkably similar to the Hertzian stress solution for a rigid flat-ended cylindrical indenter elastically penetrating the surface of a semi-infinite mass, given by equation (8.5). It appears that the liquid jet may be considered initially as a rigid punch quasi-statically loading the surface with the maximum stress occurring at the load discontinuity. The well documented, postulated pressure distribution which is hemispherical, as given in reference 15 and the uniform water hammer pressure distribution do not appear to be appropriate.

Impact duration across the impact zone is given in Fig. 8.5. It should be noted that these times include the pressure rise and decay times above a stress level of 200 lbf/in^2. The commencement of impact can be seen to be delayed in proportion to radius and is accounted for by the shaped nature of the leading edge of the jet. This will obviously be affected by jet profile and speed. However, termination of the pulses within the jet diameter seem to occur after 80-90 sec which results in shorter impact times where the maximum stress occurs.

Tests with the time scale extended in stages from 100 μ sec to 10 m sec showed no other large stresses and only small fluctuations of direct and shear stress around a low mean of little significance to erosion problems.

To gain an indication of impact load with time the average load acting on elemental rings of width $2.\delta r/d = 0.2$ (given in Fig. 8.4) were assumed to act for times given in Fig. 8.5. The load (expressed in dimensionless form as impact load/ρ cvA) versus time graph thus obtained is given in Fig. 8.7. It shows a ratio of maximum load to water hammer load of 1.6

which may be compared with a similar ratio of 1.3 taken from work by Bowden and Brunton [11], due allowance being made for the change of, c, [71] with pressure: the comparison is limited by the assumption that the impact area is defined by the jet head diameter. To compare the duration of impact with that given by Brunton the time scale may be reduced proportionately with core diameter ratio (i.e. 1.3 mm to 50 mm) which gives a similar time of three microseconds.

8.3.2 Surface shear impact stress

Maximum surface shear stress distribution, determined from the difference of the inclined strain gauges, is shown in Fig. 8.6. It can be seen that a maximum shear stress, of almost half the water hammer impact stress, occurs just within the jet diameter. There is rapid attenuation on either side of this position which tends to zero at the centre of impact and also at 0.8 jet diameters from the jet axis. Reduction of shear at the centre of the jet is likely to be due to the radial speed of contact being initially faster than 'c', the speed of compression waves in the liquid, and thus no sideways flow, or viscous shear, occuring. At larger radii the reduction of shear stress and also direct stress, is determined by the limits of influence of the jet. Brunton [17] studied flow in a liquid drop utilising the property of birefringence shown by some liquids also noticed a reduction of shear stress at the centre of impact.

The level of shear stress is remarkably high at 1,400 lbf/in^2. As a comparison, Thomas [128] has evaluated the magnitude of shear stress for turbulent boundary layer flow at a speed of 500 m/sec to be 15 lbf/in^2. Fierce jetting as water is propelled from under the converging wedge formed as the curved jet front impinges on the flat target producing velocities many times the impact velocity (as in explosive welding [3,137]) probably accounts for the high value of shearing. An interesting alternative idea is that as the liquid has already been shown to behave initially as a solid punch

it might be further considered to generate a frictional stress in which case the coefficient of friction at the circumference would be equal to 0.33.

The existence of the high level of shear stress is fully substantiated by plastic deformation in 0.005 in shim steel plate after a single jet impact. The shim steel stretches at an annulus of approximate radius 2 r/d = 0.7 to 1.1 which is the position of maximum shear stress given in Fig. 8.6. Further, the necessary surface shear force required to deform the shim steel is at least 1/4 Ton f/in^2 even if no allowance is made for the restraining frictional force between the shim steel and the supporting pressure plate.

Duration of the shear stresses is given in Fig. 8.5 and it is interesting that the shear stresses distinctly occur before direct impact and in fact reach a maximum at the moment of impact. This is again probably due to water being propelled from under the converging wedge. Shear stresses last longer at larger radii and at the jet circumference shear stresses last half as long again as the direct stresses.

The onset of shear stress across the surface shown in Fig. 8.5 gives an accurate measurement of liquid flow across the surface, which is normally very difficult to distinguish from high speed photographs [17,53]. In fact it gives a ratio of wall jet velocity to impact velocity of 16 to 1 which is considerably faster than previously recorded.

To determine the sensitivity of shear stress to surface roughness, tests were made using 2 mm thick aluminium blocks fastened with araldite to the pressure cell surface just above the relevant gauges at 2 r/d = 0.8. This resulted in more than twice the previous maximum shear stress which approached in magnitude the water hammer impact stress. The strain trace for Q_1 at this position is given in Fig. 8.1 (ii) and is identical with the exception of height to Q_1 in Fig. 8.3. A good photograph of a liquid drop

encountering a surface step is given in reference 47.

The physical implications of the direct and surface shear stress pressure distributions are that very high maximum shear stresses occur in an annulus of the impact zone: in fact the maximum shear stresses are $2\frac{1}{2}$ times greater than those at the stagnation point. This is consistent with the annulus of shear damage and discrete ring cracks which form in α-brass and Perspex erosion specimen discussed in Chapter 3. Also the slight but distinct rise in direct pressure at the stagnation point together with a steep rise in radial surface shearing stress may account for the central hole formation in ductile specimen.

8.3.3 Direct impact stress on inclined surfaces

With water jets impinging on the pressure cell at $12\frac{1}{2}^{o}$ and 21^{o} angles of inclination from the normal of the plate, a series of direct strain traces (i.e. No. 2 strain gauge) were obtained. Three typical traces at 21^{o} impact are shown in Fig. 8.1(i) and illustrate the purely compressive pulse under the point of first impact, with tensile pulses of longer duration at larger radii followed by a compressive pulse as the jet impinges.

The maximum impact stress distributions for both conditions are given in Figs. 8.8 (ii) and 8.8 (iii). They are both skew distributions with minimum values occuring at the likely positions of first contact and rising sharply on either side of this. Distance between the peaks is less with greater angles of inclination which is consistent with the experimental work in Chapter 6 concerned with measurement of an undamaged central area given by $2x_o$. The magnitude of the maximum stress is about the same as the normal impact stress.

8.3.4 Surface films

Impact tests against films of oil, grease and P.T.F.E. on the surface of the pressure cell resulted in measurements of surface shearing little different from those on normally clean surfaces.

Further tests made with 5 mm thick layers of water flowing across the platen face gave very 'peaky' oscilloscope traces and lacked the consistency of previous results and an example is given in Fig. 8.1 (iii). The maximum stress level is surprisingly not attenuated with travel through the liquid film but its position or diameter is reduced by a factor of 5, see Fig. 8.8 (i). The duration of impact stress also altered to a roughly constant value of 50 to 60 μ sec across the whole impact zone. Values of the maximum surface shear stress under these conditions were reduced to approximately half that of dry impact.

These characteristics are consistent with experimental erosion results [16,87] through liquid films; for instance

(i) rapid development of erosion craters; this is due to the longer duration of the pressure pulse;

(ii) supressed shearing and reduced mass loss; in fact the shear stress is reduced by half;

(iii) smaller diameter of erosion crater in some materials; the radius of maximum direct stress is reduced;

(iv) the depth of rock cutting with liquid jets is the same under water as in air [28]; the magnitude of the maximum direct stress is not altered by the water.

The reasons for these occurrences are not so clear: the shape of the strain pulses and the radius and level of maximum direct stress do not conform to the model [16] of a liquid - liquid impact generating compression waves in a liquid film which are subsequently reflected from liquid - solid and liquid-liquid interfaces. Although the lack of an initial tensile pulse

and the peaky nature of the traces might be suggestive of a model of this type. It seems further work with a variety of film thicknesses might shed more light on the topic.

8.3.5 Fluid flow on impact

To investigate fluid flow at impact and test the hypothesis, arising from plasticine projectiles that the central area of impact is held in its initial position, a number of high speed films from 8,000 to 15,000 fps were taken of the liquid jet. Filming perpendicular to the jet, along the impact plate surface obscured the view as the jet spread out in all directions. Further filming was therefore made along the axis of the jet and directly above a clear thick Perspex plate on to which the jet impinged and spread out into a wall jet. White and coloured pellets of various sizes and of similar density to water were initially dispersed in the die and also black streaks of ink but none of these were very successful in outlining fluid flow. More success was obtained by attaching to the Perspex impact plate a variety of markers including strips of water soluble wet paint and oil, engineers blue, white pellets and silver paper pellets on layers of grease and finally black plasticine pellets and black paper dots held on by a light film of oil. Some of the exposures from the film, taken at 15,000 frames per sec are of black paper markers being removed from the target by a water jet are shown in Fig. 8.9. Although not conclusive they do show the three markers at the centre (black dots) are held for half a milli-second while the outer markers are removed as the jet contacts the surface.

Longer than half a milli-second after impact a ring of approximately 1 in diameter is apparent within the liquid and remains until the end of the jet. This ring may be due to the change from a laminar to turbulent boundary layer in the steady state part of the jet as discussed previously but the level of surface shearing was not of sufficient magnitude to register on the pressure cell. The inference is, that it takes half a milli-second

for the transient impact condition to terminate and the steady state condition to commence.

8.4. CONCLUSIONS

The direct and surface shearing stresses resulting from normal and inclined liquid jet impact are clearly shown. Also the effect that surface protrusions, liquid films and lubricants have on impact stresses are discussed.

The stresses are shown to account for many characteristics of erosion damage and may possibly eliminate some of the mystique associated with erosion phenomena.

(i) a 2r/d = + 0·74

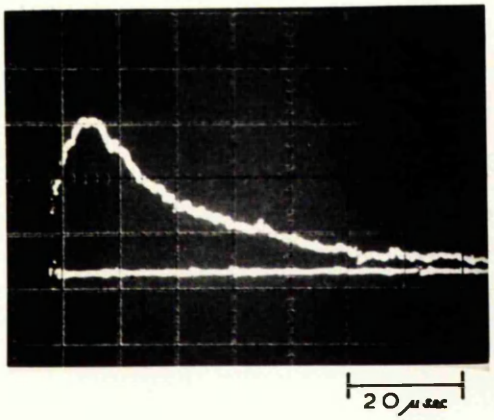

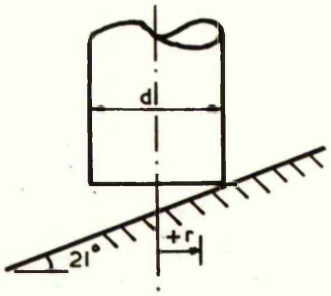

(i) b 2r/d = +0·2

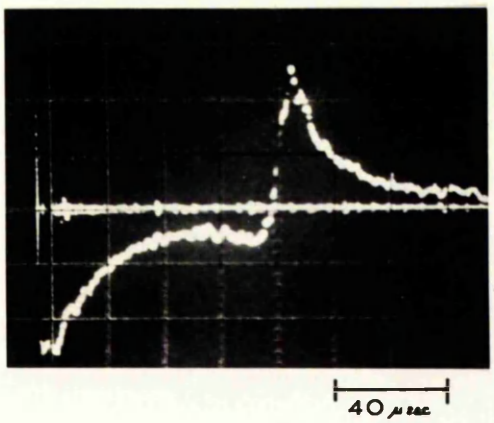

(i) c 2r/d = 0

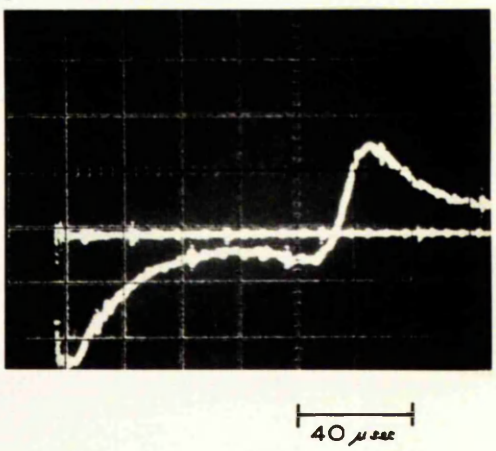

(ii) Gauge 1 , θ = 0 , 2r/d = 0·83 , 2mm. step

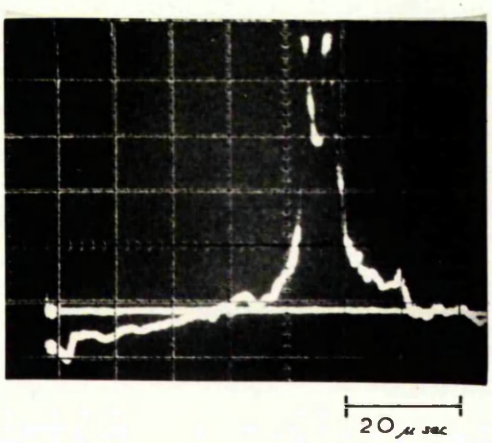

(iii) Gauge 2 , 2r/d = 0·6 , 5mm. water film

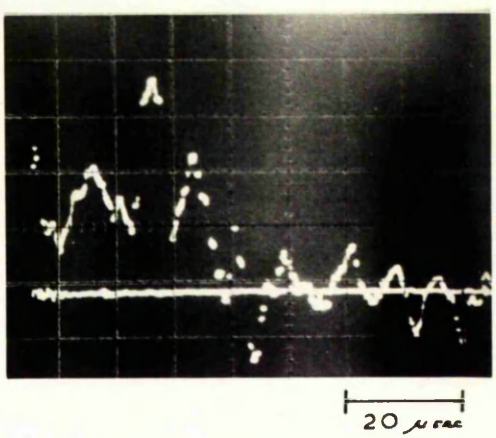

FIG. 8·1 OSCILLOSCOPE TRACES

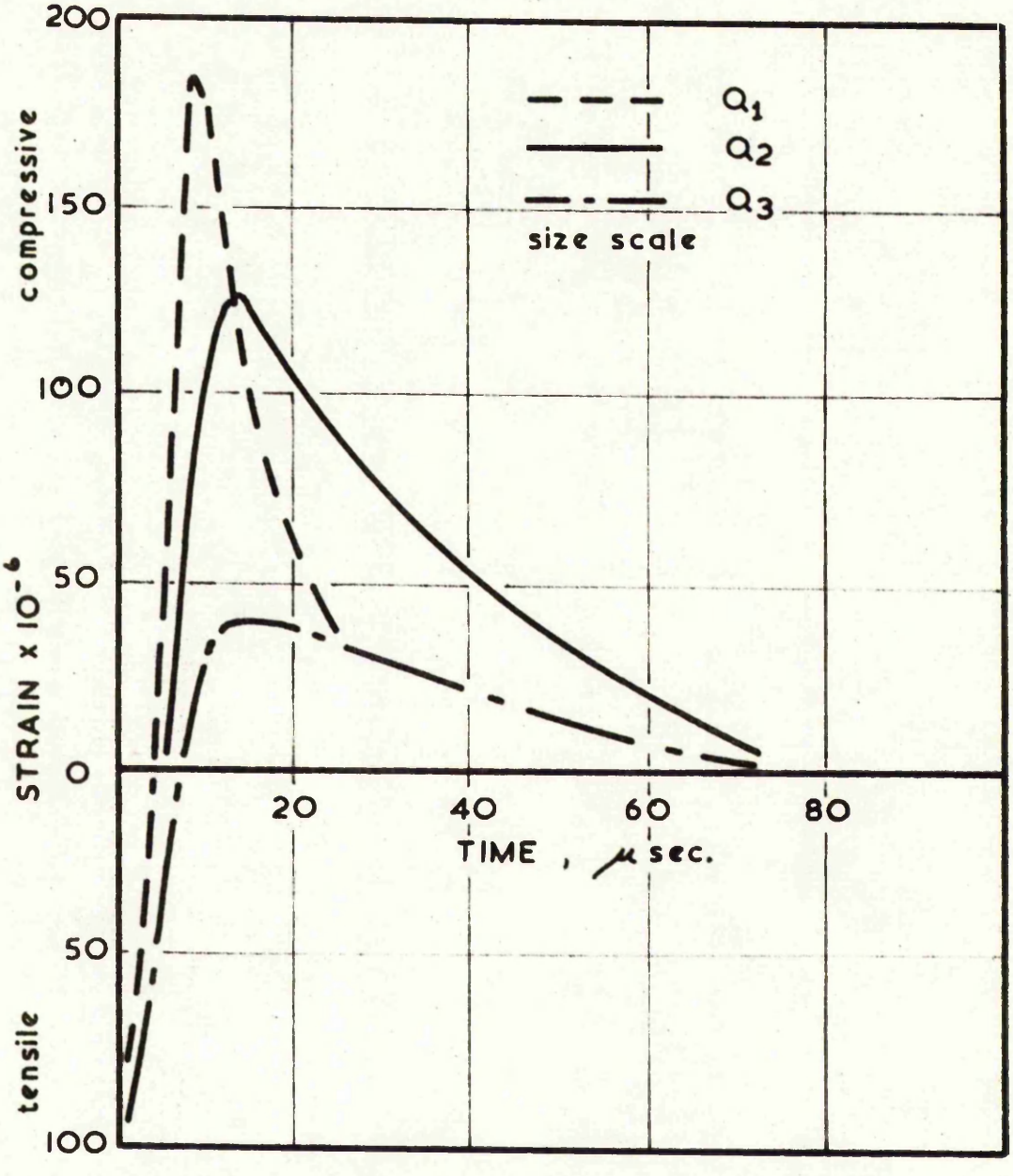

FIG. 8·2 C.R.O. STRAIN VERSUS TIME TRACE

2 r / d = 0·2

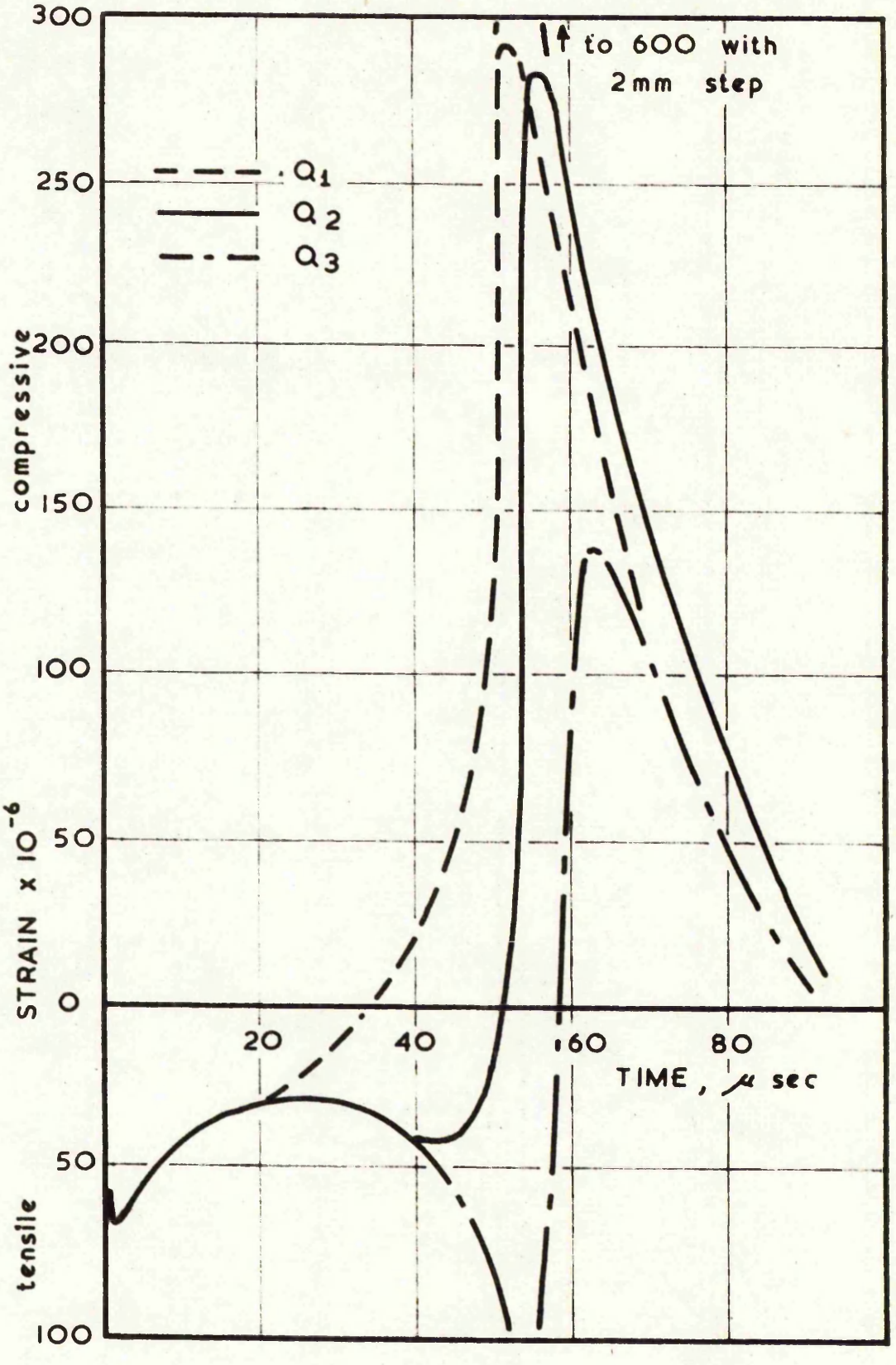

FIG. 8·3 C.R.O. STRAIN VERSUS TIME TRACE
$2r/d = 0.84$

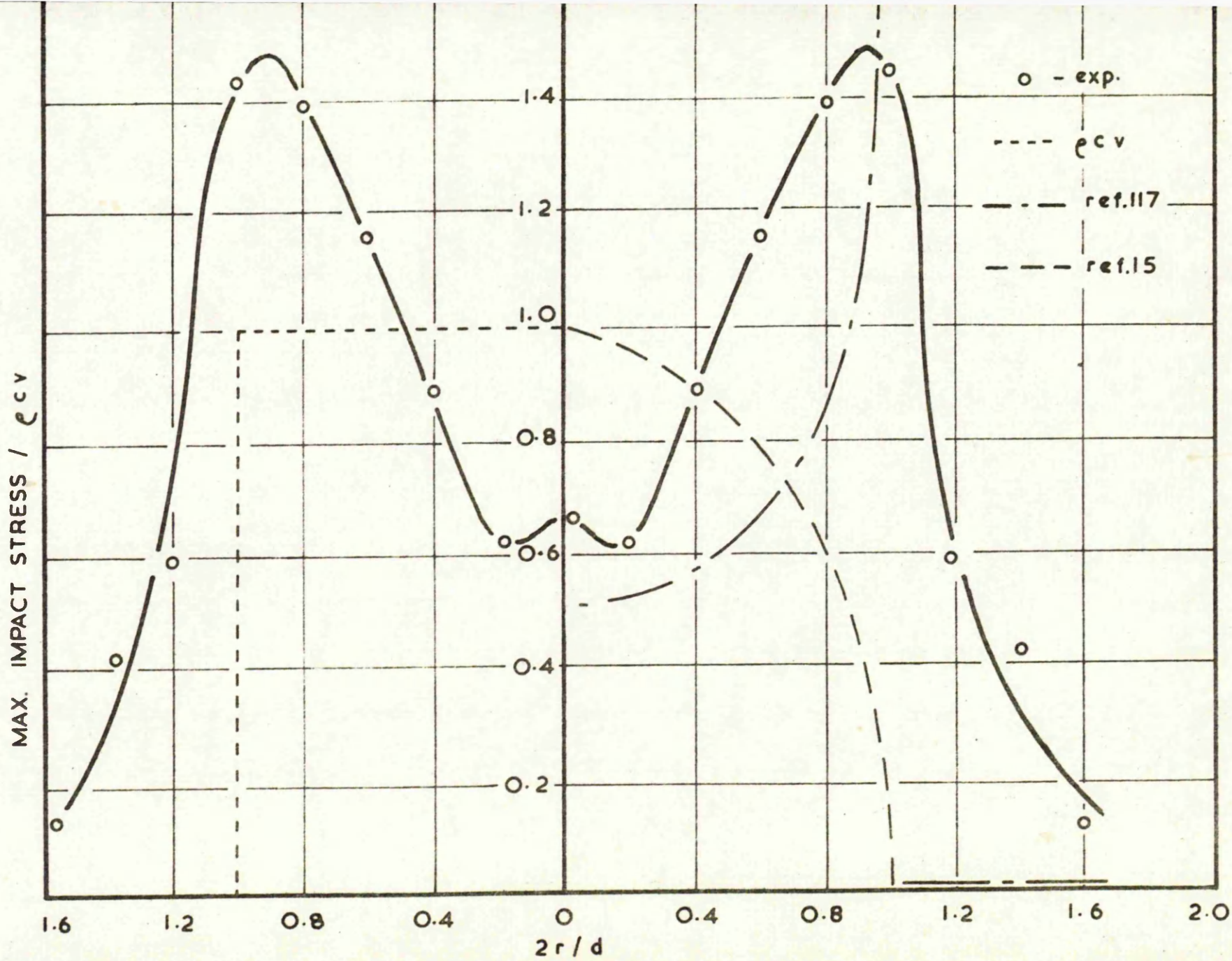

FIG. 8·4 MAXIMUM IMPACT STRESS DISTRIBUTION

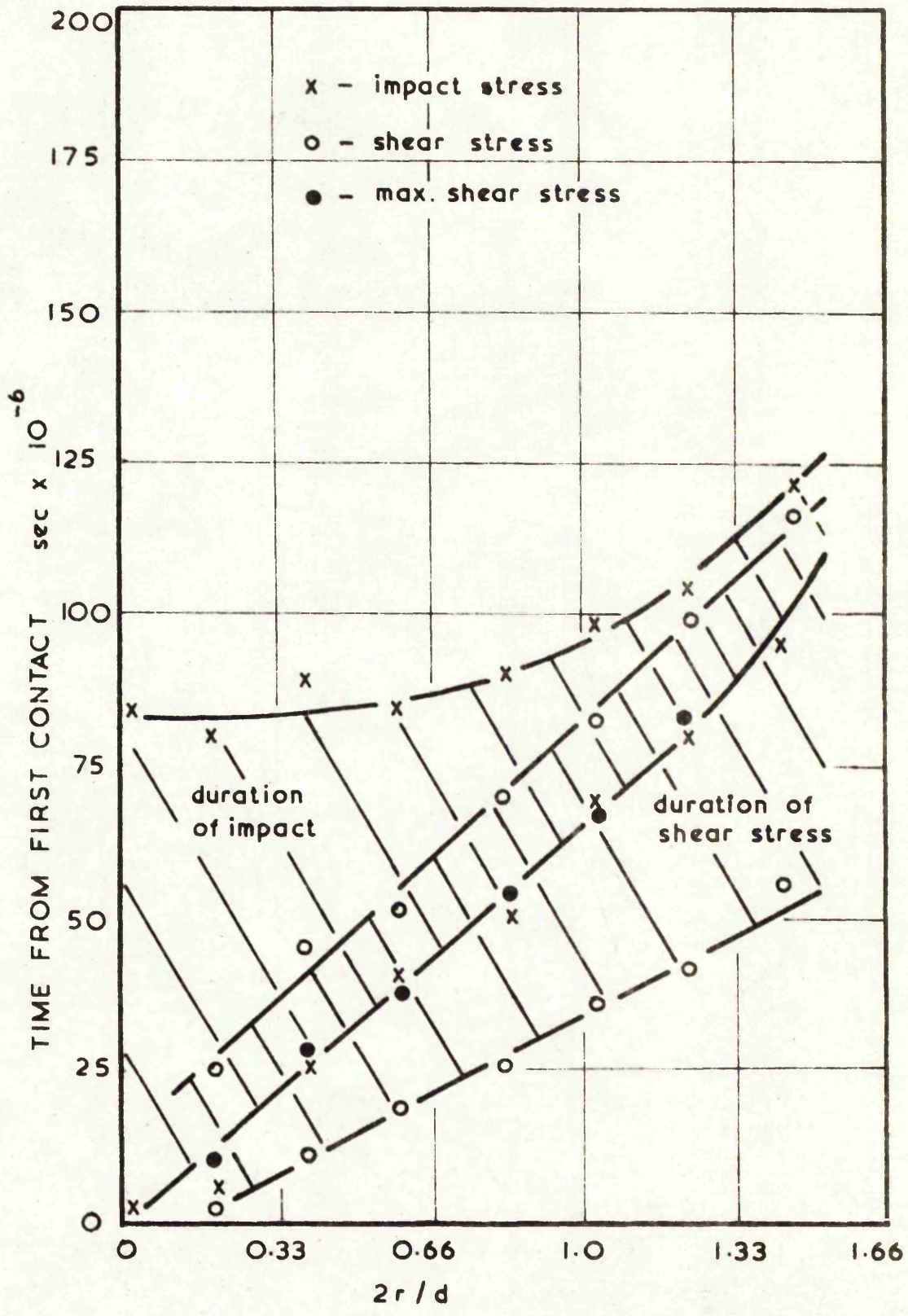

FIG. 8·5 DURATION OF DIRECT AND SHEAR STRESSES

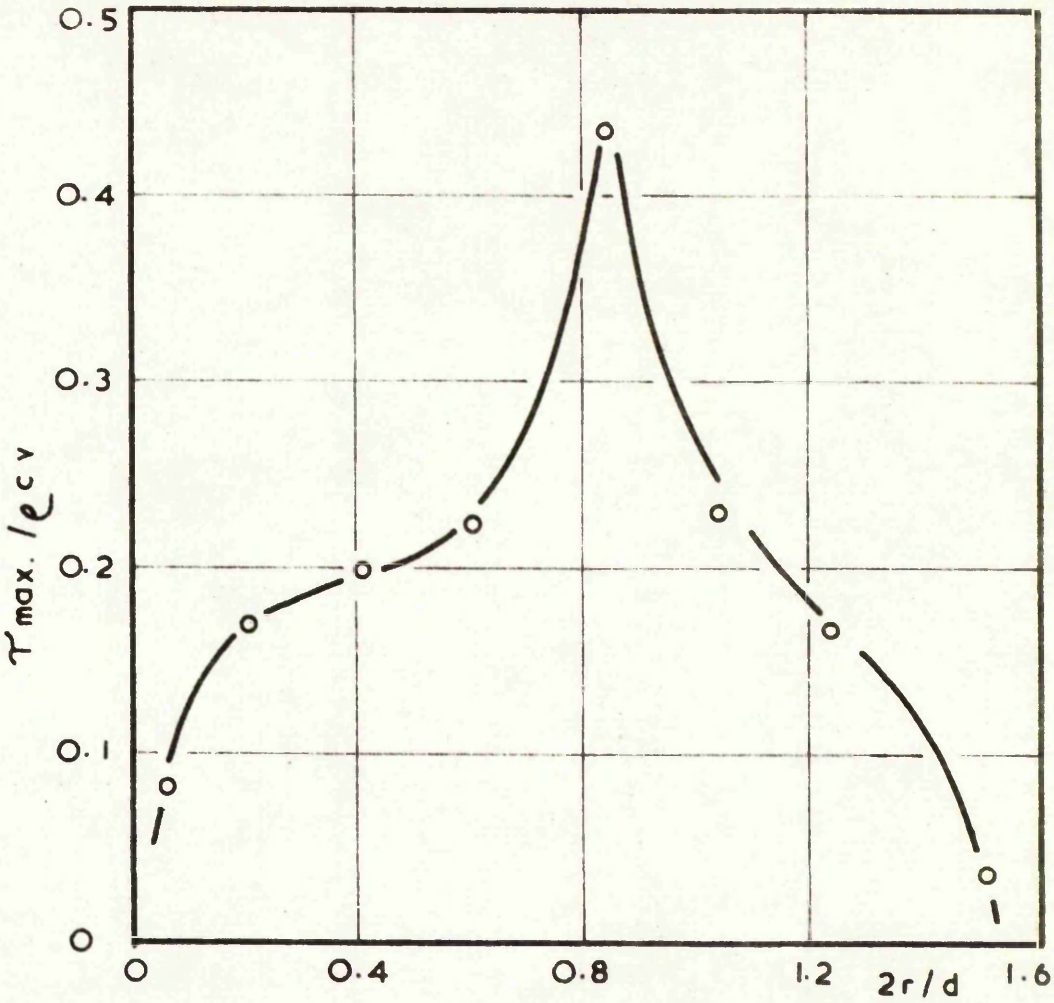

FIG. 8·6 MAX. SHEAR STRESS DISTRIBUTION

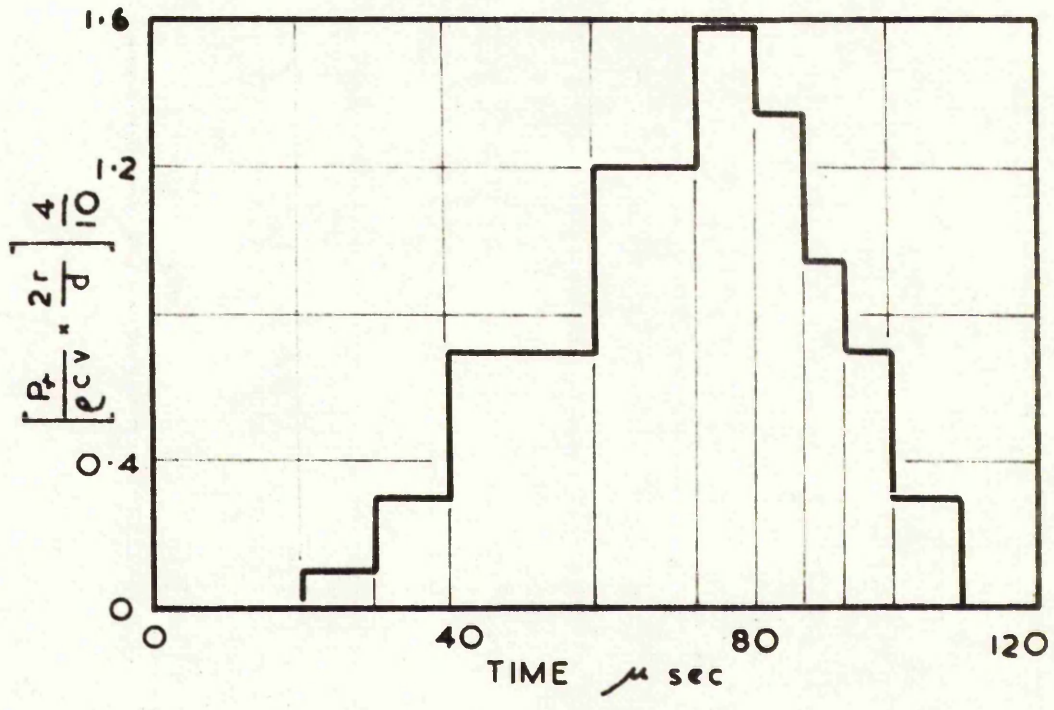

FIG. 8·7 IMPACT LOAD (ESTIMATED) VERSUS TIME

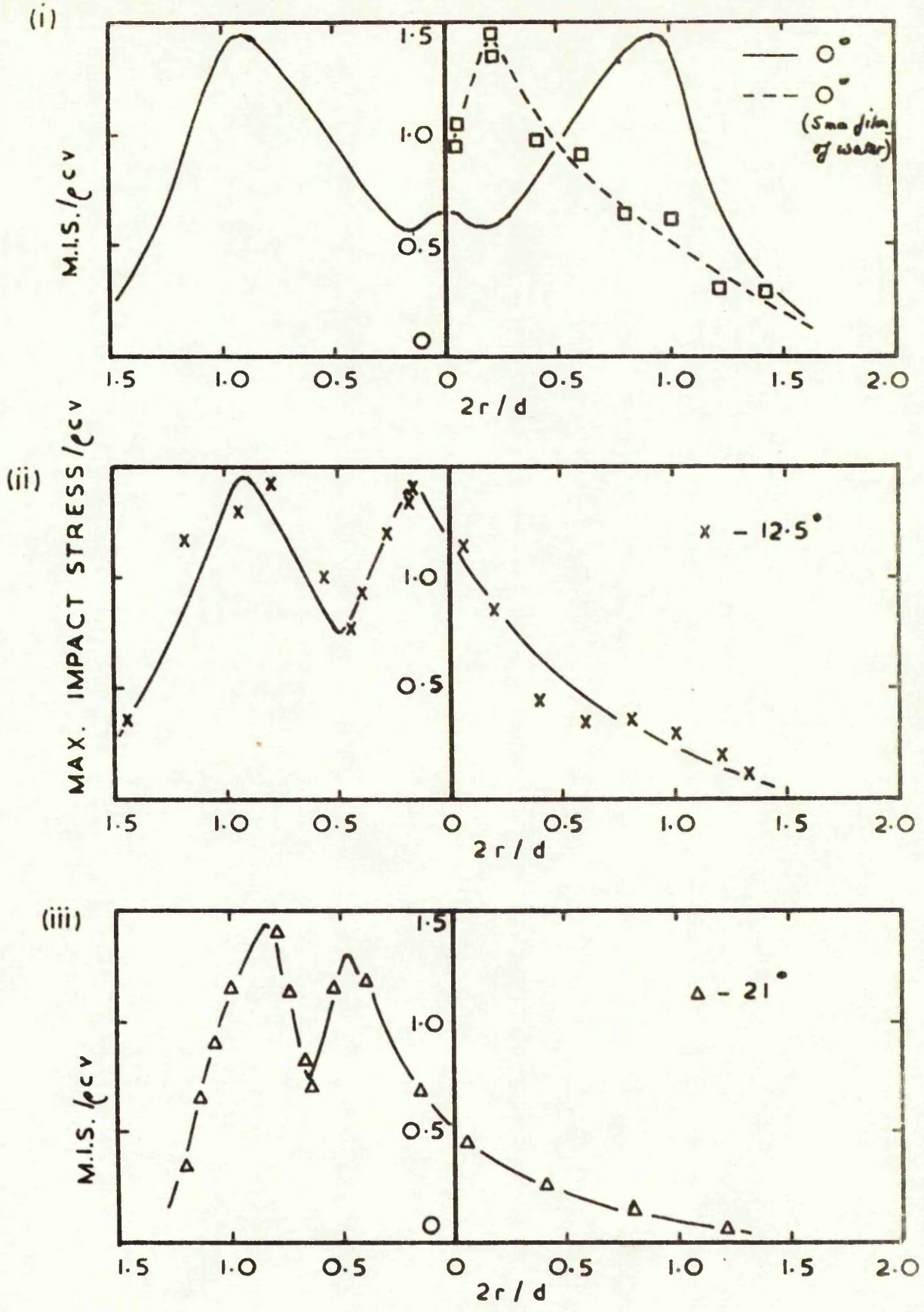

FIG. 8·8 MAX DIRECT STRESS DISTRIBUTION FOR 12·5° & 21° INCLINED & WATER FILM IMPACT

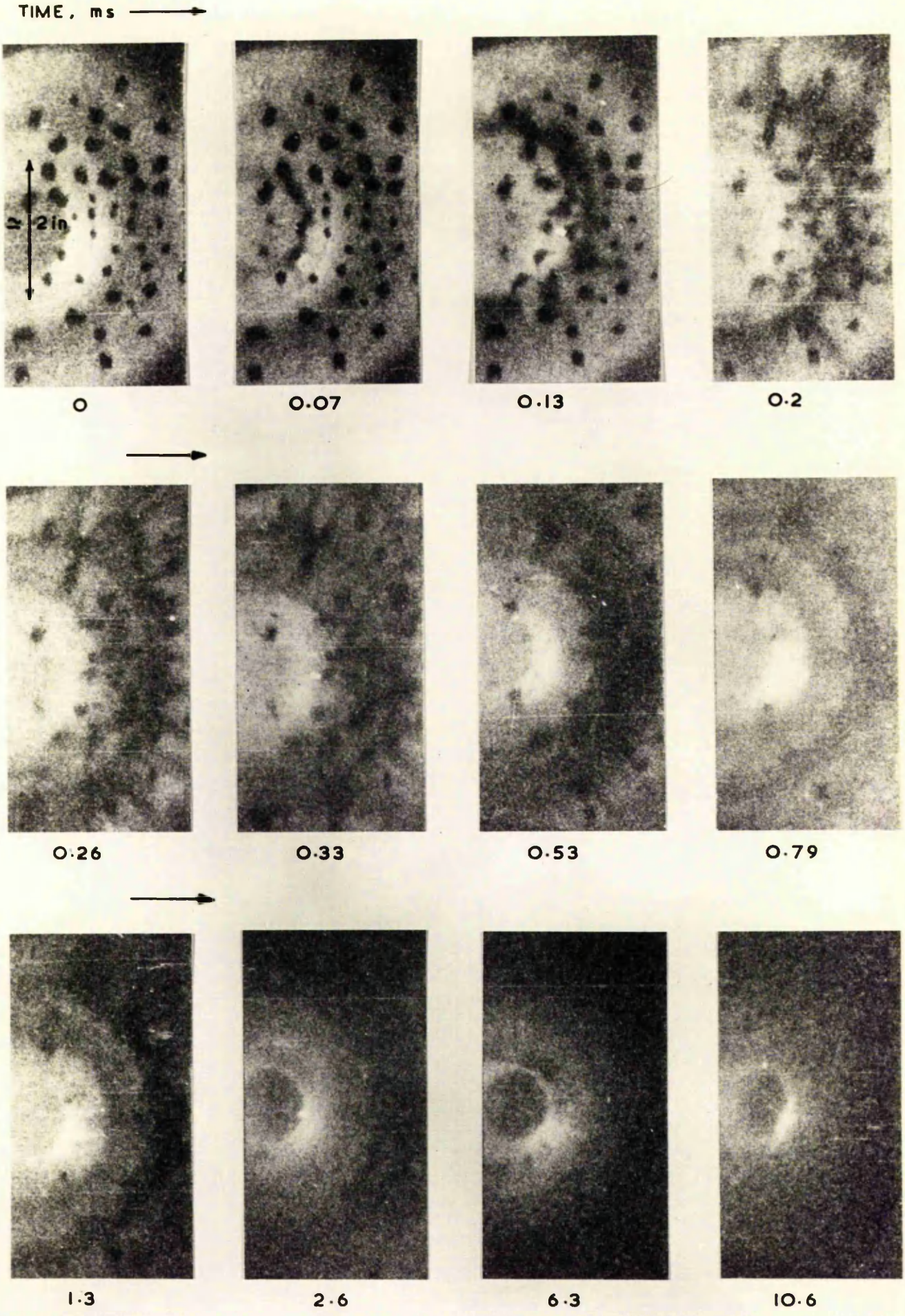

FIG. 8·9 INSTANTANEOUS VIEWS, DOWN AXIS OF JET, AS IT IMPINGES ON A PERSPEX PLATE

REFERENCES

1. ALLEN, W.A., MAYFIELD, E.B. and MORRISON, H.L. "Dynamics of a projectile penetrating sand", J. appl. Physics, 28, 370, 1957.

2. BAGREEV, V.V. "The process of impact beyond the limits of applicability of the Hertz Theory", Inzhenernyi Zhurnal, Vol. 5, No. 4, pp 796-799, 1965.

3. BAHRANI, A.S. and CROSSLAND, B. "High rate forming", Proc. I. Mech. Eng., 179, Part 1, 1964.

4. BAKER, D.W.C., JOLLIFFE, K.H., and PEARSON, D. "The resistance of materials to impact erosion damage", Phil. Trans. Roy. Soc., 260, Series A, p.193-204, 1966.

5. BECKWITH, D.J. and MARRIOTT, J.B. "Water jet impact damage in a cobalt-chromium-tungsten alloy", Erosion by cavitation or impingement, ASTM STP 408, Am. Soc. Testing Mats. p.111, 1967.

6. BECKWITH, D.J. and MARRIOTT, J.B. "Factors affecting erosion in a 12% chromium steel" Rain Erosion and Allied Phenomena, 2nd Meersburg Conference, 1967.

7. BENJAMIN, T.B. and ELLIS, A.T. "The collapse of cavitation bubbles and the pressures thereby produced against solid boundaries", Phil. Trans. Roy. Soc. 260, Series A, p.221, 1966.

8. BIRKHOFF, G., MACDOUGALL, D.P., PUGH, E.M. and TAYLOR, G.I. "Explosives with lined cavities", Journal of Applied Physics, 19, 563, 1948.

9. BIRKHOFF, G. and ZARANTONELLO, E.H. Jet, wakes and cavities, Academic Press Inc., 1957.

10. BLANCHARD, D.C., G.E. Lab Schenectady. Project Cirrus Report 7, 1948.

11. BOWDEN, F.P., and BRUNTON, J.H., "The deformation of solids by liquid impact at supersonic speeds", Proc. Roy. Soc., A263, No. 1315, 1961, p.433, 1961.

12. BOWDEN, F.P., and FIELD, J.E. "The brittle fracture of solids by liquid impact, by solid impact and by shock", Proc. Roy. Soc. A,282, 331, 1964.

13. BOWDEN, F.P., "The formation of microjets in liquids under the influence of impact or shock", Phil. Trans. Roy. Soc. 260, Series A, p.94-95, 1966.

14. BROOKS, B.W., TOBIAS, S.A. and ALI, S.M.J., M.T.D.R. Conference, 1970.

15. BRUNTON, J.H. , Ph.D. Thesis, Cambridge University, 1959.

16. BRUNTON, J.H. "Erosion by liquid shock", Rain Erosion and Allied Phenomena, 2nd Meersburg Conference, 1967.

17. BRUNTON, J.H. and CAMUS, J.J. "The flow of a liquid drop during impact", Proc. Conf. on Rain Erosion and Associated Phenomena, 1970.

18. BRUNTON, W.C. and HOBBS, J.M. "Comparative erosion tests on non-ferous materials", Part I: Drop Impact Tests, NEL Report No. 479, 1971.

19. BUSCH, H., HOFF, G., and LANGBEIN, G. "Rain erosion properties of materials", Phil. Trans. Roy. Soc. 260 , Series A, p.168-178, 1966.

20. CALDWELL, J. "Description of the damage in steam turbine blading, due to erosion by water droplets", Phil. Trans. Roy. Soc., 260 . Series A, p.204-209, 1966.

21. CANAVELIS, R. "Jet impact and cavitation damage", Trans. A.S.M.E. Series D, Journal of Basic Engineering Vol. 90, p.355-367, 1968.

22. CARRELL, J. "Cratering and perforation by means of high speed impact", M.Sc. Dissertation UMIST, 1969.

23. CHRISTIE, D.G., HAYWARD, G.W. "Erosion of steam turbine blades", Phil. Trans. Roy. Soc. 260 , Series A, p.183-192, 1966.

24. CONN, H.F., and THIRUVENGADAM, A. "Dynamic response and adhesion failures of rain erosion resistant coatings", Journal of Materials, JMLSA, Vol. 5, No. 3, pp.698-718, 1970.

25. COOK, S.S. "Erosion by water-hammer", Proc. Roy. Soc. A, 119, 481, 1928.

26. COOK, M.A. The science of high explosives, Reinhold Publishing Corp., New York, 1958.

27. COOK, M.A., KEYES, R.T. and URSENBACK, W.C. "Measurement of detonation pressure", J. Appl. Phys. 33, 3413, 1962.

28. COOLEY, W.C. and CLIPP, L.L. "High pressure water jets for undersea rock excavation", Trans. ASME, Journal of Engineering for industry, May 1970, pp.281-287, 1970.

29. DANESHI, G.H. and HAWKYARD, J.B. "A split-platen pressure cell for the measurement of pressure distribution in upsetting operations", Int. J. mech, Sci. Vol. 13, pp. 355-371, 1971.

30. DE CORSO, S.M. and KOTHMANN, R.E. "Erosion by liquid impact", Symposium on Erosion and Cavitation ASTM No. 307, June, 1961,

31. de HALLER, P., Schweiz, Bauztg. 101, 243, 260, 1933.

32. DOVE, R.C. and ADAMS, P.H. "Experimental stress analysis and motion measurement", Merrill Books, 1964.

33. EDWARDS, I.S. "Airworthiness requirements for supersonic transport aircraft in a hydrometer environment", Rain Erosion and Allied Phenomena. 2nd Meersburg Conf. R.A.E. Farnborough, 1967.

34. EINSBERG, P. "Cavitation and impact erosion-concepts, correlations, controversies", ASTM STP 474, p.3-25, 1971.

35. EISNER, E. "Design of sonic amplitude transformers for high magnification", J. ACOUST. Soc. Am., 35(9), 1367 - 1377, 1963.

36. ELLIOTT, D.E., MARRIOTT, J.B. and SMITH, A. "Comparison of erosion resistance of standard steam turbine blade and shield materials on four test rigs", ASTM STP, 474, p.127, 1970.

37. ENGEL, O.G., "Waterdrop collision with solid surfaces", Journal of Research of the National Bureau of Standards, Vol. 54, p.281, 1955.

38. ENGEL, O.G., "Erosion damage to solids caused by high-speed collision with rain", J. Res. Nat. Bur. Stand., Vol. 61, p.47, 1958.

39. ENGEL, O.G. "Impact of liquid drops", Symposium on Erosion and Cavitation, ASTM, No. 307, June, 1961.

40. ENGEL, O.G. "Written discussion", Erosion by Cavitation or Impingement, ASTM STP 408, Am. Soc. Testing Mats., p.152, 1967.

41. ENGEL, O.G. "A first approach to a microscopic model of erosion rate in drop impact and cavitation", Proc. Conf. on Rain Erosion and Associated Phenomena, 1970.

42. ESKILSSON, S. "Design rules for neoprene coatings", 2nd Inter. Meersburg Conference, Roy. Aircraft Est. Farnborough, 1967.

43. EVANS, A, and ROBINSON, J. "Erosion experiments related to steam turbine blading", Parsons' Journal, Vol. 10, No.61, p. 465-473, 1965.

44. FASSO, G. "First results of rain erosion tests in the s.3 intermittent wind tunnel of the O.N.E.R.A. modane test centre", 2nd Meersburg Conf. R.A.E. Farnborough 1967.

45. FIELD, J.E. "Stress waves, deformation and fracture caused by liquid impact", Phil. Trans. Roy. Soc. 260, Series A, p.86-93, 1966.

46. FIELD, J.E. "The importance of surface topography on erosion damage", Rain Erosion and Allied Phenomena, 2nd Meersburg Conference, 1967.

47. FIELD, J.E., CAMUS, J.J. and GORHAM, D.A. "Single impact erosion processes", Proc. Conf. on Rain Erosion and Associated Phenomena, 1970.

48. FINNIE, I, "Erosion by solid particles in a fluid stream". Symposium on Erosion and Cavitation, ASTM No. 307, June, 1961.

49. FYALL, A.A., KING, R.B. and STRAIN, R.N.C., R.A.E. Tech. note chem. 513, 1957.

50. FYALL, A.A., KING, R.B. and STRAIN, R.N.C., "Rain Erosion Aspects of Aircraft and Guided Missiles", Journal of the Roy. Aeronaut. Soc. 447, 1962.

51. FYALL, A.A., KING, R.B. and STRAIN, R.N.C. "Rain erosion aspects of aircraft and guided missiles", Journal Royal Aeronautical Soc., 1962, p.83, 1962.

52. FYALL, A.A. "Practical aspects of rain erosion of aircraft and missiles" Phil. Trans. Roy. Soc. 260, Series A, p.161-168, 1965.

53. FYALL, A.A. "Single impact studies with liquids and solids", 2nd Meersburg Conf. R.A.E. Farnborough, 1967.

54. GAINES, N. "A magnetostriction oscillator producing intense audible sounds and some effects obtained", Physics 3(5), 209-229, 1932.

55. GARCIA, R., HAMMITT, F.G. and NYSTROM, R.E. "Correlation of cavitation damage with other material and fluid properties", Erosion by Cavitation or Impingement ASTM STP 408, Am. Soc. Testing Mats. p.239, 1967.

56. GARDNER, F.W. "The erosion of steam turbine blades", Engineer, Lond., 153, 146, 202, 1932.

57. GARDNER, G.C. "Events leading to erosion in the steam turbine", Proc. Inst. Mech. Engrs. 178 , Pr.1, No.23, 1964.

58. GARDON, R. "A transducer for the measurement of heat transfer", J. Heat Tran. 82, p.396-398, 1960.

59. GARDON, R. and COBOUQUE, J. "Heat transfer between a flat plate and jet of air impinging on it", Proc. Int. Heat. Trans. Conf. 2, p.454-460, 1961.

60. GARDON, R and AKFIRAT, J.C. "The role of turbulence in determining the heat-transfer characteristics of impinging jets". Int. J. Heat Mass Transfer. Vol. 8, pp.1261-1272, 1965.

61. HAJI-IBRAHIM "Punching and drifting of thin circular plates", M.Sc. Dissertation University of Manchester, 1972.

62. HAMMITT, F.G., HUANG, Y.C., KLING, C.L., MITCHELL, T.M. and SOLOMON, L.P. "A statistically verified model for correlating volume loss due to cavitation or liquid impingement", ASTM STP 474, 1970, pp 288-312, 1970.

63. HAMMITT, F.G., LAFFERTY, J.F., CHEESEWRIGHT, R., PITEK, M.T., KEMPPAINEN, D.J. and MITCHELL, T.M. "Laboratory scale devices for rain erosion simulation", Rain Erosion and Allied Phenomena, 2nd Meersburg Conference, 1967.

64. HAMMITT, F.G., "Collapsing bubble damage to solids", Cavitation state of knowledge, ASME, 87-102, 1969.

65. HAMMITT, F.G., HUANG, J.B., MITCHELL, T.M., ROGERS, D.O. "Cavitation and droplet impingement damage of aircraft rain erosion materials", Report No. UMICH 02643 - 5 - 1. University of Michigan, 1970.

66. HANCOX, N.L., and BRUNTON, J.H. "The erosion of solids by the repeated impact of liquid drops", Phil. Trans. Roy. Soc. 260, Series A, p.121-152, 1966.

67. HATTON, A.P. "On Reynold's Analogy", Bulletin of Mechanical Engineering Education Vol. 9, No. 1, pp. 81-86, 1970.

68. HERTZ, H, J. reine angew. Math. 92, 156, 1881.

69. HEYMANN, F.J. "On the time dependence of the rate of erosion due to impingement or cavitation", Erosion by Cavitation or Impingement, ASTM STP 408, Am. Soc. Testing Mats., p.70, 1967.

70. HEYMANN, F.J. "Eine Übersicht Von Schlüssen Zu Der Verhältnissen Zwischen Der Erosionsgerschwindigkeit und Aufschlags", Rain Erosion and Allied Phenomena, 2nd Meersburg Conference, 1967.

71. HEYMANN, F.J. "On the shock wave velocity and impact pressure in high-speed liquid-solid impact", Trans. A.S.M.E., Series D, Journal of Basic Engineering, Vol. 90, p.400-402, 1968.

72. HEYMANN, F.J. "Toward quantitative prediction of liquid impact", ASTM STP 474, p.212, 1970.

73. HOBBS, J.M. and BRUNTON, W.C. "Comparative erosion tests on erosion materials", Part I: Drop Impact Tests". NEL Report No. 205, November, 1965.

74. HOBBS, J.M. "Experience with a 20 kc cavitation erosion test", NEL, Symposium on Erosion, ASTM, 1966.

75. HOBBS, J.M., LAIRD, A., BRUNTON, W.C. "Laboratory evaluation of the vibratory cavitation erosion test", NEL Report 271, 1967.

76. HOBBS, J.M., and RACKMANN, D. "Environemtally controlled cavitation tests", Characterisation and Determination of Erosion Resistance, ASTM STP 474 p.29-47, 1970.

77. HOFF, G., LANGBEIN, G., and RIGGER, H. "Material Destruction due to liquid impact", Erosion by Cavitation or Impingement, ASTM STP 408, Am. Soc. Testing Mats., 1967, p.42.

78. HOFF, G., HERBERT, W. and RIEGER, H. "Rain and sand erosion, phenomena of material destruction caused by repeated loads", Characterisation and Determination of Erosion Resistance, ASTM STP 474, p.353-376, 1970.

79. HONEGGER, E. Brown Boveris Review, 14, 95, 1927.

80. JENKINS and BOOKER "The impingement of water drops on a surface moving at high speed", Aerodynamic Capture of Particles. Pergamon Press, 1960.

81. JENKINS, D.C. "Disintegration of raindrops by shockwaves ahead of conical bodies", Phil. Trans. Roy. Soc. 260, Series A, p. 153-161, 1966.

82. JOHNSON, W. and MELLOR, P.B. "Plasticity for mechanical engineers", Van Nostrand, 1966.

83. JOHNSON, W., TRAVIS, F.W. and LOH, S.Y. "High speed cratering in wax and plasticine", International Journal of Mechanical Sciences, Vol. 10, p.593, 1968.

84. JOHNSON, W. "Impact strength of materials", Ed. Arnold, London, 1972.

85. JOLLIFFE, K.H. "The application of dislocation etching techniques to the study of liquid impact", Phil. Trans. Roy. Soc. 260, Series A, p.101-108, 1966.

86. KANTOR, A.J. and GRANTHAM, D.D. "Distribution and composition of clounds at supersonic aircraft altitudes", Rain Erosion and Allied Phenomena, 2nd Meersburg Conference, 1967.

87. KENYON, H.F. "Erosion by water jet impacts", Parts, I, II, II, IV and V. A.E.I. Ltd. Internal Report, 1967.

88. KERR, S.L. "Determination of the relative resistance to cavitation erosion by the vibratory method", Trans. Am. Soc. Mech. Engrs. 59(5) 373-397, 1937.

89. KING, R.B. "Multiple impact rain erosion studies at velocities up to 450 m/sec", Rain Erosion and Allied Phenomena, 2nd Meersburg Converence, 1967.

90. KLING, C.L. "A high speed photographic study of cavitation bubble collapse," ORA Report No. 03371-2-7 University of Michigan, March 1970.

91. KLING, C.L., HAMMITT, F.G., MITCHELL, T.M. and TIMM, E.E. "Bubble collapse near a wall in flowing systems", ASME Cavitation Forum, Detroit, Michigan, May, 1970.

92. KNAPP, R.T., DAILY, J.W. and HAMMITT, F.G. Cavitation, McGraw-Hill, 1970.

93. LANE, W.R. and GREEN, H.L. Surveys in Mechanics, Cambridge University Press, 1956.

94. LAPP, R.R., STUTZMAN, R.H. and WAHL, N.E., W.A.D.C. Reports, 53-185 and 55-308, 1955.

95. LAWS, O.J. and PARSONS, D.A., Transaction of the American Geophysical Union, TAGUA, Vol. 24, 1943, pp 452-460, 1943.

96. LEVIN, Z, and HOBBS, P.V. "Splashing of water drops on solid and wetted surfaces: hydrodynamics and charge separation", Phil. Trans. Roy. Soc. 269, Series A, P.555-585, 1971.

97. LICHTMAN, Z. "Cavitation damage resistance and adhesion of polymeric overlay materials", ASTM STP 474, p.422, 1970.

98. MARRIOTT, J.B., and ROWDEN, G. "The erosion of a cobalt-chromium alloy by liquid impact", Phil. T.R.S. 260, Series A, p.144-149, 1966.

99. MATHIESON, R. and HOBBS, J.M. "Cavitation erosion: comparative tests", Engineering Vol. 189, Jan 22 1960.

100. MORTON, W.B. and CLOSE, L.J. "Notes on Hertz's Theory of the contact of elastic bodies", Phil. Mag. 43, 320, 1922.

101. NEVINS, R.G. "The cooling power of an impinging jet", Ph.D. Thesis, University of Illinois, 1954.

102. OLUBODE, J.A. and CROSSLAND, B. "The effect of size on the yield of steels under static contact loads", Int, J. Mech. Sci. Vol. II, pp 551-573, 1969.

103. OSTROVSKII, A.P. "Deep Hole Drilling with explosives", translation from the Russian by Consultants Bureau, New York, 1969.

104. PLESSET, M.S. and DEVINE, R.E. "Effect of exposure time on cavitation damage", Journal of Basic Engineering, Trans. Am. Soc. Mech. Engrs. Vol. 88D, No.4, p.691, 1966.

105. REIGER, H. "The destruction of metals as the result of the impact of water drops at high speed", Z. Metallk., 1966, 57. Sept., 693-699. NLL Trans No. 9022.06 (5642).

106. REIGER, H. "Investigation of the influence of various test parameters on material destruction at drop impact", Proc. Conf. on Rain Erosion and Associated Phenomena, 1970.

107. RHEINGANS, W.J. "Accelerated cavitation research", Trans. Amer. Soc. Mech. Engrs. 72(5) 705-724, 1950.

108. ROSTOKER, N. "The formation of craters by high speed metallic jets", Meteoritics 1 No. 1. p11, 1953.

109. RUSSELL, F. Ph.D. Thesis Thermo and Fluids Division, 1970.

110. SCHLICHTING, H. Boundary Layer Theory, 4th ed. pp 78-83, Pergamon Press, London, 1960.

111. SCHMITT, G.F. "Polyurethane coatings for rain erosion protection" 2nd International Meersburg Conf. on Rain Erosion and Associated Phenomena, 1967.

112. SCHMITT, G.F. "Polyurethane coatings for rain erosion protection", AFML TR-67-355 Air Force Materials Laboratory, 1968.

113. SCHMITT, G.F. "Erosion Rate - Velocity Dependance for Materials at Supersonic Speeds", Characterisation and Determination of Erosion Resistance, ASTM STP 474, p.323, 1970.

114. SCHRADER, H. "Trocknung feuchter öberflächen mittels warmluftstraklen" ; Stromungsvorgange und Stoffubertragung, Forschungsh, Ver. Dtsch. Ing. 484, 1961.

115. SKALAK, R. and FELT, D. "Impact on the surface of a compressible liquid", Trans ASME (J. Engrg. for Industry) Vol. 88B, 3. 1966.

116. SMITH, A, KENT, R.P., and ARMSTRONG, R.L. "Erosion of steam turbine blade shield materials", Erosion by Cavitation or Impingement, ASTM STP 408, Am. Soc. Testing Mats. p.125. 1967.

117. SNEDDON, I.N. and HILL, R. "Progress in solid mechanics", Chap. VIII by Mucki, R., 1961.

118. TABOR, D. "The hardness of metals", Oxford Press, 1951.

119. TATNALL, G. "Military service experience and design philosophy in flight vehicle rain erosion", Proc. Conf. on Rain Erosion and Associated Phenomena, 1970.

120. TAYLOR, G.I. "The formation of enlargement of circular holes in thin plastic plate", Quart. J. Mach. App. Math., 1 . 1948.

121. TAYLOR, G.I. "Oblique impact of a jet on a plane surface", Phil. Trans. Roy. Soc. 260, Series A, p.96-100, 1966.

122. THIRUVENGADAM, A. "Intensity of cavitation damage encountered in field installations", Hydronautics, Inc., Technical Report 233-7, Feb. 1965.

123. THIRUVENGADAM, A. "The concept of erosion strength", Erosion by Cavitation or Impingement, ASTM STP 408, Am. Soc. Testing Mats. 1967, p.22.

124. THIRUVENGADAM, A. "On modeling cavitation damage", Journal of Ship Research, Vol. 13, No. 3, pp.220-233, 1969.

125. THIRUVENGADAM, A., RUDY, S.L. and GUNASEKARAN, M. "Experimental and analytical investigations on liquid impact erosion", Characterisation and Determination of Erosion Resistance, ASTM STP 474, p.249, 1970.

126. THIRUVENGADAM, A. "Cavitation Erosion", App. Mech. Rev. 24, 3 p.245-251, 1971.

127. THOMAS, G.P. "The initial stages of deformation in metals subjected to repeated liquid impact", Phil. Trans. Roy. Soc. 260, Series A, p.140-143, 1966.

128. THOMAS, G.P. Ph.D. Thesis, Cambridge University, 1966.

129. TIMM, E.E. and HAMMITT, F.G. "A repeating water gun device for studying erosion by water jet impacts", ORA Report No. 2643 - 1 - PR, University of Michigan, 1969.

130. TORZA, S., COX, R.G., and MASON, S.G. "Electrohydrodynamic deformation and bursts of liquid drops", Phil. Trans. Roy. Soc. Lond. A269, 1198, p.295-319, 1971.

131. TRAGER JOACHIM, "Photoelastic study of elastic impact on the edge of a plate", Int. J. Mech. Sci., Vol. 5, pp 275-285, 1963.

132. VAN VALKENBURG, M.E., CLAY, W.G. and HUTH, J.M. Journal of Applied Physics, Vol. 27, 1123., 1956.

133. WALTON, J.D. and GORTON, C.W. "Rain Erosion of ceramics at high mach numbers", Rain Erosion and Allied Phenomena, 2nd Meersburg Conference, 1967.

134. WEAVER, J.H. "Electroplated nickel rain erosion resistant coatings", Rain Erosion and Allied Phenomena, 2nd Meersburg Conference, 1967.

135. WHEELER, W.H. "Indentation of metals by cavitation", Journal of Basic Engineering, March, 1960, p.184-194.

136. WORTHINGTON, A.M. "A Study of splashes", Macmillan, 1963.

137. ZAID, A.I.O., HAWKYARD, J.B. and JOHNSON, W. "Experiments in plate cutting by shaped high explosive charges", Journal of Mechanical Engineering Science, Vol. 13. No.1, 1971.

APPENDIX I

If a steel ball falls freely from a height, s', travelling through two light beams during a time, t', the distance between the light beams, s, is given by,

$$s = \sqrt{2 f s'} \cdot t'$$

where f is the acceleration of the ball due to gravity.

If a water jet, or other projectile, travelling through the two light beams, spaced a distance, s, apart, takes a time, t, then its average velocity, v, is given by,

$$v = \sqrt{2 f s'} \cdot \frac{t'}{t} \tag{1}$$

Error in water jet velocity, v, due to experimental errors in s', t' and t is given by,

$$\delta v = \frac{\partial v}{\partial s'} \cdot \delta s' + \frac{\partial v}{\partial t'} \cdot \delta t' - \frac{\partial v}{\partial t} \cdot \delta t \tag{2}$$

Thus from equation (1) and (2) we have

$$\delta v = \frac{f}{\sqrt{2 f s'}} \times \frac{t}{t'} \times \delta s' + \frac{\sqrt{2 f s'}}{t} \times \delta t' - \frac{\sqrt{2 f s'} \times t' \times \delta t}{t^2} \tag{3}$$

Estimates of error are given as

$\delta s' = \pm$ 1 mm due to height of ball above photocells

$\delta t' = \pm$ 40 μsec due to alignment of ball in free flight

as it breaks the lightbeam in a slightly offset position.

$\delta t \rightarrow 0$ μsec may be considered negligible

Typical figures of $t' = 3680\,\mu$ sec, $t = 50\,\mu$ sec for nominal 220 m/sec jet

$s' = 456$ mm

$f = 9.81$ m/sec^2

Substitution of these figures into equation (3) shows that,

$$\delta v = \pm 2.6 \text{ m/sec}$$

Hence for the water jet speed of 220 m/sec the percentage error is,

$$\frac{\delta v}{v} \times 100 = 1.2\,\%$$

The error is acceptable in this work but could be further improved by reducing $\delta t'$ which is readily achieved by dropping the ball more precisely down the water jet axis.

Table I

Hardness α-brass specimens

Pre-stress MN/m^2	Vickers Hardness Number 5 kg load
0	61
7.5 b.c.	65
90 b.c.	86
180 b.c.	96
67 u.c.	85
67 u.t.	85

b.c. = biaxial compression

u.c. = uniaxial compression

u.t. = uniaxial tension

TABLE II

Plastic Indentation μm		Biaxial Compression
Water Jet *	Rigid Indenter	on Target MN/m^2
40	70	0
15	55	7.5
5	10	90
3	0	180

* Water jet travelling at 220 m/sec engendering an impact stress of 300 MN/m^2.